

Optimization of stereotactic ablative radiation therapy of malignant lung nodules presented as ground-glass opacities

Carla Cases Copestake



Aquesta tesi doctoral està subjecta a la llicència <u>Reconeixement 4.0. Espanya de Creative</u> <u>Commons</u>.

Esta tesis doctoral está sujeta a la licencia <u>Reconocimiento 4.0. España de Creative</u> Commons.

This doctoral thesis is licensed under the **Creative Commons Attribution 4.0. Spain License**.





Optimization of stereotactic ablative radiation therapy of malignant lung nodules presented as ground-glass opacities

(Optimització del tractament de radioteràpia estereotàctica fraccionada en nòduls pulmonars malignes que presenten opacitats en vidre esmerilat)

Doctoral thesis dissertation presented by Carla Cases Copestake to apply for the degree of doctor at the University of Barcelona.

Directed and tutorized by:

Meritxell Mollà, head of the department of Radiation Oncology at Hospital Clínic, researcher at the Institute for Biomedical Research August Pi i Sunyer in the group of Translational Genomics and Targeted Therapies in Solid Tumors and associate professor at the Department of Clinical Foundations in the University of Barcelona

Directed by:

Carles Gomà, medical physicist at the Institut del Cancer i Malalties de la Sang at Hospital Clínic, researcher at the Institute for Biomedical Research August Pi i Sunyer in the group of Translational Genomics and Targeted Therapies in Solid Tumors

As a part of the Doctoral Program in Medicine and Translational Research.

School of Medicine and Health Sciences. University of Barcelona.

January 2025

ACKNOWLEDGEMENTS

To my family. Both my given and chosen one. Without you I could not have had the courage and motivation to start (and even get to finish) this project. Specially to my parents, who encouraged and took good care of me in times of need.

To Berta, you went through this a while ago, and now I am just following your steps. Thanks for being there, always and unconditionally.

To my friends, the physicists, the council. Not in my wildest dreams would I have imagined finding a family like this one. You are the reason I always try to become a better version of myself.

To the colleagues, friends in most cases, of the Radiotherapy team at Hospital Clinic. For all the feedback, talks, doubts and coffees I've managed to steal from you. Specially to Meritxell Mollà and Carles Gomà, for guiding me through this process.

To the CDI colleagues, for helping me in understanding how a lung should be looked at and for analysing the images that made this project possible.

To all the patients, for sharing their data and giving me the opportunity to do this research project.

Finally, but not less important, to Maki, for being my emotional support system, my excuse to take care of my health and for teaching me that everything can be solved with love, food, exercise and moderate amounts of hate and destruction.

FUNDING

No funding was received for the development of this thesis.

TABLE OF CONTENTS

AUTORIZATION FOR THE PRESENTATION OF THE THESIS	1
STATEMENT OF THE DOCTORAL CANDIDATE AND DIRECTOR/S OF	
ORIGINALITY AND GOOD PRACTICES OF THE THESIS	2
DECLARATION OF AUTHORSHIP OF THE THESIS	3
ACKNOWLEDGEMENTS	4
FUNDING	5
TABLE OF CONTENTS	6
LIST OF FIGURES	8
ABBREVIATIONS AND ACRONYMS	10
LIST OF ARTICLES	12
RESUM DE LA TESIS EN CATALÀ	13
INTRODUCTION	16
1. Principles of Radiotherapy	16
1.1 Mechanism of action	16
1.2 Absorbed dose	
1.3 Biological effects	18
1.4 Linear-quadratic model, fractionation and biological effective dose	21
1.5 Overall treatment time	22
1.6 Fractionation schemes	23
1.7 Adverse effects and CTACE scale	24
2. Radiotherapy process	26
2.1 Radiotherapy types	27
2.2 Simulation process	27
2.3 Target delineation	28
2.4 Treatment planning	31
3. Lung Lesions	43
3.1. Lung cancer	43
3.2 Lung metastases	44
3.3 Lung screening and lung lesions follow-up	44
3.4 Lung SABR	
3.5 Lung SABR for GGO lesions	50
3.6 Lung SABR related toxicities	51

4. SABR challenges for the treatment of GGO lesions	56
4.1. Volume definition	56
4.2. Lung parenchyma changes	57
4.3. Dose calculation accuracy	58
HYPOTHESIS	50
OBJECTIVES	61
MATERIAL, METHODS AND RESULTS	52
PUBLICATION 1	62
PUBLICATION 2	73
DISCUSSION	81
1. Lung parenchyma changes evaluation strategies	81
2. Prescription fractionation and BED	83
3. Comparing TPS doses AAA vs AXB	84
4. Discussion of methodological approaches	35
5. Implications for clinical practice	87
6. Strengths and limitations	38
7. Future research directions	39
8. Key findings and concluding remarks	90
CONCLUSIONS	91
REFERENCES	92

LIST OF FIGURES

<u>Figure 1.</u> Schematic representation of radiation-induced DNA damage	17
Figure 2. Schematic representation of the cell cycle	19
Figure 3. Normal tissue complication probability (NTCP) and tumor control probability	
(TCP) as a function of dose	21
Figure 4. Effect of dose fractionation on cell survival fraction applying the linear quadratic model	23
Figure 5. Main steps of the radiotherapy process from the Simulation CT scan to the	
treatment delivery	26
Figure 6. Volume definition according to ICRU guidelines	29
Figure 7. Different approaches for the generation of the ITV volume	30
Figure 8. Depth dose distribution in water for high (MV) and low (kV) energy photons,	
electrons and protons	32
Figure 9. Dose distribution of the same plan using 3DCRT, IMRT, DCA and	
VMAT(d) techniques	34
Figure 10. Dose calculation differences between algorithms such as AAA and AXB	39
Figure 11. Differential and cumulative Dose Volume Histogram of the same radiotherapy plan	41
Figure 12. Example of PET-CT and Simulation CT scan in a patient with a lung metastasis	
close to the chest wall	45
Figure 13. Display of common malignant signs	47
Figure 14. Lung tumors with different degrees of GGO component	49
Figure 15. Radiation pneumonitis in computed tomographic images	54
Figure 16. Volume definition for a lung lesion consisting of a GGO nodule with a solid part	
at the center of the lesion	57
Figure 17. Example of a quantitative evaluation of the lung parenchyma performed on the	
pre-treatment CT scan of the right lung of a patient with a nodule	82
Figure 18. Schematic representation of the dose de-escalation approach proposed in this	
work for the three fractionation schemes analyzed	84

Figure 19. Relation between PTV size and the volumetric CTR for the patient lesions	
included in the study	.86
Figure 20. Different stages of the natural evolution of adenocarcinomas with various degrees	
of GGO component	.88

ABBREVIATIONS AND ACRONYMS

3DCRT - Three-Dimensional Conformal Radiotherapy

4DCT - Four-Dimensional Computed Tomography

AAA - Anisotropic Analytical Algorithm

AAPM - American Association of Physicists in Medicine

ADL – Activities of Daily Life

AE – Adverse Event

AI – Artificial Intelligence

AXB - Acuros XB

AXB_m – Acuros XB in medium

AXB_w – Acuros XB in water

BED - Biological Effective Dose

CCC - Collapsed Cone Convolution

COVID - Coronavirus Disease

CT – Computed Tomography

CTCAE - Common Terminology Criteria for Adverse Events

CTR - Consolidation to Tumor Ratio

CTV - Clinical Target Volume

D - Dose

DICOM - Digital Imaging and Communications in Medicine

DNA - Deoxyribonucleic acid

DVH - Dose-Volume Histogram

E – Effect

ESTRO - European Society for Radiotherapy and Oncology

ETAR - Equivalent Tissue-Air Ratio

GGO - ground-glass opacities

GTV - Gross Tumor Volume

HU – Hounsfield Units

IAEA - International Atomic Energy Agency's

ICRU - International Commission on Radiation Units

IMRT - Intensity-Modulated Radiotherapy

ITV - Internal Target Volume

LBTE - Linear Boltzmann Transport Equation

LC – Local Control

LQ - Linear Quadratic Model

MIA - Minimally Invasive Adenocarcinoma

MLD – Mean Lung Dose

NSCLC - Non-Small-Cell Lung Cancer

NTCP - Normal Tissue Complications Probability

OAR - Organ at Risk

OM - Oligometastatic

PET - Positron Emission Tomography

PBC - Pencil Beam Convolution

PTV - Planning Target Volume

RP – Radiation Pneumonitis

SABR - Stereotactive Ablative Radiotherapy

TCP - Tumor Control Probability

TPS - treatment planning system

V - Volume

VMAT – Volumetric Modulated Arc Radiotherapy

WHO - World Health Organization

LIST OF ARTICLES

Thesis in compendium of publications format.

The thesis consists of four objectives and two articles

ARTICLE 1

Cases C, Benegas M, Sánchez M, Vollmer I, Casas F, Gomà C, Mollà M. Biological equivalent dose is associated with radiological toxicity after lung stereotactic ablative radiation therapy. Radiother Oncol. 2023 Jun;183:109552.

Impact factor of 4.9 for the year 2023 and D1 according to Journal Citation Report in the category "Radiology, Nuclear Medicine and Imaging" for the year 2023.

ARTICLE 2

Cases C, Mollà M, Sánchez M, Benegas M, Ballestero M, Serrano-Rueda S, Antelo G, Gomà C. Feasibility and potential clinical benefit of dose de-escalation in stereotactic ablative radiotherapy for lung cancer lesions with ground glass opacities. Physics and imaging in radiation oncology, 32, 100681. https://doi.org/10.1016/j.phro.2024.100681

Impact factor of 3.4 for the year 2023 (year 2024 not yet available) and Q1 according to Journal Citation Report in the category "Radiology, Nuclear Medicine and Imaging". Quartile for the year 2024 is still not available.

RESUM DE LA TESIS EN CATALÀ

Optimització del tractament de radioteràpia estereotàctica fraccionada extracraneal en nòduls pulmonars malignes que presenten opacitats en vidre esmerilat

INTRODUCCIÓ

El càncer de pulmó és el més comú i letal a nivell mundial. Els pacients amb càncer de pulmó de cèl·lula no petita en estadis inicials i no operables es tracten amb radioteràpia d'alta precisió, coneguda com radioteràpia estereotàctica ablativa extracraneal (SABR, per les seves sigles en anglès). Un petit percentatge dels tumors tractats amb SABR presenten opacitats en vidre esmerilat (GGO, per les seves sigles en anglès). Aquest tractament té dos problemes principals. Primer, els algoritmes de càlcul utilitzats clínicament tendeixen a ser inexactes per a SABR de GGO, fet que pot comportar una irradiació excessiva dels teixits sans. Segon, les GGOs es tracten englobant tot el volum sospitós (que inclou la part sòlida i la component GGO), tot i que tendeixen a ser multifocals i presenten una evolució amb millor pronòstic que les lesions sòlides. A més, s'espera un augment del nombre de pacients amb tumors GGO gràcies als programes de cribratge, per la qual cosa és important optimitzar el tractament de SABR per a aquests nòduls.

HIPÒTESIS

Amb la metodologia actual, els tractaments de SABR de GGO presenten un excel·lent control local a expenses d'una irradiació excessiva als teixits sans. Utilitzant un càlcul de dosis correcte i adaptant l'administració del tractament als casos amb GGO, podrem reduir la toxicitat del tractament, mantenint el control local.

OBJECTIUS

En una primera part s'ha avaluat la toxicitat observada amb els objectius de:

- Analitzar i quantificar els canvis en el parènquima pulmonar després del tractament de radioteràpia estereotàctica fraccionada extracraneal.
- Correlacionar la toxicitat pulmonar de grau 1 amb la dosi administrada al pacient.

En una segona part, s'ha optimitzat aquest tractament, per a lesions amb component de vidre esmerilat amb els sub-objectius de:

- Avaluar l'exactitud dels algoritmes de càlcul de dosi clínica en nòduls pulmonars en presència d'opacitats en vidre esmerilat.
- Definir un enfocament per optimitzar els tractaments pulmonars estereotàctics per a lesions amb component d'opacitats en vidre esmerilat que mantingui el control local esperat mentre es redueix el risc de toxicitat associada.

MÈTODES

El primer pas ha estat analitzar retrospectivament la toxicitat radiològica observada en els pacients tractats a l'Hospital Clinic Barcelona entre 2017 i 2021, amb un total de 102 pacients i 118 lesions. Hem correlacionat aquesta toxicitat amb la dosi calculada amb els sistemes de planificació utilitzats clínicament 8Eclipse, Varian). Per a fer-ho, hem definit uns criteris per valorar la toxicitat radiològica a partir de les imatges de tomografia axial computeritzada (CT) de seguiment dels pacients, correlacionant aquesta toxicitat amb la dosi rebuda.

Paral·lelament, hem avaluat les incerteses del càlcul dosimètric en diferents sistemes de planificació emprats en la pràctica clínica per a diferents graus de GGO, tant en casos reals de pacients com en un maniquí antropomòrfic. Hem correlacionat aquestes diferències amb la quantitat de GGO present en la lesió per als diferents casos. Referent als algoritmes de càlcul s'ha utilitzat un algoritme tipus B (AAA, Eclipse) i s'ha comparat amb un algoritme tipus C, que resol la equació de transport lineal de Boltzman (Accuros, Eclipse).

Finalment, hem recalculat el pla de tractament utilitzant els dos models de càlcul de dosis disponibles, tant per a l'aproximació original, consistent en donar un sol nivell de dosi a tota la lesió, com utilitzant dos nivells de dosis diferents segons si la zona tractada correspon a la part sòlida de la lesió o a la part amb component GGO. En la selecció d'aquests dos nivells de dosi, s'ha escollit com a llindar inferior la dosis biològica efectiva de 100 GyBED₁₀, ja que és el valor aconsellat a la literatura per aconseguir un control local acceptable per a aquest tipus de lesions. Aquest nivell de dosis s'ha donat a la component GGO de la lesio mentre que la prescripció a la part sòlida de la lesió s'ha mantingut igual que en el tractament original. Hem analitzat les diferències pel que fa a dosi al pulmó i robustesa de les dues aproximacions al tractament.

RESULTATS PRINCIPALS

Hem trobat una correlació entre el volum de pulmó que rep dosis biològiques efectives superiors a 300 GyBED₃ amb l'aparició i magnitud de les toxicitats radiològiques observades. També s'ha observat que els canvis en el parènquima pulmonar tendeixen a mantenir-se o empitjorar en aquells casos on el volum amb D>300 GyBED₃ és superior a 20 cm³.

En la segona part de l'estudi, s'ha trobat una correlació positiva entre la presència de GGO i els errors de càlcul de la dosi en el cas dels càlculs sobre maniquí. Aquestes diferències disminueixen en pacients, especialment en presència de moviment respiratori. Quan es planteja un tractament aplicant una desescalada de dosis a la zona de GGO, s'aconsegueixen reduccions significatives en la dosi mitjana al pulmó, V20 i V300GyBED₃. Finalment, també s'ha observat que, optimitzant utilitzant dosis més baixes a la zona de GGO, s'aconsegueixen patrons de fluència més estables, augmentant la robustesa del tractament.

CONCLUSIONS

Dels resultats d'aquesta tesi, s'observa una correlació clara entre les dosis biològiques efectives superiors a 300 Gy i els canvis radiològics tant a curt com a llarg termini. Si es confirma en una cohort independent de pacients, aquestes troballes podrien conduir a les primeres restriccions de dosi de radioteràpia per a la toxicitat pulmonar de grau 1. Aquest estudi posa les bases per a la desescalada de dosis en el tractament SABR de lesions pulmonars amb GGO, cosa que podria conduir a un control local equivalent mentre es redueixen les toxicitats associades. Aquestes troballes estableixen els fonaments per a futurs assaigs clínic.

PARAULES CLAU

Radioteràpia estereotàctica ablativa, càncer de pulmó, opacitats en vidre esmerilat, toxicitat pulmonar, desescalada de dosi.

INTRODUCTION

1. Principles of radiotherapy

Radiotherapy is a treatment modality that uses ionizing radiation to achieve a therapeutic effect, and it is primarily used in cancer treatment.¹ In oncology, radiotherapy is one of the three main treatment modalities along with surgery and systemic treatment.² It can play a role in different phases of the disease, such as radical treatment with curative intent (either exclusive or concomitant with other treatments), adjuvant or neoadjuvant to surgery (associated or not with systemic treatment) or palliative treatment to improve symptom control and quality of life.³⁻⁵ It is estimated that nowadays, about 50% of cancer patients will benefit from radiotherapy at some point during their course of treatment.^{1,2}

1.1 Mechanism of action

The fundamental process of radiotherapy is based on the interactions between particles and molecules. These interactions cause ionization and/or excitation of the molecules, resulting in damage to the deoxyribonucleic acid (DNA) of cancer cells. This damage can ultimately lead to the death of targeted cells or their inability to further multiply.⁶

Radiation is the process by energy is deposited in the medium by electromagnetic waves or subatomic particles. When this radiation carries enough energy to ionize the medium it passes through it is classified as ionizing radiation. Ionizing radiation can originate from naturally radioactive substances, which emit it spontaneously, or from artificial sources such as X-ray generators and particle accelerators. The effect of these interaction can be broadly divided into (Figure 1):⁷

- Direct effect: Ionizing radiation directly interacts with atoms and molecules within cells. This interaction can involve several processes, including the photoelectric effect, Compton scattering, and pair production. These events result in immediate structural damage, such as breaks in the DNA chain or alterations in the nitrogenous bases, potentially leading to mutations or cell death.
- Indirect Action: A significant portion of the damage caused by ionizing radiation is mediated through the production of free radicals. These reactive oxygen species can

affect DNA integrity, leading to a variety of lesions, including single-strand breaks, double-strand breaks, damage to nitrogenous bases, and crosslinking between DNA and proteins. These complex processes, are particularly challenging for cellular repair mechanisms, increasing the risk of errors during repair or apoptosis, ultimately contributing to carcinogenesis or cell death.

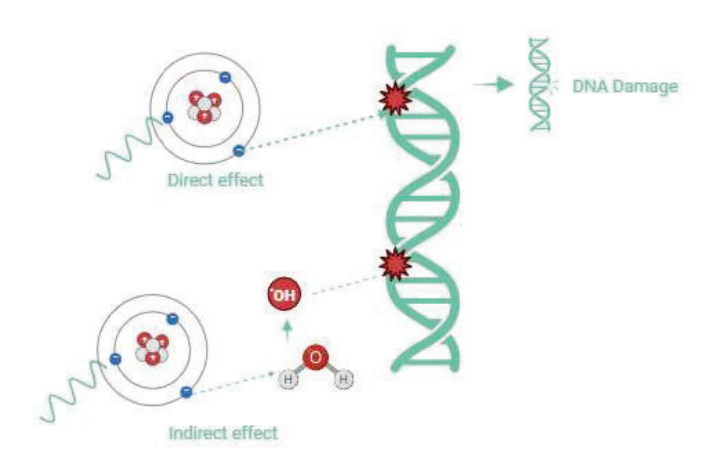


Figure 1. Schematic representation of radiation-induced DNA damage. Adapted from Frontiers in Pharmacology.

August 2019.8

The extent of the damage inflicted to the cell varies depending on how well its mechanisms of repair work. If the repair is successful, the cell resumes its normal functions. However, if the repair is incomplete or flawed, it may lead to mutations or chromosomal abnormalities, which could either make the cell sustainable or not. Viable mutations often result in cell survival but can cause aging, early differentiation, mutations, or cancer development. Conversely, non-viable mutations lead to cell death through apoptosis or necrosis.⁹

After radiotherapy, tissue repair involves a complex series of processes aimed at restoring damaged tissues. There are two main phases after radiation damage takes place. First, acute repair phase begins almost immediately after exposure to radiation. This phase is characterized by an inflammatory response triggered by cellular damage. Inflammatory cells, including neutrophils and macrophages, are activated to remove damaged cells and debris.¹⁰ This process involves the release of cytokines and growth factors that further recruit and activate additional immune cells to the site of damage.¹¹ During this phase, vascular damage can occur, leading to

impaired blood supply and hypoxia in the affected tissues. This vascular damage is a key factor that influences the subsequent stages of tissue repair.¹²

Secondly, the long-term repair phase starts. The repair process often involves fibrosis, where excess collagen deposition leads to scarring and can alter the tissue's normal function. Over time, the balance between collagen deposition and its degradation determines the quality of the tissue repair. Additionally, angiogenesis, the formation of new blood vessels, is critical for restoring blood supply to the repaired tissue and supporting ongoing repair and regeneration processes. This long-term phase can extend over months or years, depending on the extent of damage and the tissue's ability to recover.

1.2 Absorbed dose

The unit to quantify the amount of radiation delivered to a patient is the absorbed dose (D). It is defined as the energy imparted (ϵ) by the particles in a volume (V) of mass (m) as:

$$D = \varepsilon/m \tag{1}$$

The unit of absorbed dose is the gray (Gy), which corresponds to one Joule per kilogram.¹⁴ As it comes from its definition, this unit does not consider any characteristics related to the biological effects of the energy deposited, neither biological consideration regarding the irradiated volume. Although the definition of absorbed dose provides information about the degree of interaction between the particles and the target, it lacks any information to evaluate the clinical impact of the dose.

1.3 Biological effects

There are several biological factors that play a role in the biological effect of dose.

1.3.1 Cell cycle

The cell cycle consists of several phases, each phase has different characteristics in terms of cellular activities and sensitivity to radiation(Figure 2):⁷

• <u>Gap 1 Phase:</u> Cells grow and prepare for DNA synthesis. Sensitivity to radiation is relatively low during this phase.

- Synthesis Phase: DNA is replicated. Cells in this phase are more resistant to radiation because the process of DNA replication can help repair radiation-induced damage.
- Gap 2 Phase: Cells prepare for mitosis. This phase is more sensitive to radiation because cells are checking and repairing DNA before division.
- Mitosis Phase: Cells divide into two daughter cells. This phase is highly sensitive to radiation because the DNA is condensed and vulnerable.

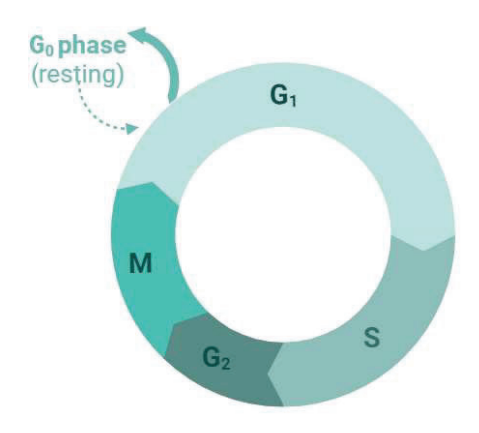


Figure 2. Schematic representation of the cell cycle. With the five phases of cell replication represented as follows:

GO phase: the normal resting state, G1 phase: RNA and proteins are produced in preparation for cell division, S

phase: DNA is produced in preparation for cell division, G2 phase: cell structurally prepares to divide, M phase:

mitosis occurs as the cell splits in half to form two identical cells. Adapted from National Cancer Institute,

SEER training module. Adapted from Randy et al.¹⁵

Tumor cells often proliferate rapidly and have shorter cell cycle durations, increasing the probability of being in the gap 2 and mitosis phases, where they are most sensitive to radiation. This makes radiotherapy particularly effective against rapidly dividing tumor cells.¹⁶

1.3.2 Repair mechanisms

Healthy cells possess several mechanisms to repair DNA damage caused by radiation. Some of the mechanisms, such as base excision repair, only repair small lesions while other mechanisms can repair double-strand break damage via homologous recombination.

Tumor cells often have defective repair mechanisms due to mutations, making them less capable of repairing radiation-induced damage compared to healthy cells. This inefficiency in repair contributes to the higher sensibility of tumor cells to radiotherapy.⁷

1.3.3 Vascularization and oxigenation

Vascularization refers to the formation of blood vessels within a tumor. Adequate blood supply is essential for delivering oxygen and nutrients. Well-vascularized tumors have a rich blood supply, ensuring high oxygen levels. This oxygen presence makes the tumor cells more susceptible to radiation, as oxygen enhances the damaging effects of radiation on DNA. Conversely, poorly vascularized tumors suffer from hypoxia (low oxygen levels), which can reduce the effectiveness of radiotherapy. Hypoxic cells are more resistant to radiation because oxygen acts as a potent radiosensitizer, stabilizing radiation-induced DNA damage and preventing effective repair.⁷

1.3.4 Therapeutic implications

All this means that, in general, the effects of ionizing radiation are more severe in tumor cells than in healthy cells, as they have a higher rate of proliferation, low differentiation, are more likely to be in the mitotic phase and have altered repair mechanisms. This differential effect on tumor cells enables a therapeutic window (Figure 3) of radiation dose where the elimination of cancer cells is greater than the loss of healthy cells, and the risk-benefit ratio of the treatment is favourable. In all cases, the objective is to maximize the probability of tumor control (TCP) and minimize the risk of complications in healthy tissue (NTCP). This balance can be optimized through the prescription dose and its fractionation, and with various factors that allow modifying and widening the difference between TCP and NTCP.¹⁷

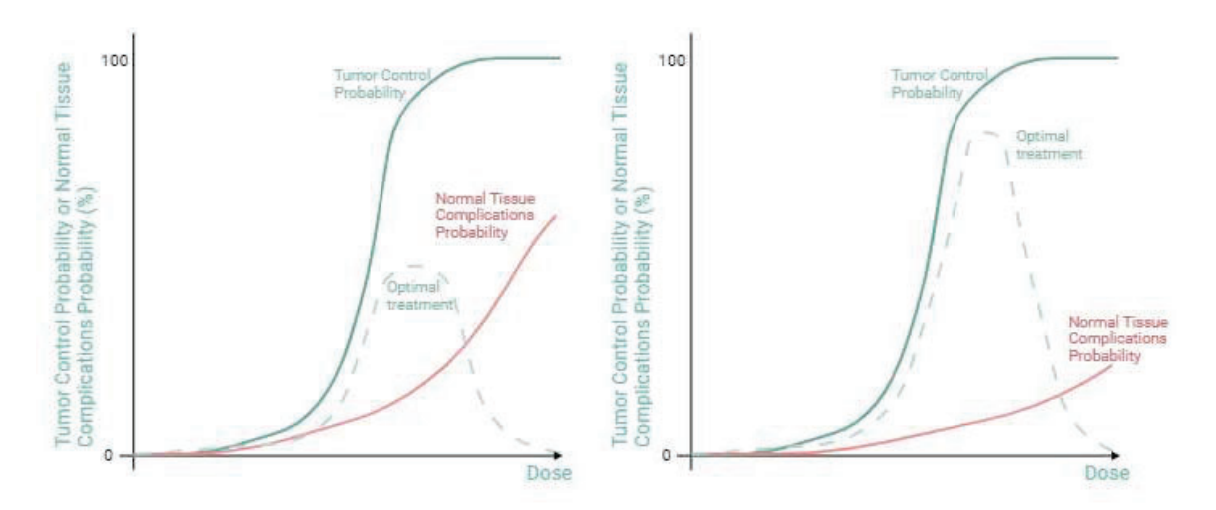


Figure 3. Normal tissue complication probability and tumor control probability as a function of dose. In the image on the left one can see a narrow therapeutic window, with a notable increase in NTCP in the area where TCP is high. Conversely, on the right, one can see how the decrease in NTCP leads to a wider therapeutic window.

Adapted from El Naga et al.¹⁸

1.4 Linear-quadratic model, fractionation and biological effective dose

One of the tools to balance TCP and NTCP is the use of fractionation for the dose delivery. During the last twenty years, several models have been defined to take fractionation effect into consideration. The most accepted approach, which has become the standard method of calculation in radiotherapy departments, parts from the linear-quadratic (LQ) model. In this model it is assumed that the effect (E) of a single radiation dose (d) is given by 21:

$$E = \propto d + \beta d^2 \tag{2}$$

This linear-quadratic equation is considered to derive from a cell-survival relationship of the form

$$S = e^{\left(-\alpha d - \beta d^2\right)} \tag{3}$$

Where S is the surviving fraction. When we deliver a certain amount of total dose (D, where D=nd) in a determined number of fractions (n)

$$\frac{\mathrm{E}}{\alpha} = D\left(1 + \frac{d}{\alpha/\beta}\right) \tag{4}$$

Fowler²² suggested the term E/α to be called the Biological Effective Dose (BED), which is a measure of the effect, in dose units, for a given biological tissue.

With the BED definition in mind, the rationale underlying the fractionation can be stated as follows. Normal tissues and tumours respond differently to a change in dose fractionation, and they can be described in terms of a single parameter: the α/β ratio.^{20,21} Late-responding normal tissues show greater changes in sensitivity in response to a change in dose per fraction than early responding tissues, and this is consistent with a higher α/β ratio (Figure 4). The survival curves for target cells and late-responding normal tissues have systematic differences. Fowler^{22,23} expressed the view that because the uncertainties in α/β ratios are considerable and because the values for some tissues have not been shown to be different from those of others, for the time being, it is logical to assume standard values for α/β of 3 and 10 Gy for most early-responding and late-responding tissues, respectively.

1.5 Overall treatment time

A typical radiotherapy course lasting 5–7 weeks allows significant cell growth in both the tumor and healthy tissues. Early reactions occur in rapidly proliferating normal tissues, which can usually withstand radiation due to their ability to quickly repopulate over several weeks. However, if the treatment duration is reduced, there's less time for this repopulation, leading to more intense early reactions.⁷ Late reactions, on the other hand, involve cells that grow slowly, so changes in the overall treatment time do not impact them as much as early reactions⁷.

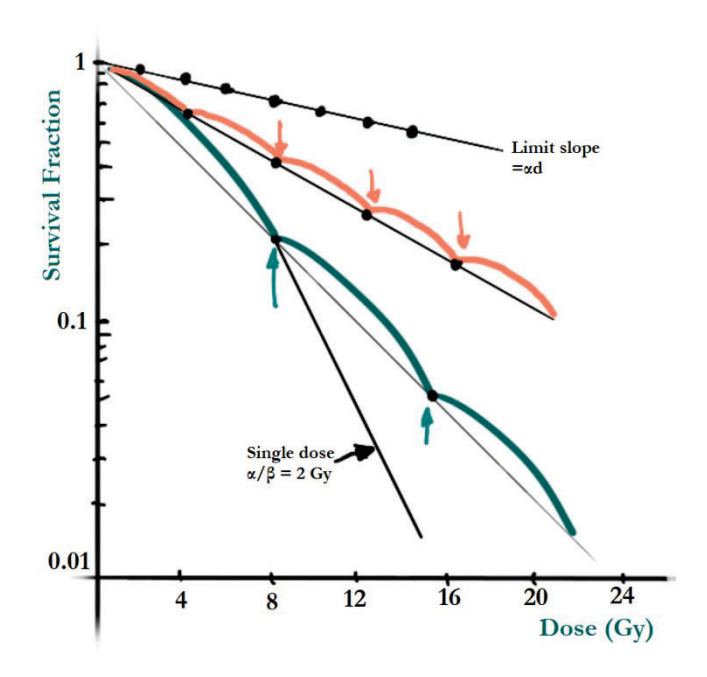


Figure 4. Effect of dose fractionation on cell survival fraction applying the linear quadratic model. Each fractionated dose represents a shoulder at the beginning of a single dose. We can see that the survival fraction increases for the same total dose because of fractionation, reaching a limit slope, at the value ad, where d is the dose per fraction. Adapted from Principles and Practice of Radiation Oncology.²⁴

Tumor cell repopulation rates can vary greatly. Despite the slow growth of most human tumors (with carcinoma volume doubling typically every three months), tumors can grow faster within a 5–7-week period. Damage and shrinkage in a tumor often trigger a rapid increase in repopulation, with doubling times sometimes less than a week.²⁵ Therefore, the overall treatment duration is crucial for tumor response. Delaying treatment by a week could significantly lower the chances of controlling the tumor. Conversely, shortening the treatment time, without reducing the total dose, might enhance local control chances.¹⁹ The existence of a lag period before repopulation starts, both in early-responding tissues and tumors, usually around 2–3 weeks must also be considered. This is particularly relevant for very short treatment courses.²⁶ Taking into consideration both lag time and repopulation, longer treatment times require higher total doses to be effective, with a calculated loss of 0.6 Gy per day due to repopulation (meaning a 2 Gy per session should be considered to have a biological effect of 1.4 Gy).²⁷

1.6 Fractionation schemes

The most direct reason why fractionation is routinely used in clinical radiotherapy is that it was empirically established. The early radiation oncologists began using single-dose treatments, but they soon realised that giving daily doses over a period of weeks also resulted in good

tumour control with less severe side effects. In retrospect, this must have occurred because the normal-tissue reactions that limit radiation therapy have a greater recovery or repair capacity than most tumors. ¹⁹ By the 1980s and 1990s, a consensus emerged that a daily dose of around 2 Gy was an optimal balance. This dose was found to be effective in controlling tumor growth while allowing healthy tissue to repair and tolerate the treatment. Over the years, the standard of 2 Gy per fraction has been defined as the standard in many radiotherapy protocols and it is referred to as normofractionation. ¹⁴

Some treatments, however, have proven to benefit from the use of a reduced number of fractions, or a larger dose per fraction. These schemes are referred to as hypofractionated schemes. A clear example of prioritizing larger fraction sizes against higher number of fractions is palliative radiotherapy where factors of cost and convenience may predominate over radiobiological principles.²⁸⁻³⁰ However, the use of large fraction sizes is on the increase, especially in stereotactive ablative radiotherapy (SABR) regimes. In these cases, a small target is treated with a high dose per fraction (larger than 6 Gy), delivering doses that are high enough to overcome the repair mechanisms of cancer cells, leading to increased cell death, thus high local control (LC) rates. This approach, where the whole treatment is usually delivered in one to eight fractions, also prevents or limits tumor repopulation from occurring during treatment. This strategy has been found effective in certain types of cancers, like lung cancer, where the treated volume is relatively small, and the risk of damage to surrounding tissues can be minimized. Numerous clinical studies have demonstrated the efficacy of SABR in various cancers, showing high rates of local control, especially in early-stage cancers.³¹ This work will be focused precisely on this context, where high doses per fraction are given over a short overall treatment time.³²

1.7 Adverse effects and CTCAE scale

We define the incidence of side effects as the probability of a certain adverse effect occurring. Just as the probability of LC increases with absorbed dose, so does the risk of adverse effects (Figure 3). Two types of effects are considered in terms of when they appear: early and late. For the latter, the follow-up time is also necessarily very long, while for early effects, a few weeks of observation, during and after radiotherapy, are enough to fully understand their incidence. ^{33,34} In

general, it can be said that the α/β value for the chronic response of healthy tissues is lower than for tumors and ranges between 1 and 6.

Thus, when we face the decision to administer certain dose levels to healthy tissue we define a range of accepted probability of harm as our tolerance level, since specific knowledge of a concrete adverse event for a specific patient is, for now, inaccessible. We say that tolerance refers to the probability of limit complications above which the treatment is not acceptable for a patient. For example, it is generally accepted that the tolerance for the maximum dose to the spinal cord is 50 Gy (given in a normofractionated scheme)³⁴ Which, in reality, means: if we irradiate the spinal cord of 2 Gy per fraction for 5 days a week up to 50 Gy, it is expected that in 5 out of every 100 of them, severe and irreversible neurological effects will occur in the long term; and this 5% seems in general, an acceptable risk compromise. To define these tolerance levels, it is necessary, first, to systematically register adverse effects related to the radiotherapy treatment.

The Common Terminology Criteria for Adverse Events (CTCAE)³⁵ is a descriptive terminology which can be utilized for Adverse Event (AE) reporting. A grading scale, accounting for the severity of the effect, is provided for each AE, defined as any unfavourable and unintended sign, symptom, or disease temporally associated with the use of a procedure.

Grade refers to the severity of the AE. The CTCAE displays grades 1 through 5 with specific clinical descriptions of severity for each AE based on this general guideline:

- Grade 1 (Mild): asymptomatic or mild symptoms which can be found by clinical or diagnostic observations only. For this AE intervention is not indicated.
- Grade 2 (Moderate): minimal, local or non-invasive intervention is indicated. Limiting
 age-appropriate instrumental activities of daily living (ADL). Where instrumental ADL
 refers to basic day to day activities such as preparing meals, shopping for groceries or
 clothes or using the telephone.
- Grade 3 (Severe or medically significant but not immediately life-threatening):
 hospitalization or prolongation of hospitalization is indicated. It is disabling and limits
 self-care ADL. Where self-care ADL refers to basic self-care activities such as bathing,
 dressing and undressing, self-feeding, using the toilet or taking medications.
- Grade 4 (Life-threatening consequences): Urgent intervention is indicated.
- Grade 5: for cases of death related to the AE.

Thus, when designing a radiotherapy treatment, it is not only relevant to seek the best LC rates, but also to minimize the risk of AE and their grade. In this thesis we will focus on optimizing SABR radiotherapy treatments with a focus on grade 1 toxicities on the lung while maintaining BED levels to ensure high LC rates.

2. Radiotherapy process

Radiotherapy treatment is a complex process (Figure 5) that needs to be adapted to the characteristics of each patient. This requires dividing the process into different phases from the decision to treat to the administration of the treatment.

After the diagnosis of the disease and its extent (achieved with a wide range of tests including biopsies, analyses and several and imaging techniques) the case is assessed, and the therapeutic approach is agreed upon, considering all available options. This is usually done by a multidisciplinary team including experts in various medical specialities. If treatment with ionizing radiation is decided, the radiotherapy process (which includes computed tomography (CT) simulation, target definition, dose prescription, treatment planning, treatment delivery and follow-up) starts.

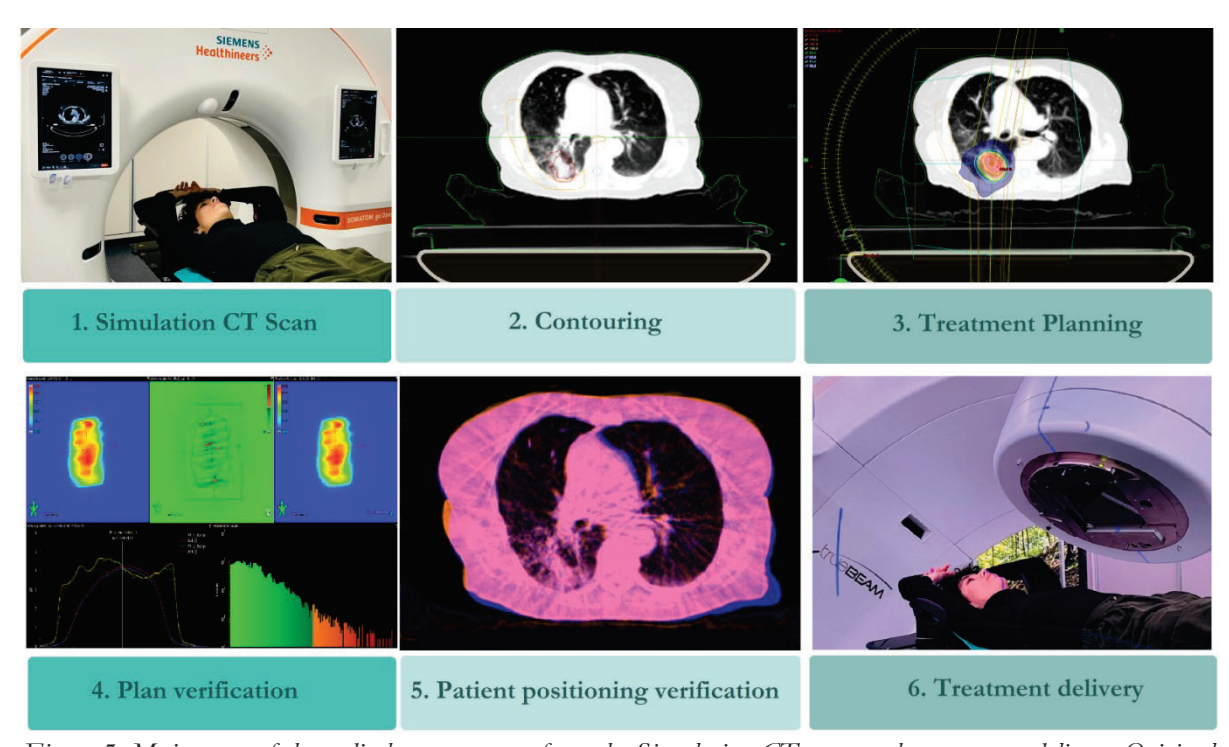


Figure 5. Main steps of the radiotherapy process from the Simulation CT scan to the treatment delivery. Original Figure from the doctoral student.

2.1 Radiotherapy types

The different types of radiotherapy are categorized by how radiation is delivered to the target area. We divide radiotherapy in two big groups:

- External radiotherapy. The radiation is produced outside the patient and directed towards the tumor.
- <u>Brachytharpy.</u> The radiation is emitted from inside the patient, in contact with or very
 close to the tumor. The radiation should be minimally penetrating to treat the area near
 the emission and irradiate the surrounding healthy tissues as little as possible.

This thesis focuses on external radiotherapy, which is the most widespread treatment modality.³⁶

2.2 Simulation process

Once external radiotherapy is decided as the treatment approach, images of the patient are acquired for treatment planning (Figure 5). The images must provide information about the shape, location, and movement of the tumor and the organs at risk (OAR) surrounding it. This image must also allow the characterization of the materials that the radiation will encounter to calculate the distribution of absorbed dose.³⁷ Furthermore, images must be acquired in the position in which the patient will be treated so that the subsequent planning is as representative as possible of the treatment situation. To achieve this a series of immobilization devices are used such as wing boards or arm supports, abdominal compression devices or vacuum bags.

CT images are usually used as they are obtained with ionizing radiation and represent a map of its attenuation in the patient, which allows establishing more easily the relationship between the grey level and the composition parameters necessary for dose calculations. This grey level is determined by the linear coefficient of attenuation of the material contained in that voxel. When breathing induced organ movement is present the most common imaging technique is the use of a four-dimensional CT (4DCT). A 4DCT is an advanced imaging technique that captures a series of CT images over different phases of a patient's breathing cycle. This method integrates the element of time (the fourth dimension) with the traditional three spatial dimensions in CT imaging, allowing for a dynamic representation of the tumor and surrounding anatomy as they move during breathing.³⁸

In some cases, supplementary images such as positron emission tomography or magnetic resonance can be used to accurately define the tumor or the surrounding OAR.

Finally, it is necessary to link the spatial coordinates of the patient with those of the accelerator so that the treatment is administered where it should be. The most common way is to use external marks or tattoos indicating the coordinate axes, although there are also other systems that use infrared marks or the three-dimensional surface of the patient.¹⁴

2.3 Target delineation

Once the images are acquired, the radiation oncologist delineates the treatment volumes and OAR. This can be done manually by contouring slice by slice or with the help of automatic segmentation tools.³⁸

Regarding target volumes, the consensus of the International Commission on Radiation Units (ICRU) establishes three main types of volume to contour.³⁹ The first is the gross tumor volume (GTV), which corresponds to the macroscopic tumor. The second is the clinical target volume (CTV), corresponding to the volume where subclinical disease may be present. If there is macroscopic tumor present, the CTV encompasses the GTV to consider the possible spread of tumor cells. Therefore, the clinical goal is to irradiate the CTV with the prescribed dose in all treatment sessions. To guarantee this, all geometrical uncertainties of the process must be considered: variability of volumes depending on who delineates them, variations in patient positioning between planning and different treatment sessions, etc. In this context, the third volume, the planning target volume (PTV), is defined, encompassing these uncertainties in an additional margin applied to the CTV. In this way, if planning is done on the PTV, it ensures that the CTV will receive the prescribed treatment (Figure 6).

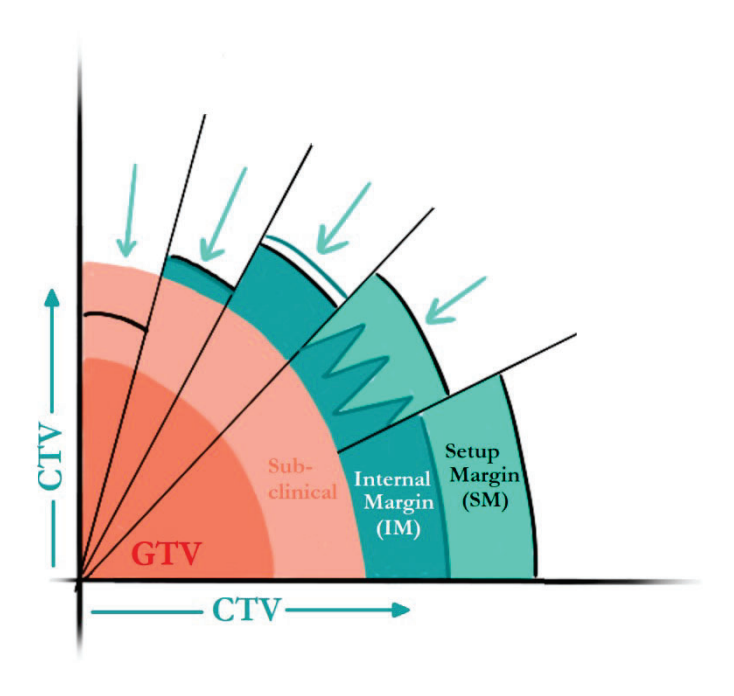


Figure 6. Volume definition according to ICRU guidelines. GTV represents the visible tumor (when present). From there, several margins are accounted for depending on the characteristics of the tumor and the proximity to organs at risk. The arrow represents the influence or the OAR on the delineation of the PTV. Adapted from ICRU Report 83.³⁹

In cases where motion of the target volume is expected to happen during treatment, the use of an internal target volume (ITV) is recommended. This volume can be defined in several ways. One example is adquiring the simulation CT scan in two extreme situations (i.e. full bladder and empty bladder) and considering that the motion expected during the treatment will fall within the limits established between the two extreme cases.

The generation of the ITV using a 4DCT is a critical process in radiotherapy planning, especially for tumors that are affected by respiratory motion. With the use of the 4DCT information the GTV/CTV position can be defined in all phases of the breathing cycle, and they can be accumulated to generate the corresponding ITV. This ITV is frequently generated in the average reconstruction of the 4DCT (Figure 7), which is then used for dose calculation. In this reconstruction, the multiple phases of the 4DCT scan, are averaged to create a single, composite image. This averaged image is a more representative depiction of the tumor and surrounding anatomy over the entire respiratory cycle. The rationale behind using the average reconstruction for dose calculation lies in its ability to provide a more stable and consistent representation of the target volume and adjacent normal tissues.

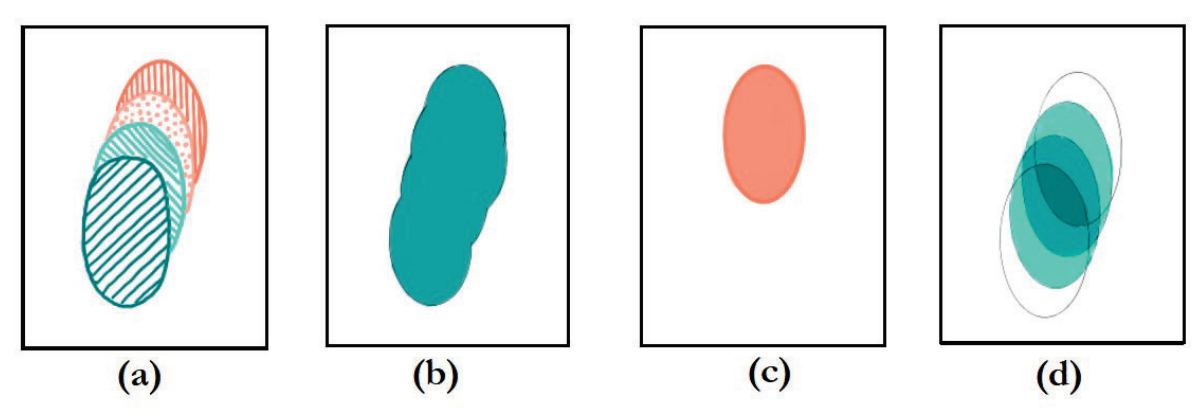


Figure 7. Different approaches for the generation of the ITV volume, to account for breathing morion during the treatment's delivery. (a) ITV encompassing all the phases of a 4DCT scan. (b) Maximum intensity projection approach (c) Gating on the most stable phases of the breathing cycle (d) Average reconstruction of the 4DCT.

Adapted from Shuxu.⁴⁰

There are several strategies to compensate for breathing tumor motion:

- ITV approach: accounts for tumor motion due to breathing by expanding the target area to encompass the entire range of tumor movement. Instead of delivering radiation to a fixed position, ITV considers both the tumor's average position and its potential displacement during respiration.
- Gating: This method involves synchronizing the radiation beam with the patient's
 breathing cycle, delivering radiation only during specific phases of respiration (for
 example, the exhalation phase). By monitoring the respiratory signals through external
 markers or internal fiducials, the radiation can be precisely timed to target the tumor when
 it is in a predefined position.
- Tracking: Tracking involves the real-time monitoring of tumor movement and adjusting
 the radiation beam accordingly during treatment. Unlike gating, which delivers radiation at
 specific times, tracking continuously follows the tumor motion, allowing for dynamic
 adaptation of the beam.
- Active breath control strategies (such as deep inspiration breath hold): is a pool of techniques where patients are instructed to voluntarily control their breathing, for example, taking a deep breath and holding it during radiation delivery. This approach needs the capacity of the patient to actively collaborate and usually focuses in using the breath hold either to push nearby OAR away or to achieve a very stable respiratory phase.

Although gating or tracking approaches permit smaller target volumes, they come at the cost of an increased treatment time and complexity. Active breath control strategies are only possible

for very fit or previously trained patients, capable of holding their breathing for prolonged periods of time. These factors make the ITV approach the most widespread breathing motion compensation technique, specially in the lung and for upper lobe tumors, as the movement for these cases tends to be smaller. In this work the analyzed patients have been treated using this approach but, nevertheless, as gating and tracking techniques are becoming more frequent, they have also been considered in this work.

2.4 Treatment planning

Once the PTV and the OAR are defined and the dose is prescribed, dosimetry technicians and medical physicists design the treatment plan using a treatment planning system (TPS). The TPS is a computer program that has access to the simulation CT images and the delineated volumes. The TPS also contains the necessary data to characterize the accelerator that will perform the treatment and incorporates dose calculation algorithms where the radiation beams to be used have been modelled.⁴¹ The program allows the creation of a radiotherapy plan which contains the configuration of the beams as needed to deliver an optimal treatment and an estimate of the absorbed dose distribution in the patient.

Different particles, techniques and optimization strategies can be used to deliver a radiotherapy treatment. In this thesis we will mainly focus on the delivery of radiotherapy using high energy photons with volumetric modulated arc therapy (VMAT) technique and inverse optimization process, all described in the following points.

2.4.1 Particles and energy used

The types of radiation used in radiotherapy are diverse. The most widespread ones are photons, electrons, and protons. Each of these particles has specific characteristics regarding how the dose is distributed in space as they penetrate the patient (Figure 8), and this characteristic shape allows them to be used in different scenarios.^{39,42} In general, changing the energy alters the penetration depth of the beam but does not modify the characteristic shape of the dose distribution in the other directions.

• <u>Electrons</u> concentrate the dose near the entry point, and they have a specific maximum range, which depends on their energy. They are mainly used in superficial treatments close to the skin.⁴³

- Low energy photons (kV) distribute the dose along their entire path, with the maximum in the entrance point and then decreasing smoothly. Photons of lower energies are mainly used to treat superficial lesions.⁴²
- <u>High energy photons (MV)</u> also distribute the dose along their entire path, but the dose reaches its maximum a few centimetres after entering the patient and then decreases smoothly as the beam loses energy. Increasing the energy increases the distance to the maximum dose and slows the subsequent dose drop. This dose distribution allows treating tumors at a wide range of depths while sparing the skin.³⁹
- Protons concentrate the dose deposition at a specific depth that depends on their energy and the material of the medium. Below this depth the dose deposition drops suddenly and can be considered negligible. The dose is lower and smoothly increases before reaching this point. By modulating the energy of the beam, the treatment of deep tumours reducing entrance and exit doses is achieved, but this dose distribution is less robust against anatomical or density changes.⁴⁴ Their use is more limited because the treatment units and dedicated centres are considerably more costly, although the number of facilities and indications is expanding.

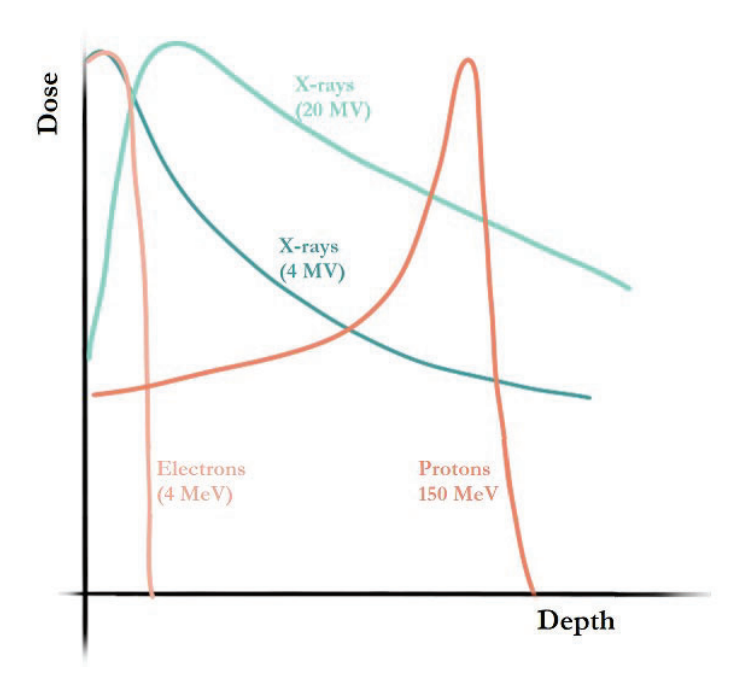


Figure 8. Depth dose distribution in water for high (MV) and low (kV) energy photons, electrons and protons.

All the depth dose profiles are normalized at their dose maximum. Original figure from the doctoral student.

Other particles, such as carbon ions, are also being used; however, their use remains limited to a small number of facilities worldwide and is primarily restricted to clinical trials.

2.4.2 Delivery technique

Treatment techniques are conditioned by the characteristics of the dose distribution. For MV photons, the dose is distributed from the entry to the exit of the patient as shown in the previous section (Figure 8), with higher values near the entry that gradually decrease until the exit. Consequently, doses can be significant before reaching the tumor, at the tumor itself, and in the tissues behind it.⁴⁵ The solution to improve the conformation of the dose to the target volume and reduce it in the rest of the tissues involves adding beams with other incidences that avoid overlaps and/or the most sensitive organs. In this way, all the beams contribute to accumulating damage to the tumor while distributing the dose to the healthy tissues and reducing the risk of side effects.

The number of beams and their configuration can be made following different considerations, giving rise to different treatment techniques (Figure 9).

- <u>Three-Dimensional Conformal Radiotherapy</u> (3DCRT): beams with static incidences are used. The intensity of the beam is not modulated using secondary collimator mechanisms and is usually flat or has a wedge shape.⁴²
- <u>Intensity-Modulated Radiotherapy</u> (IMRT) is refinement of 3DCRT in which different levels of radiation intensity can be defined in different parts of the beam. This can be achieved using the terciary collimator system either with discrete steps (step & shoot) or continuously (sliding window). This modulation of intensity allows for better conformation of the dose to the target volume.³⁹
- <u>Volumetric Modulated Arc Therapy</u> in which the number of beams and incidences increases to have a continuous arc of irradiation around the patient. Several arcs can be used in the same plans, providing more degrees of freedom. VMAT further conforms to the target volume while usually achieving a reduction in treatment time compared to IMRT.⁴⁶ A simpler approach to VMAT is called dynamic conformal arc (DCA) where the radiation is also delivered using arcs, but there is no active modulation from the terciary collimation system and its only function is to follow the outline of the PTV for each projection.

The selection of a radiotherapy delivery technique is dependent upon several of factors including the prescribed dose, the complexity of the case, equipment availability, and specific patient needs.

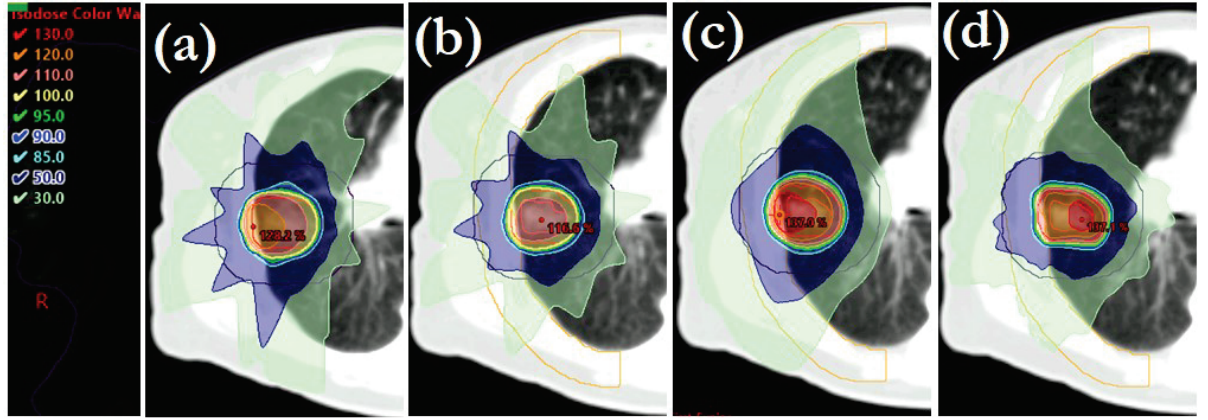


Figure 9. Dose distribution of the same plan using 3DCRT (a), IMRT(b), DCA(c) and VMAT(d) techniques. As can be seen conformity of the 50% isodose line (dark blue) improves with the complexity of the delivery technique. The Blue contour represents the volume 2cm away from the edge of the PTV (in red). The orange volume is the Chest Wall contour. Original figure from the doctoral student.

2.4.3 Treatment plan optimization

The purpose of the optimization process is to obtain the best possible treatment plan. The focus is on achieving the best dose distribution to treat the PTV while maintaining doses to OAR as low as possible. It is usually an iterative trial-and-error process where the variables are adjusted until the optimal solution is found and the objectives and restrictions are met.

The various parameters that need to be fine-tuned include the quantity and incident angles of the beams, their energies, shapes, varying intensity levels at specific points, relative contributions of each field (weights), dose rates, and, if relevant, the speeds of rotation. Diverse combinations of these factors are possible, and these approaches are generally categorized into two main groups: direct planning and inverse planning.⁴⁷

Direct planning is a manual process where the person performing the planning configures the plan, calculates it, and evaluates the degree of compliance with the objectives and restrictions. If the result is not acceptable or they believe there is room for improvement, they modify some

aspects of the plan, calculate it, check if the result improves or worsens, and repeat the process until the final plan is reached.

As the number of degrees of freedom increases the direct approach is no longer feasible. In this context, inverse planning is introduced, which automates the entire process and inverts it, as it starts from the objectives and restrictions for the system to return the optimized plan. To do so, the program iteratively minimizes its internal cost function to provide a plan as close as possible to the objectives and restrictions provided.

One of the problems associated with optimization (both direct and inverse) is the impossibility to know for sure whether there is a better plan than the one obtained. This is an inherent fact of the process since, mathematically, it is a non-convex problem where the total number of solutions, and their relationship cannot be determined a priori to discern if the minimum of the cost function is global or local.⁴⁸

2.4.4 Fluence

Dose fluence in IMRT and VMAT is a critical concept that refers to the distribution and intensity of radiation delivered to a target area. It represents the amount of radiation energy delivered per unit area and is a key factor in achieving high precision in the treatment. The optimization process tunes the fluence to achieve an optimal dose distribution, once calculated in the anatomy of the patient.

However, the intricate modulation of dose fluence also introduces certain challenges, especially in terms of treatment robustness. Robustness in radiotherapy refers to the ability of the treatment plan to remain effective and safe under different scenarios, such as patient setup errors, breathing motion or anatomical changes. The highly tailored nature of IMRT and VMAT can sometimes lead to less robust plans. For instance, small misalignments or changes in patient anatomy can lead to significant deviations from the intended dose distribution.

A specific example of this challenge is the need to remove the first millimetres of skin from the PTV when doing inverse optimization. If the skin is not removed the system will increases fluence to ensure coverage of the PTV near the skin compensating for the loss of electronic equilibrium. However, this increase in fluence would lead to unacceptable hotspots in case of slight misalignments. Another example is observed in the treatment of thoracic tumors, where the lungs' presence introduces heterogeneity.⁴⁹ The lungs, being less dense than surrounding tissues, can disrupt the lateral equilibrium of the radiation beams, leading to fluence peaks in the

area between the CTV and PTV. These peaks are areas where the radiation dose is unintentionally higher due to the beams' altered path through the different densities. This phenomenon requires careful planning and modulation to ensure the intended dose is delivered to the tumour while protecting the lung tissue.^{50,51}

The use of robust optimization, which considers different patient setup errors in the optimisation process and fluence generation, can solve these problems, but it is not yet available in most commercial TPS.⁵¹

2.4.5 Dose calculation

As mentioned in previous chapters, the information contained in the simulation CT scan, and the model of the treatment machine and beam characteristics are used by the TPS determine the dose absorbed in the patient. The uncertainties associated with the determination of the dose administered to the patient must be as low as possible to ensure that patients are treated with the intended dose.

Based on this, the ICRU³⁹ determines that the total uncertainty in the dose, including planning and administration of the treatment, should not exceed 5%, and that uncertainties associated with the dose calculation algorithm should be within 2-3% of the prescribed dose. This value is consistent with the recommendations of other organizations, such as the 2-3% requirement for TPSs in the International Atomic Energy Agency's (IAEA) TRS-430 document,⁵² or the 1-2% goal for dose calculations in heterogeneities of the Task Group 65 of the American Association of Physicists in Medicine (AAPM).⁵³

The uncertainty associated with the dose calculation algorithm will depend on the used algorithm and its limitations to account for the variables present in dose transport and deposition.

2.4.5.1 Dose calculation algorithms

The calculation algorithms estimate the dose distribution in the patient for a given treatment plan. To do this, they must characterize the beams used, the tissues and materials that the radiation will encounter, and combine it all to predict both the radiation transport (attenuation and scattering) and the energy deposition within the patient.

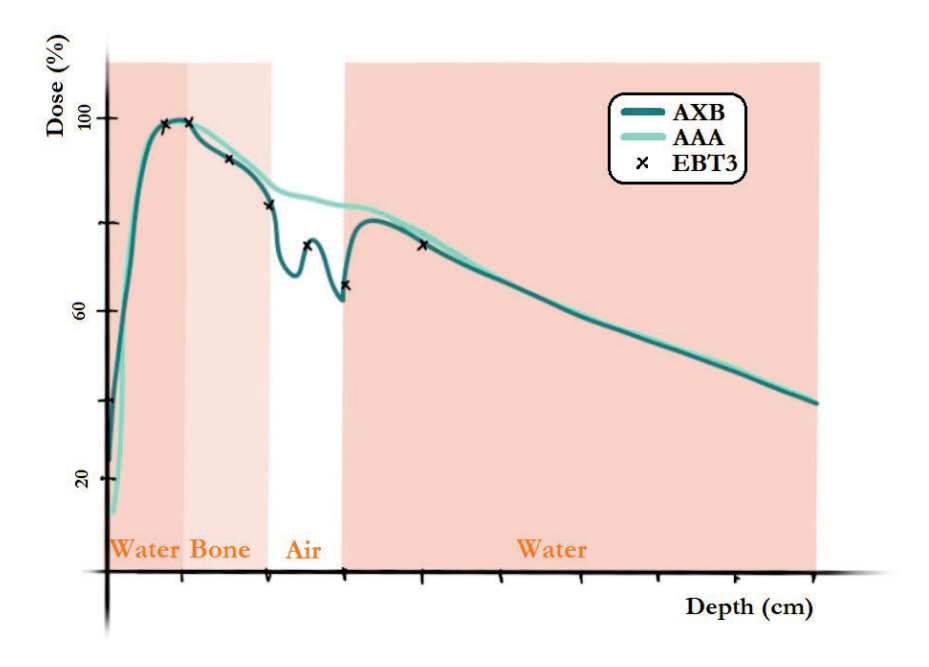
Photons emitted by the accelerator interact through different mechanisms with the matter they encounter, whether it is the patient, the accelerator head itself, or other elements like the table, immobilizers, etc. The algorithm must consider all these processes and components and, at the same time, must be efficient at calculating the dose in several minutes, so treatment planning is possible. Calculation algorithms have constantly evolved over time, becoming increasingly complex while maintaining clinically acceptable calculation times. They are divided into Type A, B or C, in increasing order of complexity.^{42,54}

- Type A: these are the simplest dose calculation algorithms, often referred to as correction-based algorithms. They include techniques like the Clarkson method or the Batho power law correction as well as the Equivalent Tissue-Air Ratio (ETAR) method. Type A algorithms assume a homogeneous medium and apply correction factors for heterogeneities. They generally use empirical or semi-empirical methods and are based on measurements in water phantoms. These type of algorithms don't take into consideration electron transport in the medium. The primary limitation of Type A algorithms is their oversimplification of tissue heterogeneity. They are not accurate in areas where there are significant changes in tissue density, such as at air-tissue or bone-tissue interfaces. This can lead to inaccurate dose calculations in thoracic, head and neck, or pelvic regions. It is no longer recommended to use these algorithms in external beam radiotherapy as they could lead to uncertainties over 3% in most clinical scenarios.
- Type B: These algorithms, also known as "model-based" algorithms, are more advanced than Type A. Examples include the Pencil Beam Convolution (PBC) method or the Collapsed Cone Convolution (CCC) algorithms. Type B algorithms incorporate more sophisticated models of radiation transport and scatter. They consider heterogeneities to a greater extent than Type A algorithms but still use some simplifications in the calculation process. While more accurate than Type A, Type B algorithms can still struggle with complex geometries and very heterogeneous areas. They might not be entirely accurate in scenarios like small fields or areas with rapidly changing densities but fall into the acceptable uncertainty range for most external radiotherapy applications. The Anisotropic Analytical Algorithm (AAA) is a commercial solution that falls within this category.
- <u>Type C:</u> These are the most advanced and computationally intensive algorithms that model the interations of individual particles, such as Monte Carlo simulations or algorithms that deterministically solve the linear Boltzman transport equation (LBTE) by modelling photon transport. Type C algorithms use few (if any), simplifications. Monte Carlo simulations, for instance, simulate the physical interactions of individual photons

and electrons with matter, providing a very detailed dose calculation. The main limitation of Type C algorithms is their computational intensity although advances in computing have partially mitigated this issue, and they have started to be routinely implemented in the clinical practice.

The use of different calculation algorithms leads to differences in the determination of the expected dose distribution (Figure 10) and they can lead to different clinical decisions. This fact is even more relevant when different densities or compositions of the medium (heterogeneities) are present. These heterogeneities affect the interactions that photons will have and the generation of charged particles, altering their transport, energy transfer, and ultimately modifying the dose distribution (Figure 10). In the context of lung lesions, for example, the use of type B algorithms may lead to an overestimate of dose in the less dense area surrounding the lesion due to the lack of lateral electronic equilibrium compared to a type A algorithm.

The information about the medium is usually obtained from the planning CT image, relating the Gray level of different points with the characteristics required by the algorithm in question. These characteristics can also be manually specified in the TPS for the volume desired and are recorded in the digital imaging and communications in medicine (DICOM) structure object.



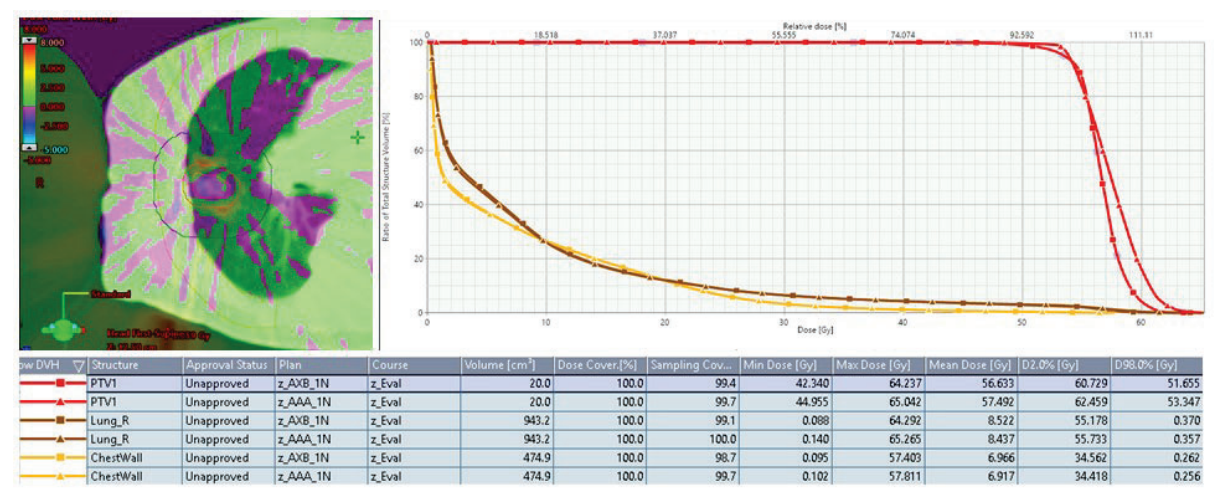


Figure 10. Dose calculation differences between algorithms such as AAA and AXB. In the top figure we can see a simplified example with the depth dose profile in a heterogeneous tissue composed of water, bone and air. Bottom figures show the differences observed in a clinical case. Differences are more prominent in the region surrounding the lesion in the lung which translate in a higher calculated dose for the PTV in the case calculated with AAA (line with triangles). Dose volume histogram (DVH) of the plans recalculated with fixed Monitor Units and dose values for the PTV (red), Chest Wall(orange) and Right Lung(brown) are provided for each calculation algorithm.

Original figure from the doctoral student.

In this thesis we will focus in two dose calculation algorithms. First AAA is a simpler convolution/superposition type algorithm that used a point type kernel implemented in the Eclipse TPS by Varian Medical Systems (Palo Alto, CA, USA) that scales the kernel in depth and in 16 lateral directions at different depths to consider heterogeneities.⁵⁵ The distributions obtained with these algorithms meet accuracy requirements in water-like tissues but may not do so if there are heterogeneities. Secondly, we will be using Acuros XB (AXB), which is a type C, LBTE-algorithm.

2.4.5.2 Dose normalization and reporting

Dose normalization in radiotherapy is a critical process that involves rescaling the calculated dose distribution to ensure the PTV receives a dose according to the prescribed dose. In most of the cases the aim is to achieve a homogeneous dose distribution within the PTV.

The ICRU³⁹ recommends that at least 95% of the PTV should receive a dose equal to or greater than 95% of the prescribed dose. This ensures adequate coverage of the target while allowing for some unavoidable variations. The maximum dose within the PTV should generally not exceed 107% of the prescribed dose. This limit helps to control the extent of hot spots

within the target area. While some level of dose inhomogeneity can be acceptable, the ICRU guidelines suggest that these areas should not exceed 110% of the prescribed dose, particularly in areas adjacent to OARs.

SABR involves delivering high-dose radiation in fewer fractions, targeting very precise locations, often near critical structures. The relationship between prescription and normalization in SABR can be more complex.

In SABR, the prescription dose might be defined to a specific isodose⁵⁶ line that encompasses the PTV. For example, the prescription could be to deliver a dose such that 95% of the PTV receives 100% of the prescribed dose. Furthermore, to achieve steep dose gradients higher maximum doses are allowed within the PTV, reaching values as high as 140% of the prescribed dose.

2.4.6 Plan evaluation

The evaluation of the quality of the treatment plan usually focuses on its theoretical dose distribution, but other factors that may cause this distribution to differ from the one finally delivered to the patient must also be considered. Among these factors are uncertainties in dose calculation, the machine's capability to irradiate the plan, and the effect of differences in the patient's positioning and anatomy compared to the planning. All these aspects are considered in the evaluation of the dose distribution, robustness, and complexity of the plan to have a broad view of its quality.

2.4.6.1 DVH

The three-dimensional distribution is visually evaluated slice by slice qualitatively. Quantitative evaluation is done using dose-volume histograms (DVH) that collect the number of voxels within a certain volume with a certain dose value. Visual inspection of DVHs can lead to identification of clinically important characteristics of an absorbed-dose distribution, such as the presence (but not the location) of regions of high or low absorbed dose, which are often difficult to assess rapidly and consistently from conventional isodose or color-wash presentations. Cumulative DVHs are histograms of the volume elements that receive at least a given absorbed dose, and they are usually expressed as either the absolute volume or the volume relative to the

total structure volume, receiving at least a given absorbed dose, D. Each point on the line of a relative cumulative DVH is described by the following:

$$DVH(D) = 1 - \frac{1}{V} \int_{0}^{D_{max}} \frac{dV(D)}{dD} dD$$
 (5)

Where V is volume of the structure and Dmax the maximum dose in the structure, and the differential DVH is defined by dV(D)/dD, which is the increment of volume per absorbed dose.

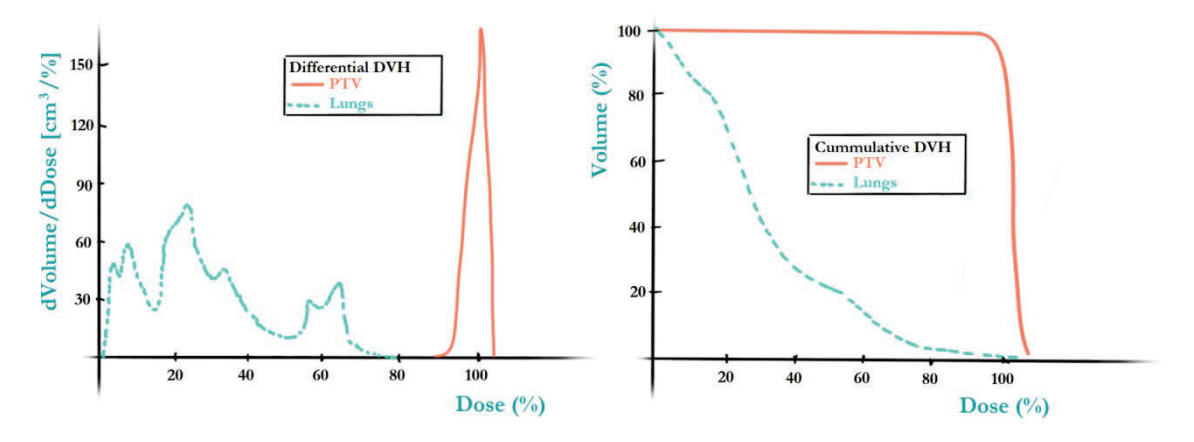


Figure 11. Differential (left) and cumulative (right) Dose Volume Histogram of the same radiotherapy plan. Two structures can be seen as an example, in orange the PTV for which the ideal scenario would be a step function in the cumulative histogram with the step at 100% of the prescribed dose. For the OAR, in this case the lungs, represented in blue, the ideal (but impossible) scenario would be to have no dose at any point of the structure.

Original figure from doctoral student.

An absolute cumulative DVH can be obtained from a relative cumulative DVH by multiplying by the volume of the structure.

2.4.6.2 OAR dose tolerances

As mentioned earlier, for the various effects that may occur and to develop appropriate treatment plans, it is important to determine tolerance doses.⁵⁷ Generally, the volume of irradiated tissue is crucial for the possibility of adverse effects to ocure, thus tolerance levels are specified as points in a DVH.⁵⁸ These DVH points are defined either with specific values as mean dose, maximum or minimum dose or by defining:

• <u>Maximum doses at a specific volume.</u> The nomenclature to define these points in the DVH is $D_{x(cm3)} < y(Gy)$ where x is the maximum volume to recieve y dose. Units can be either absolute or relative. For example, $D_{0.1cm3} < 50$ Gy for the spinal cord would translate into a maximum of 0.1cm³ of the OAR receiving 50 Gy or more.

• Maximum volumes at a specific dose. The nomenclature to define these points in the DVH is $V_{x(Gy)} < y(cm^3)$ where x is the maximum dose received by a certain volume, where units can be either absolute or relative For example, $V_{20Gy} < 20\%$ for the lung would translate into a maximum of 20% of the healthy lung to receive doses of 20 Gy or higher.

QUANTEC is an initiative that provides guidelines on the tolerance of normal tissues to radiation. It compiles and reviews data from published clinical trials, research studies, and radiobiological models to establish dose-volume constraints for various organs. Its goal is to prevent or reduce the risk of radiation-induced side effects and complications. It provides evidence-based, organ-specific dose limits that are used in treatment planning. This ensures that the guidelines reflect the latest understanding of radiation tolerance.

2.4.6.3 Complexity and robustness

Plans are usually evaluated under a static univariable scenario, but many minor changes can occur during the delivery of the treatment. It is crucial to evaluate the robustness of the treatment plan against this expected minor changes, to be sure that the dose to the PTV and OAR remain acceptable.⁵⁹

On one hand, we evaluate robustness by evaluating the impact on the dose distribution of different treatment scenarios compared to the nominal planning scenario. In MV photons, relevant scenarios are mainly due to geometrical uncertainties and to positioning errors. Although these uncertainties are partially considered in the PTV on which planning is based, there can be situations with unacceptable changes in doses to the GTV/CTV. It is advisable, therefore, to evaluate the robustness of the plan by simulating the different scenarios that may occur and studying their effect on the dose distribution.

On the other hand, plan complexity provides information on how the plan produces the dose distribution. It allows estimating whether the TPS is working under conditions where the calculation algorithm is reliable (large and regular openings, low level of conformation, etc.) and the degree of difficulty the accelerator will have in irradiating the plan accurately (speeds and accelerations of moving elements, demand for synchronizations between parameters, etc.). Different parameters and indices defined in the literature allow quantifying these aspects.

All these aspects of the plan quality must be considered in the planning process to obtain a plan with a good dose distribution, robust in all scenarios, and as simple as possible. In the case of inverse planning, this involves incorporating them into the cost function to reach the desired balance. Some TPS implement penalties for complexity. Regarding robustness, there is only one commercial system that does robust optimization on the GTV/CTV for MV photons (the PTV is not necessary in this context), unlike treatments with protons where robust optimization is the norm given their higher sensitivity to uncertainties.

3. Lung lesions

3.1. Lung cancer

Lung cancer is the most common and lethal type of cancer worldwide, accounting for 13% of cancer incidence and more than 19% of cancer-related deaths. In Spain, although the incidence is slightly lower (10%), it still accounts for 20% of all cancer-related deaths—which translates to more than 22.000 deaths per year. ⁶²

This type of cancer is a major global health burden, representing the leading cause of cancer-related mortality worldwide. According to the World Health Organization (WHO),⁶¹ lung cancer accounted for approximately 2.21 million new cases and 1.8 million deaths globally in 2020. The high mortality rate of lung cancer underscores the need to improve treatment strategies and the importance of early detection through screening.

According to the available evidence, about 75% of these lung cancer patients will receive radiation therapy (RT) at least once during their illness. Of these patients, approximately 20%—those with early-stage (T1-2N0) inoperable disease—will receive SABR. This number, however, will most likely increase in the coming years with the implementation of screening programs. While surgery is the standard treatment for medically fit early-stage non-small-cell lung cancer (NSCLC) patients, SABR has become a recommended treatment alternative for those patients who, because of co-morbidities and/or poor pulmonary function, are medically inoperable or refuse surgery as a treatment option.

3.2 Lung metastases

Lung metastases are common in patients with advanced stages of various primary tumors. It is estimated that up to 30-55% of patients with metastatic cancer will develop lung metastases

during their disease.⁶⁵ This wide range is attributable to the variability in metastatic potential across different cancer types. Metastatic stage was considered a systemic process and systemic therapy remains the treatment of choice. However, for patients with low metastatic burden, referred to as oligometastatic (OM) disease, SABR and Radiofrequency ablation have proven promising results in terms of efficacy in several randomized trials.⁶⁶⁻⁶⁹

The term OM first appeared in 1995 and defines a state between localized and widely disseminated disease.⁷⁰ Within OM we distinguish, for example: de novo OM disease where both primary and metastatic lesions are detected simultaneously in a patient without prior oncological treatment, oligorecurrence where new limited metastases appear after primary tumor has been locally controlled or oligoprogression where limited metastases occur during the systemic treatment.⁷¹

3.3 Lung screening and lung lesions follow-up

Screening for lung cancer is primarily targeted at high-risk populations, such as heavy smokers and those with a significant history of tobacco use. The primary imaging modality used for lung cancer screening is low dose CT, which has been shown to improve lung cancer treatment by detecting lesions in an earlier stage.⁷² Other techniques, such as positron emission tomography (PET) combined with CT, offer information about the metabolic activity of lesions and aiding in the selection of candidates for treatments like SABR.⁷³

Implementing lung cancer screening is challenging as it represents a significant increase in both human resources and equipment. Nevertheless, it is becoming a more common practice within health system services, and it is expected to increase lung cancer diagnosis at early stages and, by consequence SABR treatments, in the following years.^{74,75}

3.3.1. Diagnostic through imaging

Imaging studies play a pivotal role in the detection and characterization of lung lesions. The following imaging modalities are commonly used (Figure 12):

- <u>Chest Radiography</u> is often the initial imaging test, but it has limited sensitivity for detecting small lesions or distinguishing benign from malignant processes.
- <u>CT scans (usually including the use of contrast agents)</u> provide detailed images of the lung, allowing for the detection of smaller lesions, assessment of the lesion's

- characteristics (e.g., size, shape, borders), and evaluation of lymph node involvement and distant metastases.^{76,77}
- <u>PET</u> scan is often combined with CT (PET/CT), this modality helps in assessing metabolic activity of the lesions, aiding in distinguishing between malignant and benign processes, and detecting metastatic disease.⁷⁸

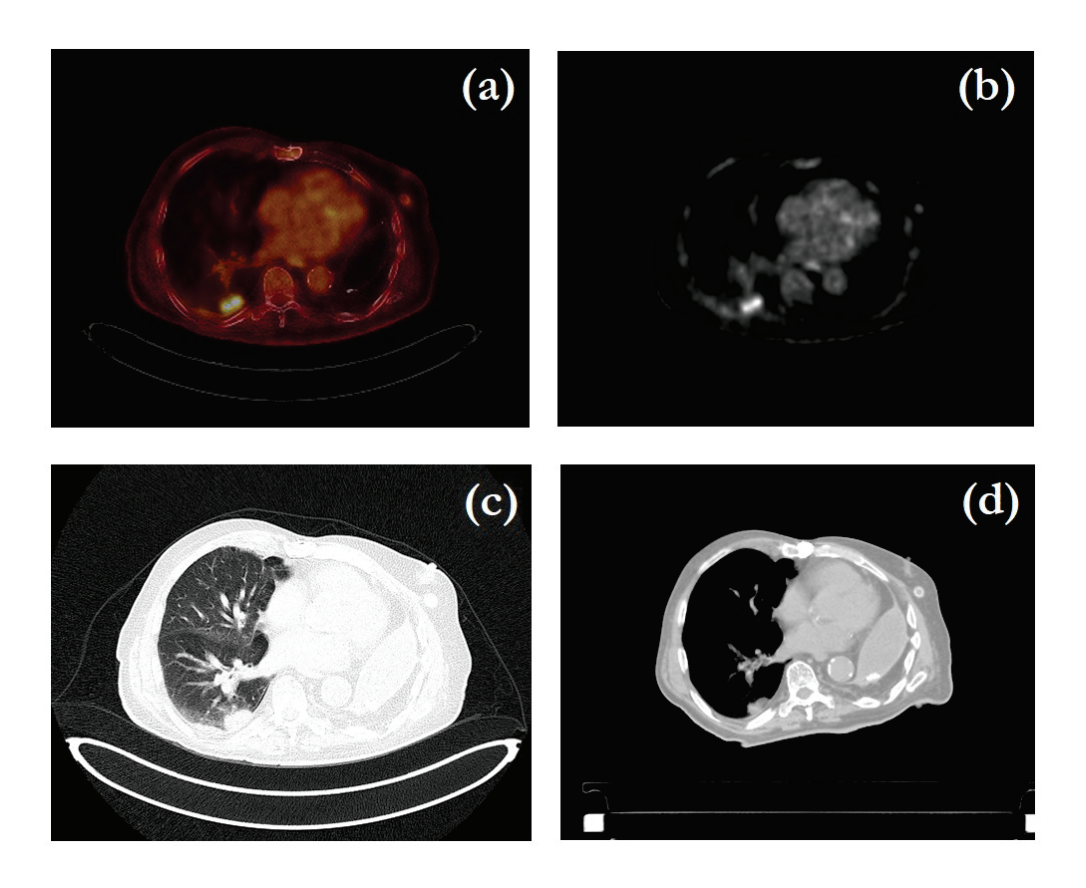


Figure 12. Example of PET-CT and simulation CT scan in a patient with a lung metastasis close to the chest wall. (a) Anatomically registered PET/CT. The red and yellow color wash indicates the PET-based captation (b) FDG-PET-scan. (c) Axial slice of the contrast enhanced planning CT. (d) Axial slice of the planning CT scan of the same anatomical area. Original figure from the doctoral student.

3.3.2. Malignancy signs in imaging

As stated before, CT scans of the chest provide are essential for the evaluation of pulmonary nodules.⁷⁹ CT can better characterize the size, shape, margins, and internal composition of lung lesions, as well as their relationship to surrounding structures. Some characteristics of lung nodules are suggestive of malignancy, these signs include (Figure 13):

- <u>Size and Growth:</u> Larger nodules (generally >8mm in diameter) and those showing growth over time are more suspicious for malignancy.⁸⁰
- <u>Borders:</u> Irregular, spiculated, or lobulated margins are more commonly associated with malignant tumors.⁷⁹
- Density: partially solid nodules are more likely to be malignant than purely solid nodules.
 Most persistent Ground Glass Opacities (GGO) are associated with malignancy, although GGO can also represent early-stage adenocarcinomas or minimally invasive adenocarcinomas.^{81,82}
- <u>Cavitation</u>: Lesions with thick-walled cavitation are suggestive of squamous cell carcinoma.⁸³
- <u>Calcification</u>: The pattern of calcification gives information about the nodule. Usually it is considered a sign of beningnity. Nevertheless, eccentric calcification might indicate malignancy, whereas central, laminar, or "popcorn" calcifications are often seen in benign lesions.⁸⁰



Figure 13. Display of common malignant signs: (A) pleura traction sign (black arrow); (B) spicule sign (white arrow); (C) lobulation sign; (D) bronchial cutoff sign; (E) air bronchogram sign (black arrow); (F) tumor vasculature sign; (G) vacuole Sign (black arrow); (H) cavity sign (white arrow). Figure by Duan et al. 84

3.3.3 Natural evolution and GGO cases

GGO in the lung refer to areas that appear hazy on a CT scan, indicating partial filling of air spaces, interstitial thickening, partial collapse of airways, or increased capillary blood volume in the lungs. Unlike solid nodules, GGOs allow for the visualization of underlying bronchial structures and pulmonary vessels due to their semi-transparent appearance. The natural evolution of persistent GGO nodules can be variable, ranging from stability over time to progression into invasive malignancy, depending on their etiology and underlying pathology.

GGO nodules can be classified (Figure 14) as pure GGOs, which lack a solid component, and part-solid GGOs, which contain both ground-glass and solid components. The management and implications of these nodules differ significantly, especially in the context of lung adenocarcinoma.⁸⁶

 Benign Causes: Many GGO nodules are benign and are transitien, resulting from conditions such as inflammation, haemorrhage, or focal fibrosis. In these cases, GGOs

- may resolve spontaneously. Infectious causes, like pneumonia or viral infections, often lead to GGOs that can resolve with medical treatment.⁷⁹
- Pre-invasive Lesions: GGO nodules can represent pre-invasive lesions, such as atypical
 adenomatous hyperplasia or adenocarcinoma in situ. These lesions have a potential for
 malignant transformation but can remain stable for years before progressing. The rate of
 growth and progression for pre-invasive lesions is generally slow, allowing for periodic
 reassessment.⁸⁴
- Minimally Invasive Adenocarcinoma (MIA): MIAs often present as part-solid GGOs and have a very slow growth. They have a high survival rate when resected, but the presence of a solid component suggests a higher likelihood of invasion compared to pure GGOs.⁸⁵
- <u>Invasive Adenocarcinoma:</u> Some GGO nodules may represent early-stage invasive adenocarcinomas. These lesions tend to grow more rapidly than pre-invasive or minimally invasive lesions. The solid component's size within a part-solid GGO is a critical factor in determining the lesion's behavior, as it is considered the invasive component, with larger solid components associated with a higher risk of invasive disease and poorer prognosis.⁷⁹⁻⁸⁷

The management of GGO nodules is guided by their appearance, size, and changes over time. A conservative approach is mostly recommended to isolated, stable pure GGOs with periodic follow-up CT scans to monitor for changes. An increase in size or the development of a solid component within a GGO nodule may indicate a need for further diagnostic evaluation.⁷⁹

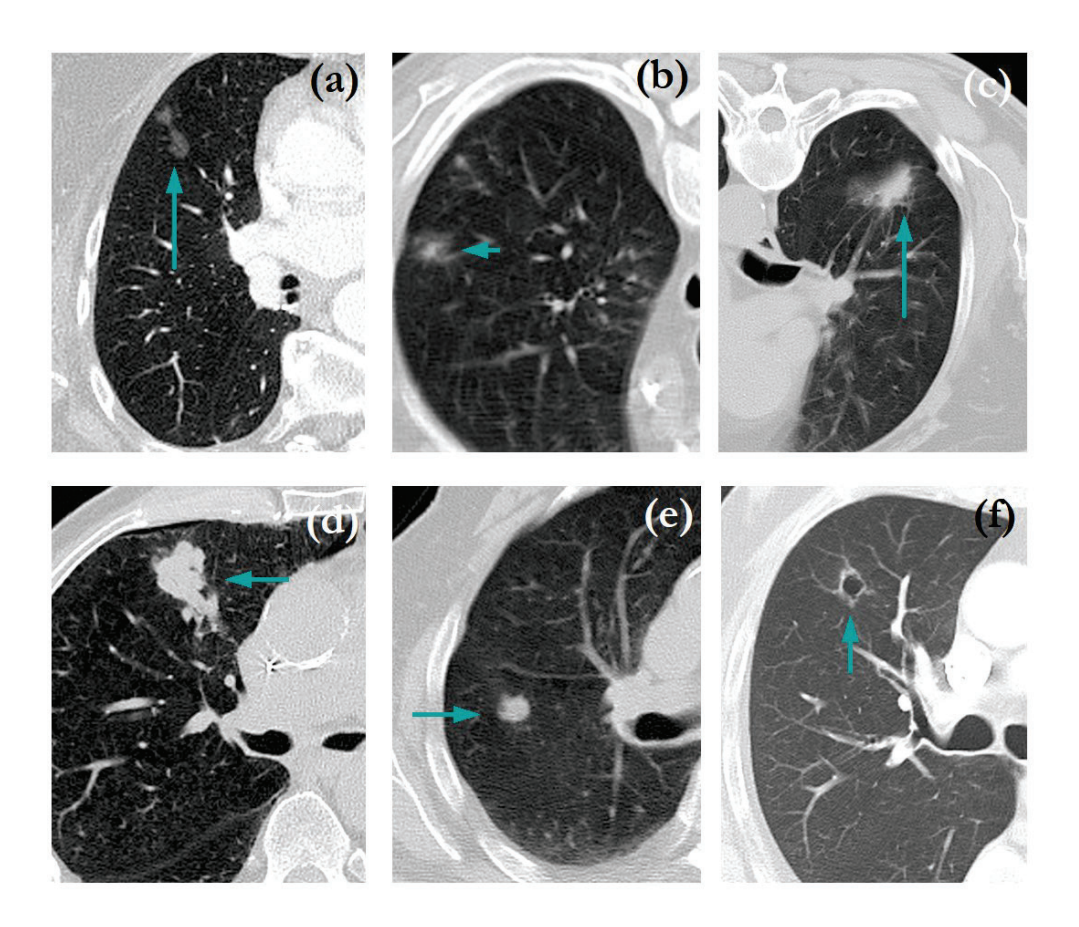


Figure 14. Lung tumors with different degrees of GGO component. (a) Pure GGO nodule. (b) Around half solid and half GGO with a Consolidation to Tumor Ratio (CTR) of 0.4 (c) Increasingly solid lesion, corresponding to a CTR of 0.7 (d) Almost purely solid lesion, with a CTR of 0.9 (e) Solid lesion (f) Cavitary lung lesion.

Original figure from the doctoral student.

3.4 Lung SABR

The technique of SABR, particularly in the treatment of lung lesions, represents a paradigm shift from conventional radiotherapy approaches. ⁸⁵ It delivers highly focused, high-dose radiation beams to a small target volume, which enables ablative doses to be delivered in a few sessions with a relatively low incidence of toxicities. ⁸⁸

One of the most critical aspects of SABR is the creation of a steep dose gradient around the target lesion. Unlike conventional radiotherapy, which often aims for a homogeneous dose distribution within the target and minimal dose to surrounding tissues, SABR prioritizes maximizing the dose to the tumor while sharply reducing the dose just outside the target boundary. While this steep gradient is essential for sparing adjacent healthy tissues and vital organs, reducing the risk of radiation-induced toxicity, it leads to higher maximum doses within the treated volume.

When talking about Lung SABR there are two main approaches which differ primarily in dose and fractionation strategies. Both schemes are designed to optimize treatment according to tumor characteristics and patient profiles.

- American Fractionation Scheme: This approach commonly uses hypofractionation with higher doses per fraction. Examples include doses of 54 Gy in 3 fractions or 50 Gy in 4 fractions. The goal is to maximize tumor control while minimizing treatment duration. Studies like RTOG 13.01 SAFRON II explore single and multifaction SABR options for pulmonary oligometastases.⁸⁹
- **Dutch Fractionation Scheme:** The Dutch approach often employs risk-adapted fractionation based on tumor location and size, delivering more conservative doses over a greater number of fractions, such as 60 Gy in 8 fractions or 55 Gy in 5 fractions. This scheme aims to minimize toxicity, especially for central lung tumors. ⁹⁰

Furthermore, fractionation schemes in lung SABR are influenced by tumor location:

- Peripheral Tumors: SABR for peripheral lung tumors often uses high-dose, hypofractionated schedules (e.g., 54 Gy in 3 fractions or 50 Gy in 4 fractions). This approach minimizes treatment time while ensuring high local control and low toxicity⁹¹. The TROG CHISEL trial confirmed the superiority of SABR over conventional radiotherapy in this context.⁹²
- **Central Tumors:** Central lung tumors require more fractionation to reduce toxicity due to their proximity to organs at risk. Common schedules include 60 Gy in 8 fractions. Studies such as the RTOG 0813 trial focus on dose escalation for central tumors while maintaining safety parameters. 93,94
- Ultracentral Tumors: Are in close proximity to the central airways or other critical structures, are treated with highly fractionated and risk-adapted schedules (e.g., 50 Gy in 10 fractions) to mitigate the risk of fatal toxicities.⁹⁵

3.5 Lung SABR for GGO lesions

The SABR treatment of GGO faces two primary challenges. The first is the standard clinical practice of treating GGO as solid nodules in terms of the prescribed dose. This approach is problematic when treating a small solid component within a larger GGO, as the risk of radiation-

induced lung toxicity correlates with the volume of lung receiving ablative doses. While this strategy effectively controls the tumor locally,⁹⁶ it increases the risk of damaging healthy lung tissue. Moreover, the presence of GGO component has been related to better LC rates.⁹⁷ This suggests that a uniform radiation dose for all pulmonary tumors may not be optimal, particularly for GGO tumors, which are often multifocal and may require multiple subsequent irradiations.

The second challenge involves the potential for large dose calculation errors by some commercial dose calculation algorithms, due to the increased heterogeneity of GGO lesions compared to solid nodules. 98-100 To our knowledge, no studies have yet evaluated the dose calculation errors in GGO lesions treated with SABR or its possible impact on healthy tissue toxicity. Furthermore, challenges related to fluence peaks during optimization should be considered, as they lead to less robust dose distributions. These fluence peaks are relevant when using type C algorithms, like AXB, and need to be addressed, as these can significantly affect dose distribution and accuracy in heterogeneous tissues like GGO. 101 Several approaches have been presented for solid lesions to mitigate this effect and achieve a fluence with a robustness level similar to that obtained when optimizing using type B algorithms, such as AAA. 102,103 This work focusses on optimizing the treatment of lung nodules containing GGO component, considering both possible approaches to reduce OAR toxicities while ensuring an accurate and robust dose distribution.

3.6 Lung SABR related toxicities

Like all therapeutic interventions, lung SABR is associated with specific toxicities. The frequency and severity of these side effects can vary based on several factors including the location of the tumor within the lung, the total radiation dose, the fractionation schedule, and the patient's underlying health status.¹⁰⁴ The most common toxicities associated with lung SABR, categorized by their CTCAE³⁵ grade are:

Radiation Pneumonitis

Is one of the most common complications, occurring in approximately 10-20% of patients treated with SABR for lung tumors.³¹

• Grade 1 (mild): Asymptomatic or mild symptoms.

- Grade 2 (moderate): Symptomatic; medical intervention indicated; limiting instrumental Activities of Daily Life (ADL).
- Grade 3 (severe): Severe symptoms; limiting self-care ADL; oxygen indicated.
- Grade 4 (life-threatening): Life-threatening respiratory compromise; urgent intervention indicated (e.g., ventilatory support).

Rib Fracture

The risk of rib fracture following SABR is reported to be around 2-10% when the treatment volume is adjacent to the chest wall.¹⁰⁵

- Grade 1: Asymptomatic; clinical or diagnostic observations only.
- Grade 2: Symptomatic and limiting instrumental ADL.
- Grade 3: Hospitalization or surgical intervention indicated.

Chest Wall Pain

Chest wall pain incidence varies widely, and it is reported up to 30-50% in some series, especially for tumors close to the chest wall.³¹

- Grade 1-2: Pain can often be managed with over-the-counter pain medications.
- Grade 3: Severe pain; limiting self-care ADL; narcotic analgesia or other interventions may be required.

Skin Toxicity

Although it is relatively uncommon with SABR, some mild skin reactions are obsevred in a small percentage of patients.¹⁰⁵

- Grade 1: Faint erythema or dry desquamation.
- Grade 2: Moderate to brisk erythema; patchy moist desquamation, mostly confined to skin folds and creases; moderate edema.
- Grade 3: Moist desquamation in areas other than skin folds and creases; bleeding induced by minor trauma or abrasion.

Esophagitis

Occurs in a small percentage of patients, more commonly when treating lesions close to the mediastinum. 106

- Grade 1: Asymptomatic or mild symptoms.
- Grade 2: Symptomatic; altered eating/swallowing; oral supplements indicated.
- Grade 3: Severely altered eating/swallowing; tube feeding, or hospitalization indicated.

Fatigue

Although it is common it is also usually only observed in a mild form, but usually mild (grade 1 or 2).

Brachial Plexopathy

It is a rare toxicity, occurring in less than 1% of patients, typically with tumors located in the upper lobes or apices of the lungs.¹⁰⁵

- Grade 1-2: Mild to moderate symptoms; intervention may include physical therapy or pain management.
- Grade 3-4: Severe symptoms; may include sensory loss and motor deficits; often requires more intensive management strategies.

3.6.1 Lung toxicities

In this work we will focus on radiation pneumonitis. Radiation pneumonitis is an inflammation of the lung tissue that can occur after exposure to radiation. Its development is influenced by various factors, including the total radiation dose, the volume of lung irradiated, the dose per fraction, and individual patient sensitivity (Figure 15).

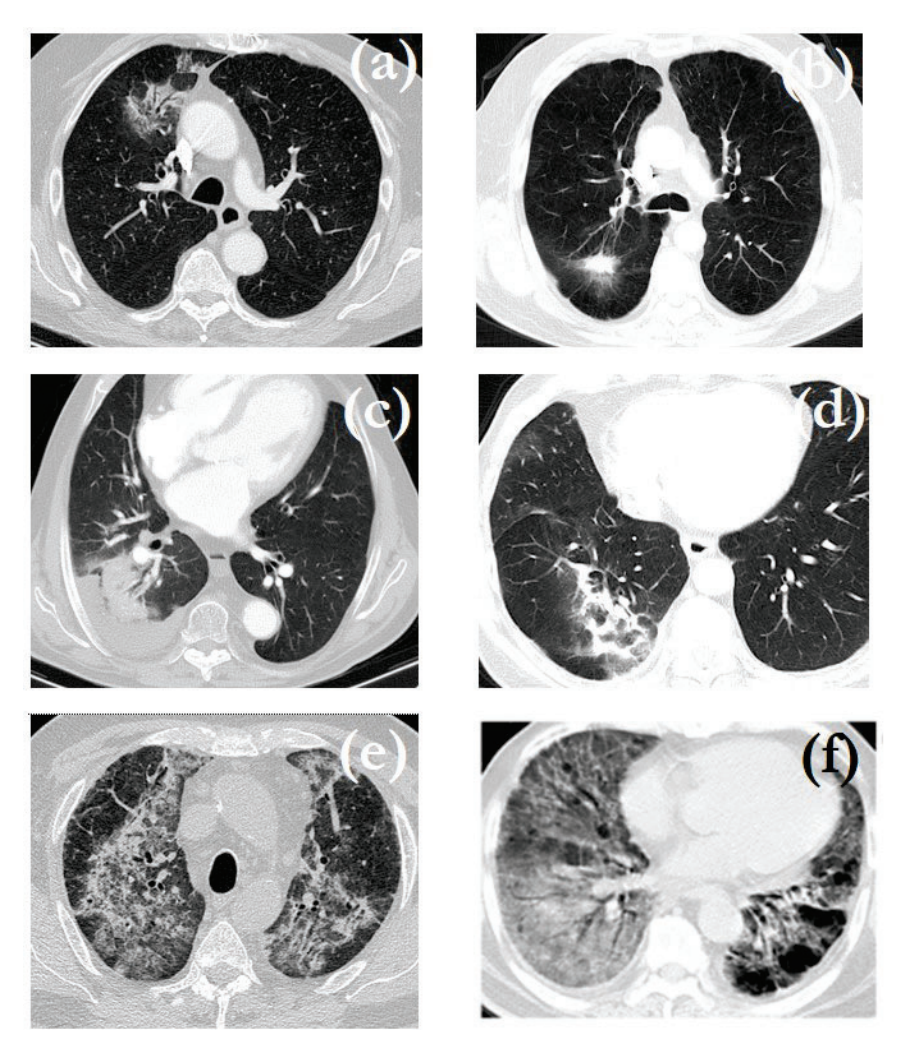


Figure 15. Radiation pneumonitis (RP) in CT images: (a) to (d) different patients with grade 1 lung parenchyma changes, (e) grade 2, and (f) grade 4-5. Original figure from the doctoral student.

3.6.1.1. Grade 2 and higher

Grade 2 radiation pneumonitis involves symptomatic presentations that may include persistent cough, low-grade fever, and dyspnea on exertion. Unlike grade 1, which is mostly asymptomatic and detected incidentally on imaging, grade 2 pneumonitis actively affects patients and requires medical treatment. Its management often involves corticosteroids to reduce inflammation, along with supportive care measures. 31

The prevalence of grade 2 and higher radiation pneumonitis in patients undergoing lung SABR varies widely in the literature, ranging from as low as 10% to as high as 30%. The variation in reported incidence rates can be attributed to differences in patient populations, treatment protocols, and definitions of pneumonitis across studies. However, the incidence of severe (grade 3 or higher) pneumonitis is generally lower, reported to be around 1-5% in most series. The series of the prevalence of

Several factors have been identified that increase the risk of developing grade 2 or higher radiation pneumonitis following lung SABR:

- <u>Dose-Volume parameters:</u> V20Gy is a commonly cited dosimetric parameter associated with the risk of pneumonitis for normofractionated regimes, and it is usually onscidered for SABR treatments. Higher V20Gy values are linked to an increased risk. Other parameters, such as the mean lung dose (MLD) and V5Gy, have also been correlated with pneumonitis risk, ¹⁰⁸ but their relation is less clear.
- <u>PTV size</u>: Larger PTVs have been associated with a higher risk of pneumonitis, as larger volumes of lung tissue are exposed to radiation.¹⁰⁷
- <u>Tumor location:</u> Tumors located centrally or near critical structures such as the main bronchus are associated with a higher risk of pneumonitis due to the proximity of larger volumes of lung tissue to high-dose radiation areas. ¹⁰⁵ In lung SABR the proximity to the main bronchial tree is the main criteria to choose among different fractionation schemes. Lower lobes tumors have also been identified as being more prone to radiation pneumonitis.
- <u>Underlying lung function</u>: Patients with pre-existing lung conditions or compromised pulmonary function are at increased risk for developing pneumonitis.³¹
- Concurrent chemotherapy on immunotherapy: The use of systemic treatments in conjunction with radiation therapy has been shown to increase the risk of pneumonitis, although this is less commonly a factor in SABR due to its typical use in a standalone setting for early-stage or oligometastatic disease.¹⁰⁸

3.6.1.2. Grade 1 toxicities

The diagnosis of grade 1 radiation pneumonitis is primarily based on imaging findings, given the lack of or minimal clinical symptoms. ¹⁰⁹ In the early stages, radiographic findings may be subtle or even absent, making CT scans a more sensitive tool for detection. ¹¹⁰ These changes might appear only during the acute phase and then resolve or remain as permanent changes in the lung parenchyma.

Imaging Changes in Lung Parenchyma

On imaging, especially high-resolution CT scans, several changes can be observed in the lung parenchyma indicative of radiation pneumonitis (Figure 15):

- <u>Ground-Glass Opacities</u> are a common early finding and may represent mild interstitial inflammation or edema.¹¹¹
- <u>Consolidation</u> refers to a region of homogenous increase in pulmonary parenchymal attenuation that obscures the margins of vessels and airway walls. It indicates more significant inflammation and may be accompanied by air bronchograms.¹¹²
- <u>Volume loss</u>: There may be evidence of volume loss in the affected lobe, characterized by crowding of pulmonary vessels and bronchi, and displacement of interlobar fissures. ¹¹⁰
- Septal thickening and traction bronchiectasis: As the inflammation progresses, there can be interstitial thickening and development of traction bronchiectasis, which suggests the beginning of lung fibrosis.¹¹¹

These imaging findings are typically confined to the radiation field and may show a sharp demarcation corresponding to the treatment area, which can help differentiate radiation-induced changes from other causes of pneumonitis.¹⁰⁹

Grade 1 radiation pneumonitis management primarily involves observation and monitoring for progression to higher-grade pneumonitis. 110 Preventive measures, such as minimizing exposure of healthy lung tissue to radiation and optimizing radiation delivery techniques, are crucial in reducing the risk of pneumonitis. 112

4. SABR challenges for the treatment of GGO lesions

The SABR treatment of GGO faces two primary challenges. The first is the standard clinical practice of treating GGO as solid nodules. The second involves the possibility of significative dose calculation errors in the semisolid area of the lesion. In the following sections we develop these points, which are the fundamental areas of research of this work.

4.1. Volume definition

The approach of treating GGO lesions as solid lesions in terms of volume is problematic when treating a small solid component within a larger GGO (Figure 16), as the risk of radiation-induced lung toxicity correlates with the volume of lung receiving a high radiation dose. While this strategy effectively controls the tumor locally. 55, it increases the risk of damaging healthy

lung tissue. Moreover, the presence of GGO component has been related to better LC rates.⁹⁷ As stated before, this questions the approach of using a uniform radiation dose for all pulmonary tumors, specifically for GGO tumors. Thus tailoring SABR treatments for this kind of lesion seems reasonable.

Considering these facts, this thesis focuses on analysing the dosimetric impact of a dose deescalation regime for SABR for lesions with GGO component, with the goal of informing future clinical application. Specifically, it analyses the feasibility of such technique from a technical point of view as well as the related expected benefits for patients in terms of associated grade 1 toxicities in the lung.

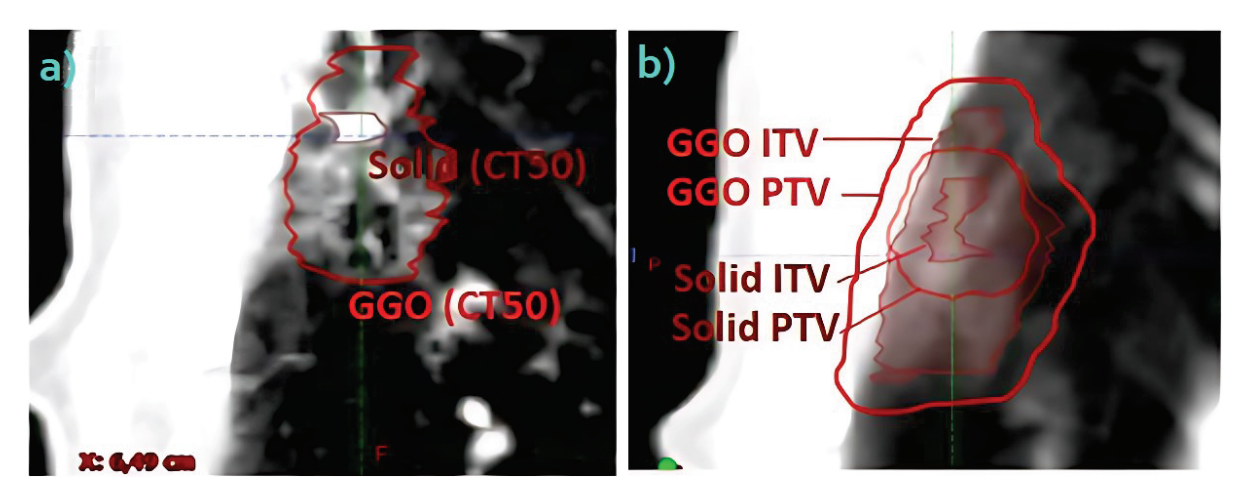


Figure 16. Volume definition for a lung lesion consisting of a GGO nodule with a solid part at the centre of the lesion. (a)
In Red we can see the static CTV of the whole lesion and in brown the static CTV of the solid lesion. In (b) we can see
their corresponding ITV and PTV. Original figure by the doctoral student.

4.2. Lung parenchyma changes

The first question that arises when considering a de-escalation SABR treatment for GGO lesions is whether this approach would lead to reduced changes in the lung parenchyma. In the last years, concerns around grade 1 toxicities have risen in the context of oligometastatic patients, where multiple lesions are treated and the accumulation of patches of affected lung parenchyma may lead to clinical toxicities. This is especially true for patients undergoing SABR, who usually present previous pathologies restricting their respiratory function. Furthermore, with the implementation of screening programs, it is expected to diagnose and treat younger patients, likely to receive multiple lung treatments.

In addition, the use of immunotherapy in combination with SABR¹¹⁵ has also become the standard of care for advanced NSCLC and oligometastatic patients.^{96,116} This combination increases the treatment related toxicities, thus making it more relevant to reduce the impact of the SABR treatment.

Radiation-induced lung injury after SABR is a dynamic process that affects the lung parenchyma surrounding the target lesion. The radiological pattern evolves during follow-up, and it is typically classified in acute (< 6 months) or late phase changes (>6 months).¹¹⁷

It is not only a concern about toxicity, as consolidation areas surrounding the lesion also make it challenging to differentiate between LC and local recurrence (LR) of the tumor. In case of LR and due to reirradiations, where clinical toxicities are more prevalent, in a fine delineation of the tumor volume is critical, as the volume of the re-irradiated area in correlated with the risk of grade ≥ 2 toxicities.

To the best of our knowledge, before this work, there was a lack of literature relating the delivered SABR dose with purely radiological toxicity of the lung parenchyma. Some studies have analyzed the impact of different SABR regimes in terms of BED and its relation to local control¹²² and clinical toxicity. Over the last years, lower BED regimes have been prioritized to reduce toxicities. These regimes, below the threshold of 130 GyBED₁₀, come at the cost of lower LC rates. Despite the low incidence of clinical toxicities there is a big prevalence of grade 1 toxicities.

4.3. Dose calculation accuracy

As stated before, a second challenge in treating GGO lesions involves the potential for large dose calculation errors by commercial dose calculation algorithms, owing to the increased heterogeneity of GGO lesions compared to solid nodules. To our knowledge, no studies have yet evaluated the dose calculation errors in GGO lesions treated with SABR or its possible impact on healthy tissue toxicity. Furthermore, challenges related to fluence peaks during optimization should be considered, as they lead to less robust dose distributions. These fluence peaks are relevant when using type C algorithms, like AXB, and need to be addressed, as these can significantly affect dose distribution and accuracy in heterogeneous tissues like GGO. Several approaches have been presented for solid lesions to mitigate this effect and achieve a fluence with a robustness level like that obtained when optimizing using type B algorithms, such as AAA.

In conclusion, this thesis emphasizes in the challenges and optimization strategies for lung lesions with GGO component treaded with SABR. Through two published studies, we first evaluate the correlation between the BED and the incidence of subclinical radiological toxicities in a series of patients that underwent SABR in our institution between 2017 and 2021. In this first study we found a statistically significant association between high lung BEDs and the appearance of organizing pneumonia patterns and lung affectation over both short and longterm follow-ups. This study was published under the title "Biological effective dose is associated with radiological toxicity after lung stereotactic ablative radiation therapy". Secondly, in a study entitled "Feasibility and potential clinical benefit of dose de-escalation in stereotactic ablative radiotherapy for lung cancer lesions with ground glass opacities" we explored the feasibility and optimization of dose de-escalation regimes for GGO lesions in SABR, focussing on the balance between minimizing dose to the lung while maintaining high doses to the solid region of the tumour. At the same time ensuring accurate dose calculation and robust treatment plans. These investigations collectively propose a foundation for refining radiotherapy dose constraints to mitigate grade 1 pulmonary toxicity and lay the groundwork for future clinical protocols aimed at enhancing local control while minimizing the toxicity profile for lung lesions with GGO components.

HYPOTHESIS

- 1. There is an association between the dose delivered to the healthy lung tissue and grade 1 toxicities observed after SABR treatment.
- 2. SABR treatment of lung malignancies containing GGO can be optimized to maintain local control while reducing grade 1 lung toxicities.

OBJECTIVES

First part, toxicity evaluation:

- 1. Analyze and quantify the lung parenchyma changes after stereotactic radiation therapy.
- 2. Correlate grade 1 lung toxicity with the dose delivered to the patient.

Second part, optimization of stereotactic ablative radiation therapy:

- 3. Evaluate the accuracy of clinical dose calculation algorithms in lung nodules in the presence of ground glass opacities.
- 4. Define an approach to optimize stereotactic lung treatments for lesions containing ground glass opacities component that maintains the expected local control while reducing the risk of associated toxicity.

MATERIAL, METHODS AND RESULTS PUBLICATION 1

Cases C, Benegas M, Sánchez M, Vollmer I, Casas F, Gomà C, Mollà M. Biological equivalent dose is associated with radiological toxicity after lung stereotactic ablative radiation therapy. Radiother Oncol. 2023 Jun;183:109552.



Contents lists available at ScienceDirect

Radiotherapy and Oncology

journal homepage: www.thegreenjournal.com



Original Article

Biological equivalent dose is associated with radiological toxicity after lung stereotactic ablative radiation therapy



Carla Cases ^a, Mariana Benegas ^{b,c}, Marcelo Sánchez ^{b,c}, Ivan Vollmer ^{b,c,d}, Francesc Casas ^{a,c}, Carles Gomà ^{a,e,*}, Meritxell Mollà ^{a,c,e,f}

* Department of Radiation Oncology; * Department of Radiology; * Thoracic Oncology Unit, Hospital Clinic de Barcelona; * Translational Research in Pulmonary Vascular Diseases: Cell Proliferation and Apoptotic Mechanisms in Pulmonary Arterial Hypertension; * Translational Genomics and Targeted Therapies in Solid Tumors, Institute for Biomedical Research August Pi i Sunyer (IDIBAPS); and * Department of Clinical Foundations, University of Barcelona, Barcelona Spain

ARTICLE INFO

Article history: Received 20 September 2022 Received in revised form 18 January 2023 Accepted 6 February 2023 Available online 21 February 2023

Keywords: Radiotherapy Biological equivalent dose Radiologic toxicity SABR

ABSTRACT

Introduction: Stereotactic ablative radiation therapy (SABR) is the standard of care for inoperable earlystage non-small-cell lung cancer. Although the probability of grade \geq II toxicities is low, many patients present radiological subclinical toxicities usually associated with long-term patient management challenges. We evaluated radiological changes and correlated them with the received Biological Equivalent Dose (BED).

Methods: We retrospectively analyzed chest CT scans of 102 patients treated with SABR. An experienced radiologist evaluated the radiation-related changes 6 months and 2 years after SABR. The presence of consolidation, ground-glass opacities, organizing pneumonia pattern, atelectasis and the extent of affected lung were recorded. Dose-volume histograms of the lung healthy tissue were transformed to BED. Clinical parameters such as age, smoking habits, and previous pathologies were registered and correlations between BED and radiological toxicities were drawn.

Results: We observed a positive and statistically significant correlation between lung BED over 300 Gy and the presence of organizing pneumonia pattern, the degree of lung affectation and the 2-year prevalence and/or increase of these radiological changes. Radiological changes in patients receiving BED > 300 Gy to a healthy lung volume \geq 30 cc increased or remained in the 2 years follow-up scan. We found no correlation between radiological changes and the analyzed clinical parameters.

Conclusions: There seems to be a clear correlation between BEDs higher than 300 Gy and radiological changes both short and long term. If confirmed in an independent patient cohort, these findings could lead to the first radiotherapy dose constraints for grade I pulmonary toxicity.

© 2023 Elsevier B.V. All rights reserved. Radiotherapy and Oncology 183 (2023) 109552

Lung stereotactic ablative radiotherapy (SABR) has proven to be an effective treatment for inoperable lesions with a very good local control (LC) and a very low incidence of grade \geq II toxicities [1–4]. It is well known, though, that over 60% of the patients treated with SABR present post radiotherapy radiological changes in the lung parenchyma [5]. Although in most cases these changes have no direct clinical impact, they present a challenge in the long-term management of the patient.

Firstly, consolidation areas surrounding the lesion makes it challenging to differentiate between LC and local recurrence (LR) of the tumor [6]. In case of LR and need for re-irradiation, where clinical toxicities are more prevalent [7,8], a fine delineation of

the tumor volume is critical, as the volume of the re-irradiated area is correlated with the risk of grade $\geq II$ toxicities [9,10]. Secondly, concerns around grade I toxicities have risen in the

Secondly, concerns around grade I toxicities have risen in the context of oligometastatic patients, where multiple lesions are treated and the accumulation of patches of affected lung parenchyma may lead to clinical toxicities. This is especially true for patients undergoing SABR, who usually present previous pathologies already restricting their respiratory function [11]. Furthermore, with the implementation of screening programs, it is expected to diagnose and treat younger patients, likely to receive multiple lung treatments.

In addition, the use of immunotherapy in combination with SABR [12] has also become the standard of care for advanced NSCLC and oligometastatic patients [13,14]. This combination increases the treatment related toxicities, thus making it more relevant to reduce the impact of the SABR treatment.

https://doi.org/10.1016/j.radonc.2023.109552 0167-8140/© 2023 Elsevier B.V. All rights reserved.

^{*} Corresponding author at: Department of Radiation Oncology, Hospital Clinic de Barcelona, Carrer de Villarroel 170, 08036 Barcelona, Spain. E-mail address: goma@clinic.cat (C. Gomà).

One last concern has risen lately with the global pandemic of COVID-19, where it has been seen that COVID-19 could be a risk factor for patients receiving radiotherapy [15].

To the best of our knowledge, there is a lack of literature relating the delivered SABR dose with purely radiological toxicity of the lung parenchyma. Some studies have analyzed the impact of different SABR regimes in terms of Biologically Equivalent Dose (BED) and its relation to local control [16] and clinical toxicity [4,17,18]. Over the last years, lower BED regimes have been prioritized in order to reduce toxicities. These regimes, below the threshold of 130 GyBED₁₀ (where the subscript refers to the alpha/beta ratio), come at the cost of lower LC rates [19]. Despite the low incidence of clinical toxicities (between 9 and 28%) [1,2,4], there is a big prevalence of grade I toxicities. If we consider these toxicities as a precursor of higher toxicities, we can utilize this information to determine BED levels that associate with the presence of more extensive and durable radiological toxicity cases. To the authors knowledge, no study has been published yet that correlates the received BED with the presence, magnitude and durability of radiological changes in the lungs after SABR.

Radiation-induced lung injury after SABR is a dynamic process that affects the lung parenchyma surrounding the target lesion. The radiological pattern evolves during follow-up and it is typically classified in acute (<6 months) or late phase changes (>6 months)

In this study we analyzed the acute and long-term radiationinduced lung changes in terms of presence or absence of several radiological findings. We also analyzed if any of the clinical parameters previously associated with clinical toxicities in the literature [19,21] were predictive of radiological toxicity.

Materials and methods

We retrospectively analyzed the pre-treatment, simulation and follow up CT scans of the patients treated with SABR in the lung between 2017 and 2021 at our institution, and who met the following criteria:

- A lung pre-treatment CT scan was available
- At least a 6 months follow-up chest CT scan was available
- No local recurrence was observed

Patients that presented local recurrence were removed from the study to assure that the consolidation surrounding the tumor did not include tumor growth.

Our patients were treated following the Radiation Therapy Oncology Group 0236 trial protocol [22]. We prescribed three fractionation schemes, depending on the size, centrality or proximity to organs at risk of the tumor. The schemes consisted of 3 fractions of 18 Gy, 5 fractions of 11 Gy and 8 fractions of 7.5 Gy. We immobilized the patients using a vacuum bag and abdominal compression and acquired a 4DCT. The radiation oncologist defined the internal target volume (ITV) using the 10 phases of the 4DCT. An isotropic margin of 3 mm was added to the ITV to define the planning target volume (PTV). The dose calculation (Eclipse AAA13.7/16.0) was performed on the Average CT reconstruction. We assessed the plan conformity and the dose gradient using R100 and R50 respectively (ratio between the volume receiving the prescribed dose or the 50% of the prescribed dose and the PTV). The maximum dose at 2 cm from the PTV was maintained as established by the protocol [22]. For the healthy lung dosevolume histogram (DVH) parameter, the total lung volume minus the ITV was taken into account. We optimized and delivered the treatment using Volumetric Modulated Arc Therapy; with a dose normalization to ensure that the 100% isodose level encompassed 95% of the PTV. Treatments were delivered using either a 6 MV photon beam in a Varian Clinac2100 or a 6 MV flattening-filter free beam in a Varian TrueBeam linear accelerator. We performed daily image guidance using Cone Beam CT.

After SABR treatment, follow-up CT scans were performed at 3 months, 6 months and annually. All patients underwent a chest CT [scanners: Somatom Definition Flash (128 slices), Somatom Go Top (64 slices), Somatom Sensation64 (64 slices) and Somatom Emotion 16 (16 slices), Siemens Healthineers, Erlangen, Germany), with or without intravenous contrast, in supine position and suspended deep inspiration. The images were reconstructed using mediastinal and lung kernels with slice thickness from 1 to 3 mm. An experienced thoracic radiologist evaluated the changes in the lung parenchyma for the 6 months and 2 years follow-up scans (Fig. 1). The baseline characteristics of the lung lesions in the pretreatment CT were: density, size and pulmonary lobe. The presence of emphysema or bronchiectasis was also recorded. In the follow-up CT at 6 months and 2 years, the presence or resolution and size of the lesion was recorded. Pneumonitis and atelectasis were recorded following the CTACE score. To allow us to further assess and subcategorize radiological differences that fall within grade I toxicities, radiation-induced changes were also analyzed according to the presence or absence of: consolidation, residual atelectasis and organizing pneumonia-like changes. Organizing pneumonia-like changes were defined as peribroncho vascular opacities with perilobular distribution and/or the presence of the reverse halo sign [23]. The lung extent of the features was scored visually in 25% steps. Additionally, we recorded the volume of the PTV and the superior-inferior position of its centre of mass [19].

To analyze the correlation between clinical and radiological toxicities with the BED, we exported the dose-volume histograms (DVH) of the lung and transformed each point of the DVH curve by applying the linear quadratic model.

$$BED = nd \left[1 + \frac{d}{(\alpha/\beta)} \right]$$

where n represents the total number of fractions, d stands for the dose per fraction and the value of alpha beta was considered to be 3.

Once the BED volume histogram was obtained, we extracted VxGyBED₃ (cc) (with x ranging from 10 to 500 in 10 GyBED₃ steps) [24]. The analyzed dosimetric and clinical parameters are detailed in Table 1.

We evaluated the statistical significance with univariate correlations using Pearson (for quantitative variables), Chi-Square test (qualitative variables), or ANOVA analysis (other cases) and we considered the results statistically significant for p < 0.05.

Results

102 patients (with a total of 118 lesions) who met the above-described inclusion criteria were treated in our institution between 2017 and 2021. For 48 of these patients (51 lesions) a 2-year follow-up CT scan was also available. Baseline clinical and dosimetric characteristics are summarized in Table 1. The median age was 73 and 32 patients were female. Smoking history was available for 61% of the patients: 20% of those never smoked, 56% were ex-smokers and 24% current smokers. The vast majority presented other pathologies such as hypertension (65%), history of cardiac pathologies (67%) or Chronic Obstructive Pulmonary Disease (COPD) (64%). The median tumour size was 20 mm, and the median PTV volume was 23 cc.

Immunotherapy was prescribed to 9 of the 102 patients with a 6 months follow and to 3 of the patients with a 2 year follow up.

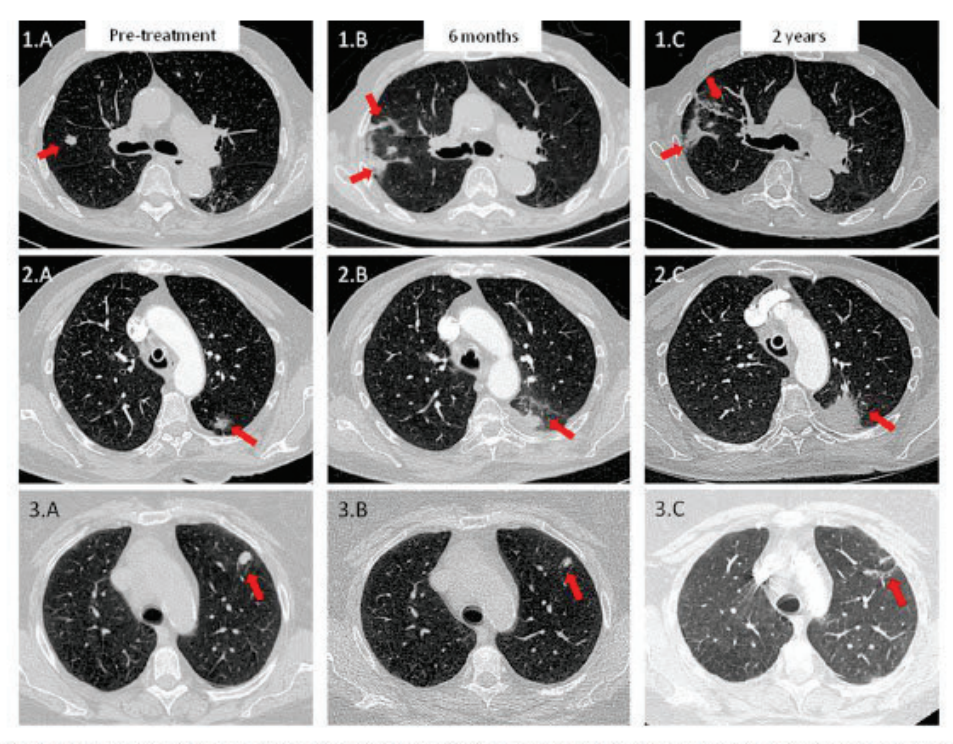


Fig. 1. Examples of axial chest CT images (lung window) used for the evaluation of the radiation-induced lung changes. 1.A) Solid pulmonary nodule in the right upper lobe. 1. B) Organizing pneumonia pattern surrounding the nodular lesion at 6 months 1.C) Organizing fibrosis changes at 2 years 2.A) Sub-solid pulmonary nodule in the left lower lobe. 2.B) Small focal consolidation and ground-glass opacities at 6 months. 2.C) Increased consolidation at 2 years, 3.A) Solid pulmonary nodule in the left upper lobe. 3.B) Decrease in size at 6 months. 3.C) Resolution of the lesion at 2 years with the presence of linear atelectasis.

Although 2 were receiving immunotherapy during the 2 years of follow up, one of them started immunotherapy between the 6 months and 2 years time point and another stopped between the 6 months and 2 years follow up scan due to immunotherapy-associated grade II pneumonitis. This latter patient was treated for a Merkel cell carcinoma with pembrolizumab, then the patient presented a primary NSCLC treated with SABR. The patient presented a grade II immunotherapy-related pneumonitis related to the Merkel treatment. We found no statistically significant relation between immunotherapy and lung parenchyma changes. For the remaining patients we found no statistically significant correlation between any of the clinical variables and the observed radiological changes. The majority of the lesions (57%) were treated in 5 fractions, 17% in 3 fractions and the rest were treated with 8 fractions.

Some of the patients were treated during the COVID pandemic and 2 presented COVID-related lung parenchyma changes before irradiation. These patients did not present any unexpected response to the treatment.

Table 1 shows a summary of the pre-treatment CT characteristics of the lung parenchyma and the radiation-induced changes observed at 6 months and 2 years follow-up CT. In the pre-treatment chest CT scan, emphysema was observed in 53 patients, but with only 14 cases of severe emphysema. Bronchiectasis was present in 47% of the patients. 22 patients presented both emphysema and bronchiectasis. In the 6 months follow-up CT scan, lung parenchyma changes were maintained within the irradiated area for the majority of the cases, with only 22% of the cases extending to other lung lobes, and were within the treated lung for all of the patients except for one patient that presented grade II pneumonitis

associated with the concurrent immunotherapy treatment. Only 20% of the patients did not show any radiological change of the lung parenchyma, while over 50% presented various types of acute parenchyma changes after irradiation. While only 10 patients had a percentage of lung affectation of more than 50%, 67 had a percentage of affectation between 25% and 50%. In the 2-years follow-up scan, organizing pneumonia-like changes were reduced in 45% of the patients, the presence of residual atelectasis in 60%, and the size of the consolidation in 64%. The percentage of lung affectation presented a distribution similar to the 6 months follow-up scan. Only 4 of our patients did not show any radiological lung parenchyma change in the 2-year follow-up scan compared to the baseline CT.

When comparing the 6 months CT scan with the baseline scan, we found a statistically significant correlation for the percentage of affected lung and dose levels over 280 GyBED3, Dmax, D1cc and D5cc (except for the Merkel case who had a percentage of lung affectation above 75%). The strength of the correlation was very strong (p < 0.001) for dose levels between 300 GyBED3 and 400 GyBED3. The presence of organizing pneumonia-like changes and the extent of consolidation were also strongly correlated (p < 0.01) for doses between 300 GyBED3 and 400 GyBED3. Conversely, the presence of atelectasis was not correlated with any dose level.

Fig. 2 shows the relation between the percentage of lung affectation and organizing pneumonia-like changes at 6 months and the volume receiving 100, 300 and 400 GyBED₃ with each correspondent p-value.

Table 1

Summary of patient characteristics, dose distribution and CT features analyzed in the lung parenchyma for the pre-treatment CT scan, and in the 6 months and 2-years CT follow-up scan.

PATIENT CHARACTERISTIC		
	Average (Min-Max)	
Age	73 (37- 9 1)	
	Number of patients	
	(percentage)	
Smoking habits*		
Never	13 (20%)	
Ex-smoker	35 (56%)	
Current smoker	15 (24%)	
Sex		
Male	70 (69K)	
Female Other	32 (31%) 0	
	0	
Other Pathologies Hypertension	66 (65%)	
Cardiac diseases	68 (67%)	
COPD	65 (64%)	
Immunotherapy		
At 6 months	9 (9%)	
At 2 years	3 (6%)	
2000		
	Number of lesions	
	(percentage)	
Tumor Location	ec (ecv)	
Right Lung Left Lung	66 (56%) 52 (44%)	
Lower Lobes	67 (56%)	
Upper Lobes	51 (44%)	
Fractionation scheme	70.0000	
3 × 18 Gy	30 (25%)	
5 x 11 Gy	67 (57%)	
8 × 7,5 Gy	20 (17%)	
	Average (Min-Max)	
PTV size (cc)	23 (2-97)	
Dose Distribution		
V5 GyBED ₃ (cc)	482 (119-1375)	
V20 GyBED ₃ (cc)	254 (44-809)	
V50 GyBED ₃ (cc)	139 (16-548)	
V100 GyBED ₃ (cc)	79 (7-335)	
V150 GyBED ₃ (cc) V200 GyBED ₃ (cc)	53 (4-246) 38 (2-184)	
V300 GyBED ₃ (cc)	17 (0-112)	
V400 GyBED ₃ (cc)	9 (0-88)	
Dmax (GyBED ₃)	430 (233-700)	
D1 cc (GyBED ₃)	388 (193-644)	
D5 cc (GyBED ₃)	354 (89-958)	
CT FEATURES		
Pre-Treatment scan		
	Percentage of patients (N)	
Emphysema	52% (53)	
Severe	27% (14)	
Light to moderate	73% (39)	
Bronchiectasis	46% (47)	
Emphysema and Bronchiectasis	22% (22)	
	6 months scan	2 years scan
Number of patients	102	48
Number of lesions	118	51

Table 1 (continued)

PATIENT CHARACTERISTICS		
	Average (Min-Max) Percentage of lesions (N)	Percentage of lesions (N)
Lung toxicity		77770000000000
(pneumonitis) Grade 0	19% (23)	8% (4)
Grade I	77% (91)	88% (45)
Grade > I	3% (4)	0% (0)
% Affected Lung		
<25%	35% (41)	29% (15)
25%-50%	56% (67)	53% (27)
>50%	8% (10)	18% (9)
Organizing pneumonia- like changes	50% (59)	31% (16)
Atelectasis	52% (61)	47% (24)
No changes	20% (23)	8% (4)

^{*} Available for 61% of the patients.

The majority of the cases without organizing pneumonia-like changes have V300GyBED₃ below 30 cc, with only two outlier cases having V300GyBED₃ above 30 cc who presented an organizing pneumonia pattern in the 2 year follow up scan. Furthermore, all of the cases that received a dose over 300 GyBED₃ to a volume greater or equal to 30 cc presented permanent changes in the lung parenchyma. The percentage decreased to 90% when the volume of the lung encompassed by BED₃ \geq 300 Gy was over 20 cc.

We also found a positive and statistically significant (p < 0.05) correlation between the increase or persistence of long-term organizing pneumonia-like changes and the percentage of lung affectation with respect to the 6 months CT for dose levels over 300 GyBED₃. Furthermore, almost all patients receiving 300 GyBED₃ to a volume above 30 cc, presented a percentage of lung affectation over 25% and/or organizing pneumonia pattern.

Focusing on a qualitative analysis, Fig. 3 shows the evolution of the lung parenchyma changes in two patients. The first patient received 300 GyBED₃ to a volume of 31 cc. Even though at 6 months changes surrounding the lesion consisted of a small increase in size of the lesion as focal consolidation, long-term parenchyma affectation with organizing pneumonia pattern appeared at 2 years. Conversely, the second patient received V300 GyBED₃ = 0. In this case, although a consolidation pattern was present at 6 months, in the two-year follow-up scan a significant decrease was observed.

Fig. 4 shows the distribution of the long-term evolution of the lung parenchyma, classified in patients that received 300 GyBED $_3$ to less or more than 20 cc. It can be noticed that the patterns of the evolution are clearly different between the two groups. While in the first group (V300GyBED $_3$ < 20 cc) the majority of the patients decreased or maintained the changes, the second group (V300GyBED $_3$ \geq 20 cc) had a clear tendency to increase the observed changes, with only a minority of the patients decreasing or maintaining those changes.

In general, organizing pneumonia pattern tended to increase with time, with over 85% of our patients either increasing or maintaining the organizational CT changes between the 6 months and 2 years follow-up CT scans. Lastly, most of the patients kept the percentage of lung involvement stable (Fig. 4).

Discussion

In this study we described and analyzed the changes in the lung parenchyma observed in a cohort of 102 patients (118 lesions) treated with SABR. We related these changes with the delivered BED to the healthy lung tissue. We found that dose levels over

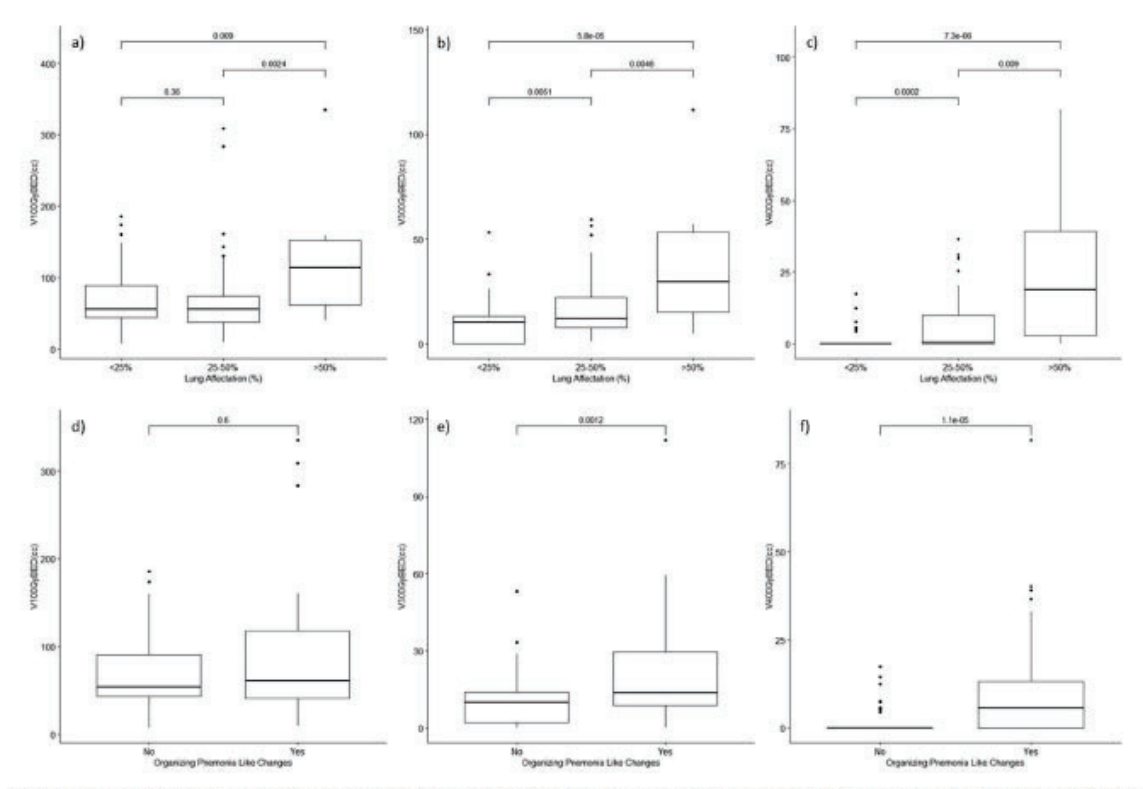


Fig. 2. Distribution of Lung affectation percentage (a, b,c) and Organizing Pneumonia-Like changes (d, e, f) at 6 months for three different dose levels corresponding to: 100 GyBED₃ (a and d), 300 GyBED₃ (b and e) 400 GyBED₃ (c and f). The p-value of the correlation between BED and lung changes (ANOVA test) is shown. Figure a shows that a significant correlation only exists for patients with a lung affectation between 50–70%, but as dose increases this effect extends to lower percentages of lung affectation. The same trend is shown in figures d-f, where organizing pneumonia-like changes are not statistically significant for low doses, while they achieve significance for doses above 300 GyBED.

300 GyBED₃ to the lung were associated with long-term radiological changes in the lung parenchyma. Furthermore, we observed that patients receiving doses over 300 GyBED₃ to volumes greater than 20 cc had a significant risk of presenting the aforementioned changes. This relation was further validated as we found no clinical toxicity that could explain the different evolution of the lung parenchyma changes. This dose level is comparable to the level described in the literature as the threshold where local control rates decrease [18]. The fact that the same threshold for LC applies to the presence and severity of grade I toxicities suggests that volumes encompassed by this dose level should be considered carefully.

It has been reported that lower lobe tumor location is correlated with grade ≥ II toxicities [4,21], but in this study we found no such correlation. This finding could have two possible explanations. On the one hand, it could evidence that purely radiological changes (which represent 96% of our patients) are independent of the localization of the irradiated area [21]. On the other hand, lower lobe lesions tend to have a larger respiratory motion due to their proximity to the diaphragm, which leads to larger treated volumes [25]. The fact that in our study the PTV volume was taken into account to determine the fractionation scheme [22] might have limited the impact of lower lobe location as a risk factor.

Similarly to the grade \geq II results reported in the literature, we found no correlation between clinical variables and grade I toxicity.

Neither did we find any statistically significant relation between the use of immunotherapy and radiological changes, although the low number of patients receiving immunotherapy (below 10% in both groups) was not sufficient to draw any conclusions.

There is extensive literature on the evaluation of radiological images post-SABR to assess local control and other risk factors [6,20,26]. Similarly, CTCAE score describes toxicities based on clinically observed parameters, but it does not consider a subdivision within all the radiological changes that do not have a clinical impact, as they all fall within grade 1 toxicities. To the authors knowledge, there are no unified criteria to assess post-SABR patterns regarding associated radiological toxicities. In the current study, the most frequent pulmonary radiological findings after SABR were described.

Although the results of this study seem to be sound, there are inherent limitations to consider. Firstly, the retrospective nature of the study made it impossible to evaluate the effect of fractionation independently from tumor variables such as size or position. Secondly, the unicentric nature of the study makes it advisable to validate the results in an independent cohort. Lastly, the application of the linear-quadratic model to calculate BED does not explain all biological effects related to dose fractionation at high doses per fraction. In spite of the above-mentioned limitations, our study has also several strengths worth mentioning. To the best of our knowledge, this is the first study analyzing grade I toxicities in the lung parenchyma and describing the evolution of these

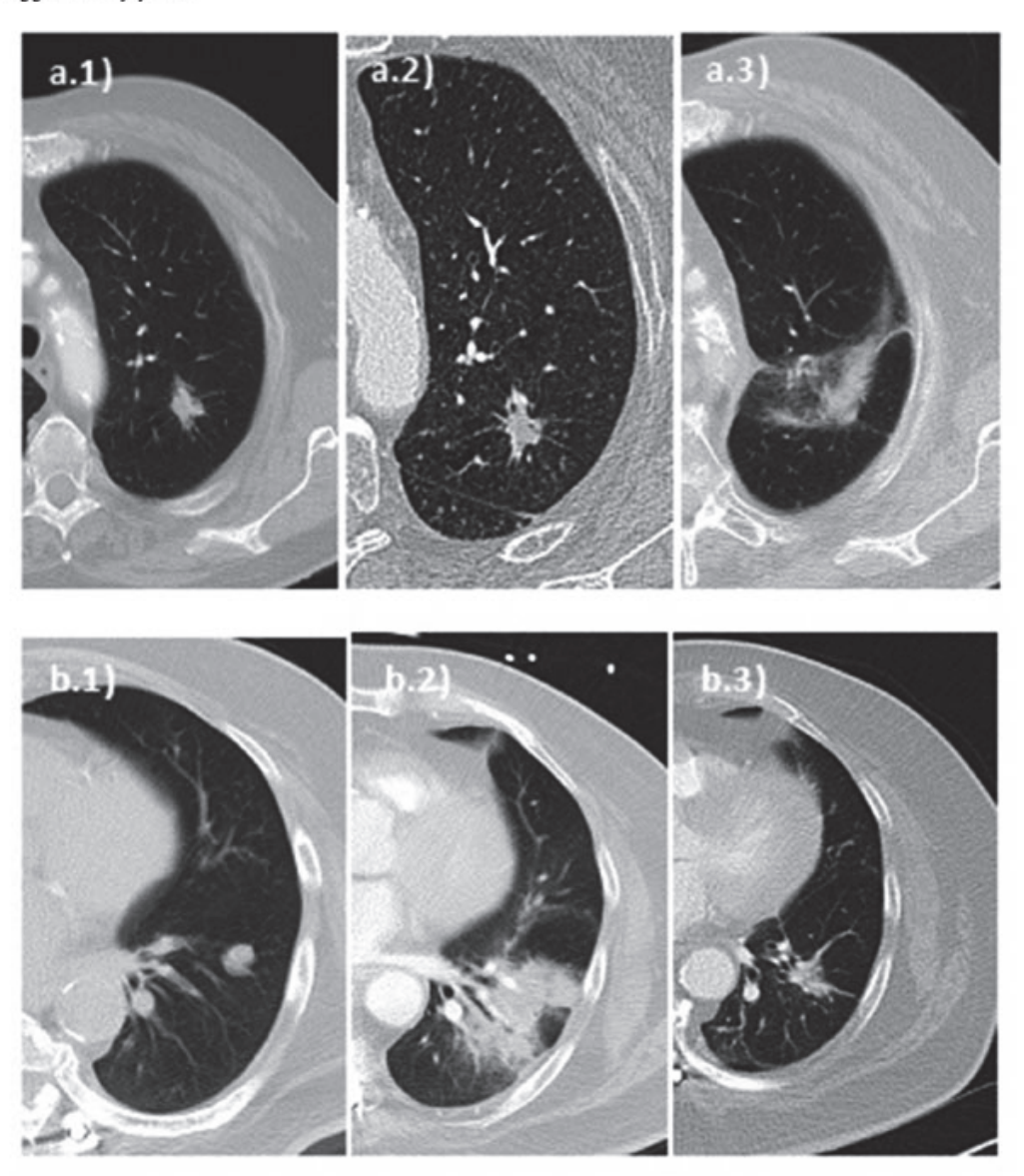


Fig. 3. A.1) pre-treatment, a.2) 6 months and a.3) 2 years follow-up axial chest CT scans (lung window) for a patient who received V300 GyBED₃ = 31 cc and suffered late changes in the parenchyma with an organizing pneumonia pattern. b.1) Pre-treatment, b.2) 6 months and b.3) 2 years follow-up axial chest CT scans (lung window) for a patient who received V300 GyBED₃ = 0 cc, and whose changes in the lung parenchyma with consolidation in the 6 months follow-up scan improved at 2 years with a significant decrease of the consolidation and presence of residual atelectasis.

changes throughout the patient follow up. We were also able to identify a window of BED for which the changes in the lung parenchyma clearly correlate with the dose received in the healthy lung tissue, independently of previous patient conditions or tumor

location. Not only we found that the acute changes observed in the 6 months scan clearly correlated with doses above 300 GyBED₃, but the long-term prevalence of these changes also correlated with a similar dose range.

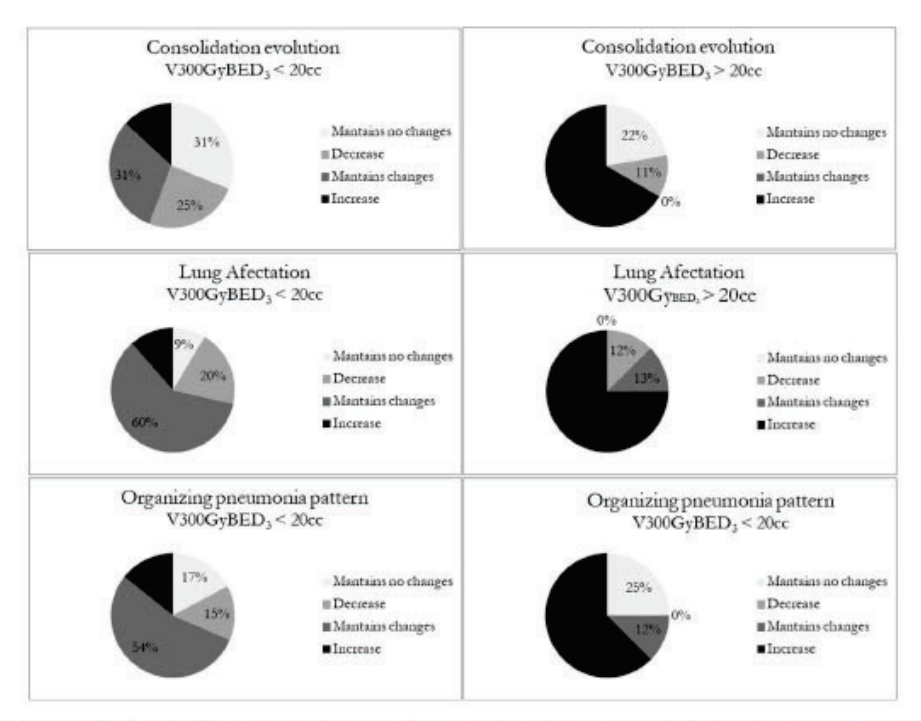


Fig. 4. Long-term evolution of the lung parenchyma in terms of the evolution of the consolidation (top), percentage of lung affectation (middle) and organizing pneumonia pattern (bottom); classified between patients that received 300 GyBED₃ to a volume smaller than 20 cc (left) and greater than 20 cc (right).

Conclusions

This study shows a clear correlation between the irradiation of healthy lung volumes greater than 20 cc to doses over 300 GyBED₃ and the presence of grade I toxicities. This work lays the foundations for the first radiotherapy dose constraint for lung radiological toxicity.

Funding

Research data are not available at this time.

Conflict of Interest

None.

References

- Barriger RB, Forquer JA, Brabham JG, Andolino DL, Shapiro RH, Henderson MA, et al. A dose-volume analysis of radiation pneumonitis in non-small cell lung cancer patients treated with stereotactic body radiation therapy. Int J Radiat Oncol Biol Phys 2012;82:457–62. https://doi.org/10.1016/j.ijrobp.2010.08.056. Epub 2010 Oct 29 PMID: 21035956.
- Epub 2010 Oct 29 PMID: 21035956.
 Bongers BM, Botticella A, Palma DA, Haasbeek CJ, Warner A, Verbakel WF, et al. Predictive parameters of symptomatic radiation pneumonitis following stereotactic or hypofractionated radiotherapy delivered using volumetric modulated arcs. Radiother Oncol 2013;109:95–9. https://doi.org/10.1016/j.radonc.2013.10011_Epub 2013 Oct 31 PMID: 24183862.
 Matsuo Y, Shibuya K, Nakamura M, Narabayashi M, Sakanaka K, Ueki N, et al.
- Dose Volume metrics associated with radiation pneumonitis after stereot actic body radiationtherapy for lung cancer. Int J Radiat Oncol Biol Phys 2012;83: e545-9. https://doi.org/10.1016/j.ijrobp.2012.01.018. Epub 2012 Mar 19 PMID: 22436782

- [4] Saha A, Beasley M, Hatton N, Dickinson P, Franks K, Clarke K, et al. Clinical and dosimetric predictors of radiation pneumonitis in early-stage lung cancer treated with Stereotactic Ablative radiotherapy (SABR) - An analysis of UK's largest cohort of lung SABR patients. Radiother Oncol 2021;156:153-9. https://
- doi.org/10.1016/j.radonc.2020.12.015. Epub 2020 Dec 14 PMID: 33333139.

 [5] Nanda RH, Liu Y, Gillespie TW, Mikell JL, Ramalingam SS, Fernandez FG, et al. Stereotactic body radiation therapy versus no treatment for early stage non-small cell lung cancer in medically inoperable elderly patients: A National Cancer Data Base analysis. Cancer 2015;121:4222–30. https://doi.org/10.1002/
- corc 79540. Epub 2015 Sep 8 PMID: 26348268.

 [6] Ronden MI, Palma D, Slotman BJ, Senan S. Advanced radiation technology committee of the international association for the study of lung cancer. Brief Report on radiological changes following stereotactic ablative radiotherapy (SABR) for early-stage lung Tumors: A pictorial essay. J Thorac Oncol 2018;13:855-62. https://doi.org/10.1016/j.jtho.201802.023. Epub 2018 Mar 6 PMID: 29518554
- 6. PMD: 29518854.
 [7] Horne ZD, Dohopolski MJ, Clump DA, Burton SA, Heron DE, Thoracic reirradiation with SBRT for residual/recurrent and new primary NSCLC within or immediately adjacent to a prior high-dose radiation field. Pract Radiat Oncol 2018;8:e117-23. https://doi.org/10.1016/j.prro.2017.11.011. Epub 2017 Dec 8. PMID: 29724402.
 [8] John C, Dal Bello R, Andratschke N, et al. In-field stereotactic body radioth erapy
- (SBRT) reirradiation for pulmonary malignancies as a multicentre analysis of the German Society of Radiation Oncology (DEGRO). Sci Rep 2021;11:4590.
- https://doi.org/10.1038/s41598-021-83210-3 Maranzano E, Draghini I, Anselmo P, Casale M, Arcidiacono E, Chirico I, et al. Lung reirradiation with stereotactic body radiotherapy. J Radiosurg SBRT 2016;4:61-8. PMID: 29296427; PMCID: PMC5658839.
- [10] Peulen H, Karlsson K, Lindberg K, Tullgren O, Baumann P, Lax I, et al. Toxicity after reirradiation of pulmonary tumours with stereotactic body radiotherapy.

 RadiotherOncol 2011;101:260-6. https://doi.org/10.1016/j radone 2011-90-12. Epub 2011 Nov 5 PMID: 2205534.
 [11] Qiao X, Tullgren O, Lax I, Sirzén F, Lewensohn R. The role of radiotherapy in
- treatment of stage I non-small cell lung cancer. LungCancer 2003;41:1-11. https://doi.org/10.1016/90169-5002(03)00152-1. PMID: 12826306.

 [12] Borghaei H, Paz-Ares L, Horn L, Spigel DR, Steins M, Ready NE, et al. Nivolumab versus docetaxel in advanced nonsquamous non-small-cell lung cancer. N Engl J Med 2015;373:1627-39. https://doi.org/10.1056/NEJMoa1507643. Epub 2015 Sep 27. PMID: 26412456; PMCID: PMC5705936.

 [13] Palma DA, Olson R, Harrow S, Gaede S, Louie AV, Haassbeek C, et al. Stereotactic
- ablative radiotherapy for the comprehensive treatment of oligometastatic

- cancers; long-term results of the SABR-COMET phase II randomized trial. J ClinOncol 2020;38:2830-8. https://doi.org/10.12
- Jun 2. PMID: 32484754; PMCID: PMC7460150. [14] Chalkidou A, Macmillan T, Grzeda MT, Peacock J, Summers J, Eddy S, et al. Stereotactic ablative body radiotherapy in patients with oligometastatic cancers: a prospective, registry-based, single-arm, observational, evaluation study. Lancet Oncol 2021;22:98–106. https://doi.org/10.1016/51470-2045(20) 30537-4. PMID: 33387498.
- 30537-4, PMID: 33387498.

 [15] Cella I, Gagliardi G, Hedman M, Palma G. Injuries from asymptomatic COVID-19 Disease: new hidden toxicity risk factors in thoracic radiation therapy. Int J Radiat Oncol Biol Phys 2020;108:394-6, https://doi.org/10.1016/j. ijrobp.2020.06.055, PMID: 32890518; PMID: PMIC7462877.

 [16] Klement RJ, Sonke JJ, Allgauer M, Andratschke N, Appold S, Belderbos J, et al.
- Correlating dose variables with local tumor control in stereotactic body radiation therapy for early-stage non-small cell lung cancer: A modeling study on 1500 individual treatments. Int J Radiat Oncol Biol Phys 2020;107:579–86. https://doi.org/10.1016/ii/robp.2020.03.005. Epub 2020 Mar 15 PMID:
- 32188579.
 [17] Huang BT, Lu JY, Lin PX, Chen JZ, Li DR, Chen CZ. Radiobiological modeling analysis of the optimal fraction scheme in patients with peripheral non-small cell lung cancer undergoing stereotactic body radiotherapy. Sci Rep 2015;11:18010. https://doi.org/10.1038/srep18010. PMID: 26657569. PMCID: PMC4676016
- PMCID: PMC4676016
 [18] Woody NM, Videtic GM, Stephans KL, Djemil T, Kim Y, Xia P. Predicting chest wall pain from lung stereotactic body radiotherapy for different fractionation schemes. Int J Radiat Oncol Biol Phys 2012;83:427–34. https://doi.org/10.1016/jijrobp.2011.06.1971. Epub 2011 Dec 23 PMID: 22107887.
- [19] Bradley JD, Hope A, El Naça I, Apte A, Lindsay PE, Bosch W, et al. A nomogram to predict radiation pneumonitis, derived from a combined analysis of RTOG 9311 and institutional data. Int J Radiat Oncol Biol Phys 2007;69:985–92.

- https://doi.org/10.1016/Lijrobp.2007.04.077. Epub 2007 Aug 6. PMID: 17689035: PMCID: PMC2196217.
- 17689035; PMCID: PMC2196217.

 [20] Dahele M, Palma D, Lagerwaard F, Slotman B, Senan S. Radiological changes after stereotactic radiotherapy for stage I lung cancer. J Thorac Oncol 2011;6:1221-8. https://doi.org/10.1097/ITO.0b013e318219aac5.

 [21] Hope AJ, Lindsay PE, El Naqa I, Alaly JR, Vicic M, Bradley JD, et al. Modeling radiation pneumonits risk with clinical, dosimetric, and spatial parameters. Int J Radiat Oncol Biol Phys 2006;65:112-24. https://doi.org/10.1016/ji.limbp.2005.11.045. PMID: 16618575.

 [22] Timmerman R, Paulus R, Galvin J, Michalski J, Straube W, Bradley J, et al. Stereotactic body radiation therapy for inoperable early stage lung cancer. J Am Med Assoc 2010;303:1070-6. https://doi.org/10.1001/jama.2010.261. PMID: 202333825. PMICD: PMC2907644.
- PMID: 20233825; PMCID: PMC2907644.
- [23] Travis WD, Costabel U, Hansell DM, King Jr TE, Lynch DA, Nicholson AG, et al. Committee on idiopathic interstitial pneumonias, an official American thoracic society/European Respiratory Society statement: Update of the international multidisciplinary classification of the idiopathic interstitial pneumonias. Am J Respir Crit Care Med 2013;188:733-48. https://doi.org/10.1164/rccm.201308-1483ST. PMID: 24032382; PMCID: PMC5803655.
- 1483ST, PMID: 24032382; PMCID: PMC5803655.
 [24] Gay HA, Niemierko A. A free program for calculating EUD-based NTCP and TCP in external beam radiotherapy. PhysMed 2007;23:115–25. https://doi.org/10.1016/j.ejmp.2007.07.001. Epub 2007 Sep 7 PMID: 17825595.
 [25] Sarudis S, KarlssonHauer A, Nyman J, Bäck A. Systematic evaluation of lung tumor motion using four-dimensional computed tomor motion using four-dimensional computed tomorphy. Acta Oncol 2017;56:525–30. https://doi.org/10.1080/0284186X.2016.1274049. Epub 2017 Jan 11 PMID: 28075183.
 [26] Palma DA, Sepan S, Handheld CAA Mothidel WISAN Management and Computed tomorphisms.
- [26] Palma DA, Senan S, Haasbeek CJA, Verbakel WFAR, Vincent A, Lagerwaard F. Radiological and Clinical pneumonitis after stereotactic lung radiotherapy:a matched analysis of three-dimensional conformal and volumetric-modulated arc therapy techniques. Int J Radiat Oncol 2011;80;506–13. https://doi.org/ 10.1016/j.ljrobp.2010.02.032.

CORRIGENDUM TO PUBLICATION 1



Contents lists available at ScienceDirect

Radiotherapy and Oncology

journal homepage: www.thegreenjournal.com



Original Article

Corrigendum to "Biological effective dose is associated with radiological toxicity after lung stereotactic ablative radiation therapy" [Radiother. Oncol. 183 (2023) 109552]



Carla Cases a, Mariana Benegas b,c, Marcelo Sánchez b,c, Ivan Vollmer b,c,d, Francesc Casas a, Carles Gomà a,c., Meritxell Mollà a.e.f

* Department of Radiation Oncology, Hospital Clinic de Barcelona, Bara-brus, Spain; * Department of Radiology, Hospital Clinic de Barcelona, Barcelona, Spain; * Translational Research in Pulmonary Vaccular Diseases: Gell Proliferation and Apoptotic Mechanisms in Pulmonary Actebral Hypertension, Institute for Biomedical Research August Pi i Sunyer (IDIBAPS), Barcelona, Spain; *Translational Genomics and Tangeted Therapies in Solid Tumors, Institute for Biomedical Research August Pi i Sunyer (IDIBAPS), Barcelona, Spain; * Department of Clinical Foundations, University of Barcelona, Barcelona, Spain

After publication of the abovementioned article, the authors regret that an inaccuracy has been noticed. In the title, abstract

and text the term "Biological Equivalent Dose (BED)" should read "Biological Effective Dose (BED)".

The authors apology for any inconvenience caused.

https://doi.org/10.1016/j.radonc.2023.109776 0167-8140/ 0 2023 Elsevier B.V. All rights reserved.

DDI of original article: https://doi.org/10.1016/j.radonc.2023.109552

* Corresponding author at: Department of Radiation Oncology, Hospital Clinic de Baucelona, Carer de Villarres! 170, 0856 Barcelona, Spain.

E-mail address: gomi-Petinic.cat (C. Gomi).

PUBLICATION 2

Cases C, Mollà M, Sánchez M, Benegas M, Ballestero M, Serrano-Rueda S, Antelo G, Gomà C. Feasibility and potential clinical benefit of dose de-escalation in stereotactic ablative radiotherapy for lung cancer lesions with ground glass opacities. Physics and imaging in radiation oncology, 32, 100681. https://doi.org/10.1016/j.phro.2024.100681



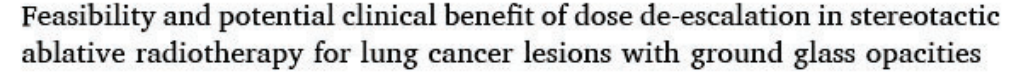
Contents lists available at ScienceDirect

Physics and Imaging in Radiation Oncology

journal homepage: www.sciencedirect.com/journal/physics-and-imaging-in-radiation-oncology



Original Research Article





- Department of Radiation Oncology, Hospital Clinic, Barcelona Spain
 Translational Genomics and Targeted Therapies in Solid Tumors, Institute for Biomedical Research August Pi i Sunyer (IDIBAPS), Barcelona, Spain
 Department of Clinical Foundations, University of Barcelona, Barcelona Spain
 Thoracic Oncology Unit, Hospital Clinic, Barcelona Spain

- * Department of Radiology, Hospital Clinic, Barcelona Spain

ABSTRACT

Introduction: Treatment of neoplasic lung nodules with ground glass opacities (GGO) faces two primary challenges. First, the standard practice of treating GGOs as solid nodules, which effectively controls the tumor locally, but might increase associated toxicities. The second is the potential for dose calculation errors related to increased heterogeneity. This study addresses the optimization of a dose de-escalation regime for stereotactic ablative radiotherapy (SABR) for OGO lesions.

Materials and Methods: We used the CT scans of 35 patients (40 lesions) with some degree of GGO component treated at our institution between 2017 and 2021. We first assessed the dose calculation accuracy as a function of the GGO component of the lesion. We then analysed the advantages of a dose de-escalation regime in terms of lung dose reduction (Dmean, V20Gy and V300GyBED3) and plan robustness.

Results: We found a positive correlation between the presence of OGO and the dose calculation errors in a phants m scenario. These differences are reduced for patient data and in the presence of breathing motion. When using a de-escalation regime, significant reductions were achieved in mean lung dose, V200y and V3000yBED3. This study also revealed that lower doses in GGO areas lead to more stable fluence patterns, increasing treatment robustness.

Conclusions: The study lays the foundation for an eventual use of dose de-escalation in SABR for treating lung lesions with GGO, potentially leading to equivalent local control while reducing associated toxicities. These findings lay the groundwork for future clinical trials.

1. Introduction

Lung stereotactic ablative radiotherapy (SABR) has proven to be an effective treatment for inoperable lesions, offering good local control (LC) and a low incidence of grade ≥ II toxicities [1-4]. Most lung SABR treatments target solid pulmonary nodules. However, an increasing percentage are administered to nodules with some component of ground-glass opacity (GGO). These opacities are present in minimally invasive adenocarcinomas, lepidic-predominant adenocarcinomas, and invasive mucinous adenocarcinomas and exhibit a more indolent clinical course [5-8]. Furthermore, the GGO component is considered to correspond to a non-invasive histology, while the solid component is considered as the invasive part of the lesion [9]. Nonetheless, with the widespread use of screening [10], small-sized pulmonary nodules, especially those containing GGO component, are increasingly detected [11].

Over the years, several SABR regimes have been used to treat lung lesions. Some studies have analyzed different SABR regimes in terms of biologically effective dose (BED) and its relation to local control [12] and/or clinical toxicity [4,13,14]. Over the last years, lower BED regimes have been prioritized to reduce toxicities. However, it has been reported that lowering the prescribed BED below the threshold of 100 Gybedio (where the subscript 10 refers to the alpha/beta ratio considered for calculation) comes at the cost of lower LC rates [15,16].

In this context, which sets a lower threshold to grant acceptable LC rates, and an upper threshold to reduce associated toxicities, some groups have studied the use of different dose levels within the lesion for specific cases. Dose de-escalation has been proposed to avoid chest wall toxicity, while maintaining LC rates [17]. Conversely, others have analyzed the outcomes of using a simultaneously integrated boost for larger lesions [18] achieving promising LC rates.

The SABR treatment of GGO faces two primary challenges. The first is the standard practice of treating GGO as solid nodules. This approach is problematic when treating a small solid component within a larger GGO, as the risk of lung toxicity correlates with the volume of lung receiving a high dose [19]. While this strategy effectively controls the

E-mail address: cases@clinic.cat (C. Cases).

https://doi.org/10.1016/j.phro.2024.100681

Received 24 April 2024; Received in revised form 20 November 2024; Accepted 20 November 2024 Available online 29 November 2024

2405-6316/© 2024 The Authors. Published by Elsevier B.V. on behalf of European Society of Radiotherapy & Oncology. This is an open access article under the CC BY-NG-ND license (http://creativecommons.org/licenses/by-nc-nd/4.0/).

^{*} Corresponding author.

tumor locally [20], it increases the risk of damaging healthy lung tissue to a lesion expected to have better LC rates [21]. Tailoring SABR treatments for this kind of lesion seems advisable, as GGO tumors are often multifocal and may require multiple subsequent irradiations.

The second challenge involves the potential for large dose calculation errors by commercial dose calculation algorithms, owing to the increased heterogeneity of GGO lesions [22–24]. To our knowledge, no studies have yet evaluated the dose calculation errors in GGO lesions. Furthermore, challenges related to fluence peaks during optimization should be considered, as they lead to less robust dose distributions [25]. This effect is especially significant when optimizing with type C algorithms and several approaches have been presented for solid lesions [26,27]. With all the aspects in mind, optimizing SABR treatment for GGO malignancies is an essential step to ensure the best treatment option for these malignancies, which are expected to be increasingly diagnosed.

In this study we focus on analyzing the feasibility of performing a dose de-escalation that ensures dose calculation accuracy and robustness. We propose a method to efficiently implement dose de-escalation for lung lesions containing varying amounts of GGO component and report the expected differences in lung dose, robustness, and dose accuracy compared to the standard approach of a single dose level.

2. Materials and methods

To assess the technical feasibility of dose de-escalation, we used two datasets. First, we analyzed dose calculations performed on the CT scan of a thoracic static anthropomorphic phantom (IMRT Thorax phantom, CIRS, SUN Nuclear, Norfolk). Second, we evaluated the dose calculation accuracy, dose reduction achieved, and the robustness of the plan on the CT scans of 40 lesions (from 35 patients) treated at our institution between 2017 and 2021, which exhibited some component of GGO in the lesion.

To describe the amount of GGO present in the lesion, we used the consolidation to tumor ratio (CTR), defined as the diameter of the solid part of the lesion divided by the total diameter [28]. In this study, we have also included the volumetric CTR (CTR $_{\nu}$), defined as the volume of the solid component divided by the total lesion volume.

Our patients were originally treated following the Radiation Therapy Oncology Group (RTOG) 0236 trial protocol and the giudelines included in the clinical study approved by the ethics board at our institution. We prescribed two fractionation schemes, depending on the size, centrality, and proximity of the tumor to organs at risk. The schemes consisted of 3 fractions of 18 Gy or 5 fractions of 11 Gy. The radiation oncologist defined the internal target volume (ITV) using the 10 phases of the 4DCT, as it allowed a better differentiation of the solid and GGO component. An isotropic margin of 3 mm was added to the ITV to define the planning target volume (PTV). We optimized the treatment using volumetric modulated arc therapy (VMAT), with a dose normalization ensuring that the 100 % isodose level encompassed 95 % of the PTV.

The BED of the two considered fractionation schemes for the GTV are $115~\mathrm{Gy}$ geD10, and $151~\mathrm{Gy}$ geD10 for the 5, and 3 fractions case, respectively. Our dose de-escalation strategy was to lower the dose to the GGO component of the PTV to $100~\mathrm{Gy}_{\mathrm{BED10}}$, while maintaining the dose to the solid part as per the original prescription, thus reducing the prescribed dose to the GGO component to $10~\mathrm{Gy}$ and $14~\mathrm{Gy}$ for the 5 and 3 fraction case respectively.

2.1. Evaluation of dose calculation accuracy as a function of GGO component

To evaluate the dosimetric impact of the algorithm used, we first used the CT scan of the thoracic phantom. We contoured a set of spherical lesions in the lung region with diameters of 10, 15, 20, 30, and 40 mm; and CTRs of 0, 0.25, 0.50, 0.75 and 1 for every diameter. We manually assigned a physical material value to each region inside the

PTV: water (1 g/cm³) for the solid kernel and lung (0.6134 g/cm³) for the GGO shell (Fig. 1). Regarding the clinical cases, we studied two scenarios: (i) the average reconstruction of a 4DCT scan simulating an ITV approach, and (ii) the 50 % expiration phase of the 4DCT scan, to simulate the results in the case of a gated treatment, which could further improve the dose reduction [32]. The solid component and the GGO component were delimited in each phase of the CT scan, and a solid ITV (ITVs) and a GGO ITV (ITVGGO) were defined. Their corresponding PTVs were also defined by adding a 3 mm margin to their corresponding ITV

To evaluate dose inaccuracies in both datasets, we calculated (Eclipse v16.0) VMAT treatment plans with a dose prescription of 55 Gv in 5 fractions. We optimized and calculated the dose distribution using AAA and then recalculated these plans using AXB_{m,m} (m,m indicates transport in medium, dose to medium) with fixed monitor units (MU). Optimization was performed with heterogeneity corrections activated during the optimization process, using coplanar half arcs with couch structures included. Normal Tissue Objective (NTO) parameters were set manually to ensure a fast dose fall off beyond the PTV. To ensure a correct dose calculation it was crucial to take into consideration the multileaf collimator (MLC) characterization as well as the accuracy of the planning system for small fields [29]. The MLC was characterized in the treatment planning system following the recommendations by Saez et al [30]. Minimum jaw field size was set to 35 mm, while the output of smaller fields, conformed with MLC, was verified using EBT4 radiochromic films [31]. To reduce complexity of the plans the aperture shape controller was set to high strength and total MU were limited according to the prescribed dose per session in the optimization process. This ensured an acceptable dose distribution while avoiding unnecessary MLC modulation.

We analyzed the relationship between CTR and the relative differences between D98% (Gy) and D2% (Gy) on the PTV. Furthermore, Dmean was analyzed for the PTV-ITV area, where the differences are expected to be more appreciable due to density differences. For ease of interpretation we divided the sample in two groups, the first one with CTRs ranging from 0 and 0.33 (low CTR) and the second one with CTRs above 0.33 (mid-high CTR).

2.2. Evaluation of lung dose reduction after dose de-escalation

To evaluate the treatment plans with the least amount of variability, we reoptimized and recalculated with ${\rm AXB_{m,m}}$ the dose distribution for the 40 lesions with a limited set of optimization parameters. The same physicist optimized the plans with the original dose prescription and with a dose reduction to the GGO component and following the same optimization procedure. For the standard approach, dose was normalized to ensure 100 % of the prescribed dose covered 95 % of the PTV. For the de-escalation case, dose was normalized to ensure 100 % of the prescribed dose covered 95 % of the solid PTV. The dose to the GGO component of the PTV (Fig. 1) was lowered as much as possible, but always granting that at least 100 % of the lower dose covered 95 % of the GGO PTV. Maximum doses were limited to 140 % of the prescribed dose. Other parameters were optimized following the RTOG 0236 trial protocol. The characteristics of the analysed lesions in terms of CTR, CTRv, lesion size and prescription are summarized in Table 1.

We analyzed the lung dose reduction in terms of the mean lung dose (Dmean) and the percentage of volume receiving 20 Gy (V20Gy), as they are associated with grade II or higher toxicities. We also analyzed the absolute volume of the lung receiving V300Gy_{BED3}, as it has recently been correlated with radiological toxicity [19]. Furthermore, for those patients with more than one lesion, we analyzed the same parameters considering the treatment of both lesions simultaneously.

We statistically analyzed the differences for Dmean, V20Gy and V300GyBgD3 between the standard prescription and the de-escalation protocol using a paired t-test using RStudio software version 2022.07.2. We also analyzed the correlation between the lung dose

2

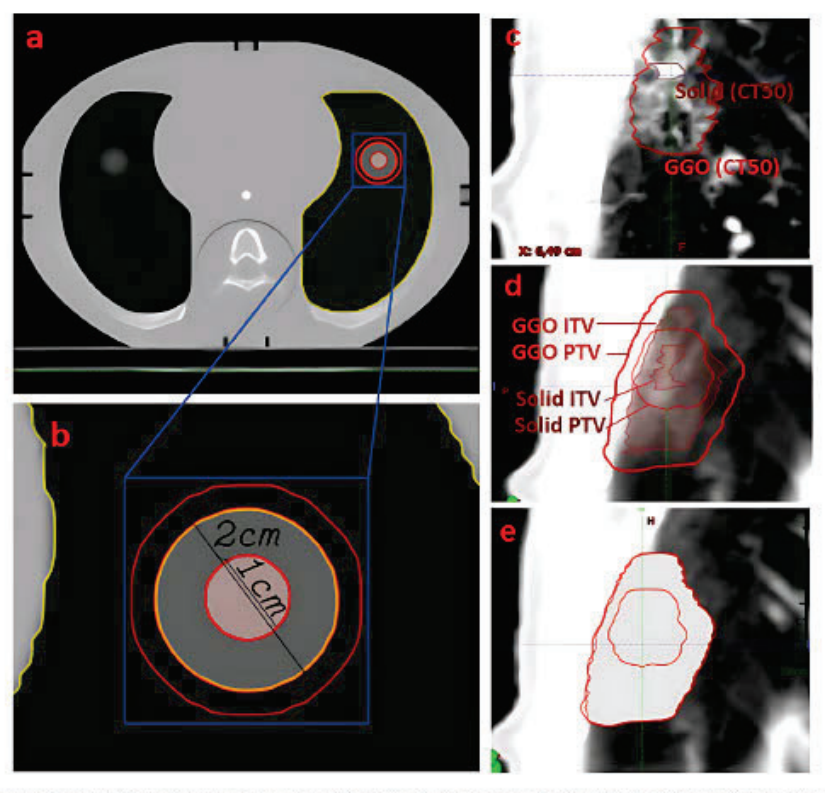


Fig. 1. Definition of target volumes. (a) Lung Phantom with a soomed figure to a lesion corresponding to CTR of 0.5. Figure (c) is an example of the GTV volume delineation of a patient lesion on the 50 % expiration phase (CTS0). The accumulated GTV was generated in the Average reconstruction of the 4DCT (d) to create the ITV. A 3 mm margin was added to generate the PTV. In Figure (e) we can see the structure set with the PTV area density and material overwritten to water to evaluate robustness.

reduction and the CTR and CTR_v using the Spearman's Ranks correlation

2.3. Evaluation of dose distribution robustness

To evaluate the robustness of the treatment when optimizing with two dose levels with AXB $_{\rm m,m}$, we used three datasets: Firstly, we used the plan optimized using AAA dose calculation algorithm with one dose level. Secondly, the same plan optimized using AXB $_{\rm m,m}$ with one dose level and, finally, a plan optimized using AXB $_{\rm m,m}$ with two dose levels (dose reduction to the GGO). These plans were optimized using the average CT scan of the 4DCT.

We then recalculated $(AXB_{m,m})$ with fixed MU these three plans to a new average CT with the PTV volume overridden (material and HU) to water (Fig. 1). When recalculated in water, possible fluence peaks in the area surrounding the ITV become apparent and comparison between algorithms is performed under the same dose transportation and deposit conditions. The analysis of these peaks allowed us to evaluate robustness of the plan against any motion of the GTV within the PTV region. To evaluate the magnitude of these fluence peaks, we compared the mean dose to the ITV with the dose to the ring between the ITV and the PTV (DmeanP-I/DmeanITV). Differences between the three scenarios were evaluated using a one-way ANOVA test.

3. Results

3.1. Evaluation of dose calculation accuracy as a function of GGO component

In the phantom case, we found relevant differences between the dose distributions calculated by the two algorithms in correlation with the CTR value. As shown in Fig. 2, the low CTR group (high GGO component) presented higher differences than the mid-high CTR group for the D2% parameter. While for the low CTR group the average difference between algorithms was 2 %, for the high CTR group this difference was reduced to 1 %. These differences were statistically significant (p = 0.04) and were also correlated with CTR for D98% (p = 0.04), going from an average difference of 2.5 % to 2 %.

In the clinical cases, the lesions led to PTVs with an equivalent sphere diameter ranging from 9.8 to 24.5 mm and CTRs from 0.00 to 0.90. Both variables were roughly normally distributed. Dose differences between both algorithms were found as previously reported in the literature. Differences in D2% were on average 1 % ranging from 0.5 % to 5.4 %. Differences in D98% between both algorithms were higher, with an average value of 6 % ranging from 0.5 % to a 20 %. In this case, however, neither the ITV scenario (Average CT) nor the gated scenario revealed any statistically significant difference between the two CTR groups.

3.2. Evaluation of lung dose reduction after dose de-escalation

The lung dose reduction obtained in terms of V300GyBED3, Dmean

3

Table 1
Summary of patient treatment characteristics, lesion volumes and CTR and lung dose, for the standard treatment and the dose de-escalation case.

	Average [min; max]	
PTV Volume (cm³)	06.54.643	
Sòlid PTV Volume	26 [4; 64]	
(cm ³)	12 [0; 35]	
GGO PTV Volume	13 [2; 44]	
(cm ³)	15 (2, 44)	
CTRv	0.52 [0; 0.93]	
CTR	0.69 [0; 0.97]	
	N	
Number of lesions	40	
3 @ 18 Gy	9	
5 @ 11 Gy	31	
Patients with 1 lesion	30	
3 @ 18 Gy	7	
5 @ 11 Gy	23	
Patients with two	5	
lesions		
3 @ 18 Gy	1	
5 @ 11 Gy	4	
Lung Dose Evaluation	Standard	Dose de- escalation
Dmean (Gy)	3.5 [1; 8]	3.1 [1; 7]
V20Gy (%)	4.3 [1; 13]	3.6 [1; 10]
V300GyBED3 (cm²)	15.6 [2; 57]	7.1 [0; 29]
Multiple lesion patients		
Dmean (Gy)	5.0 [3,1; 7,1]	4.4 [2.5; 7]
V20Gy (%)	6.1 [5,0; 8]	5.4 [3.5; 7]
V300GyBED3 (cm ³)	21.5 [6,5; 34]	5.1 [0.7; 16]

and V20Gy can be seen in Fig. 3. An average reduction of 9 % (0.5 Gy) of Dmean was obtained. A reduction of V20Gy, from 3.6 % to 4.2 % and V300Gy_{BED3} going from an average volume of $16~{\rm cm}^3$ to $7~{\rm cm}^3$ were also observed. Differences in all three variables were statistically significant

(p < 0.01). When focusing the subgroup with a GGO volume above 20 cm³, the reduction in Dmean and V20Gy increased to a 5.3 % and 8.5 % respectively and we observed an average V300Gy_{BED3} reduction of 21 cm³.

For V300Gy_{BED3} the number of lesions with an absolute lung volume greater than 20 cm³ went from 11 to 2 cases. The number of lesions with V300Gy_{BED3} > 30 cm³ went from 4 to none.

Spearman's correlation between CTR or CTRv (Fig. 4) with the differences observed in lung doses ranged between 0.3 for V20Gy to 0.53 for V300Gy_{BED3}, indicating a low to moderate correlation (p < 0.05). The correlation was clearer when we analyzed the lung dose reduction in terms of the absolute volume of the GGO component of the lesion, ranging from a correlation of 0.56 for V20Gy to 0.78 for V300Gy_{BED3} (p < 0.05). As it can also be seen in Fig. 4, the patients with GGO above 20 cm³ all achieved a significant reduction in lung dose, with an average V300Gy_{BED3} reduction of 21 cm³, a reduction of Dmean of 0.5 % and a reduction in V20Gy of 1.1 %.

It is compelling to analyze the 5 patients with 2 lesions (Table 1). For these patients a mean lung dose reduction of 14 % (0.5 Gy) was obtained, with V20Gy going from 6 % to 5.4 %. The most significant reduction was obtained for V300GyBED3 with 3 out of 5 patients going from volumes above 20 cm³ to all of them being below 20 cm³, and an average reduction of 16 cm³.

3.3. Dose distribution robustness

As it has been previously reported, we observed fluence peaks in the low-density area surrounding the PTV (Fig. 5). This effect was more evident when using $AXB_{m,m}$ during the optimization process and led to bigger fluence peaks compared to AAA (p = 0.02). When recalculated to water, the average dose for the region between the ITV and the PTV had an average dose of 0.98 for the AAA case compared to the ITV average dose. This value increased to an average of 1.015 for the $AXB_{m,m}$ case, showing a higher average dose on the area between the ITV and the PTV than within the ITV.

The analysis of the same parameters for the dose de-escalation case can be seen in Fig. 5. As it can be seen the fluence peaks were almost nonexistent (with an average value of 0.96 compared to the ITV dose value), similarly to the AAA-optimized scenario (p > 0.05) but clearly lower than the original AXB_{m,m} optimization (p < 0.01).

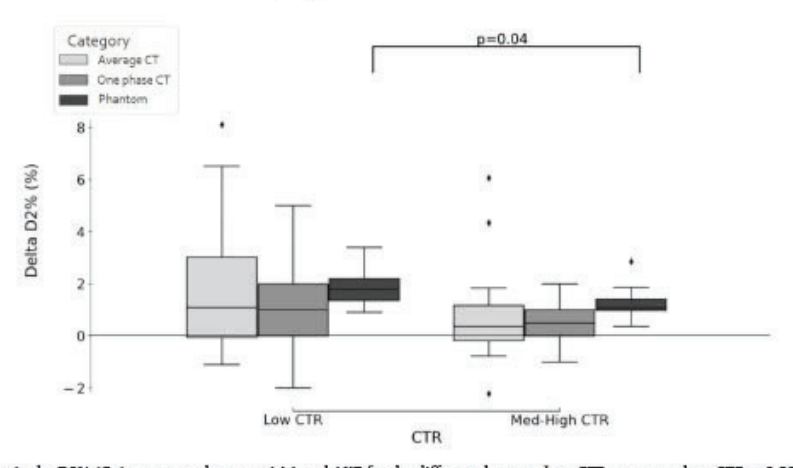


Fig. 2. Relative difference in the D2% (Gy) parameter between AAA and AXB for the different datasets. Low GTR corresponds to GTR < 0.33, while Med-High to GTR > 0.35. Differences are statistically significant only for the phantom case.

4

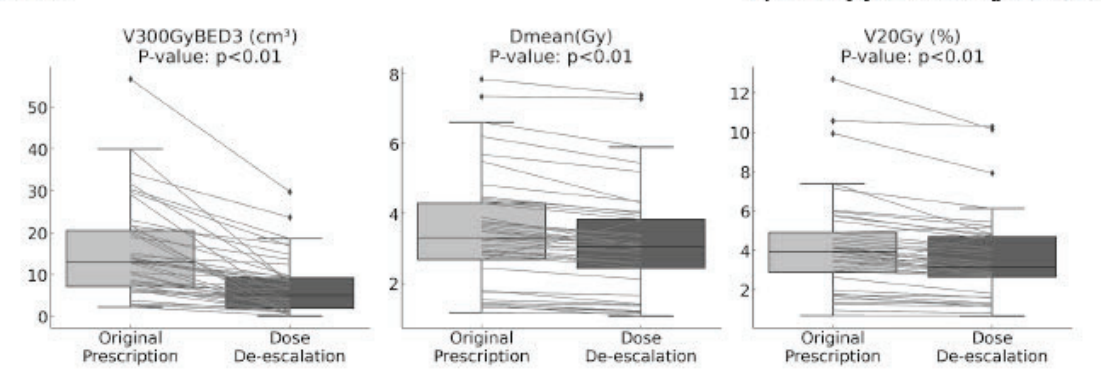


Fig. 3. Dose differences in the lung between the standard dose prescription and the dose de-escalation approach. Left: Reduction of V300GyBED3, with an average difference from 16 cm³ to 7 cm³. Center: Differences in lung Dmean, with an average reduction of 0.5 Gy. Right: V20Gy (%) showing a reduction from 4.2 % to 3.6 %.

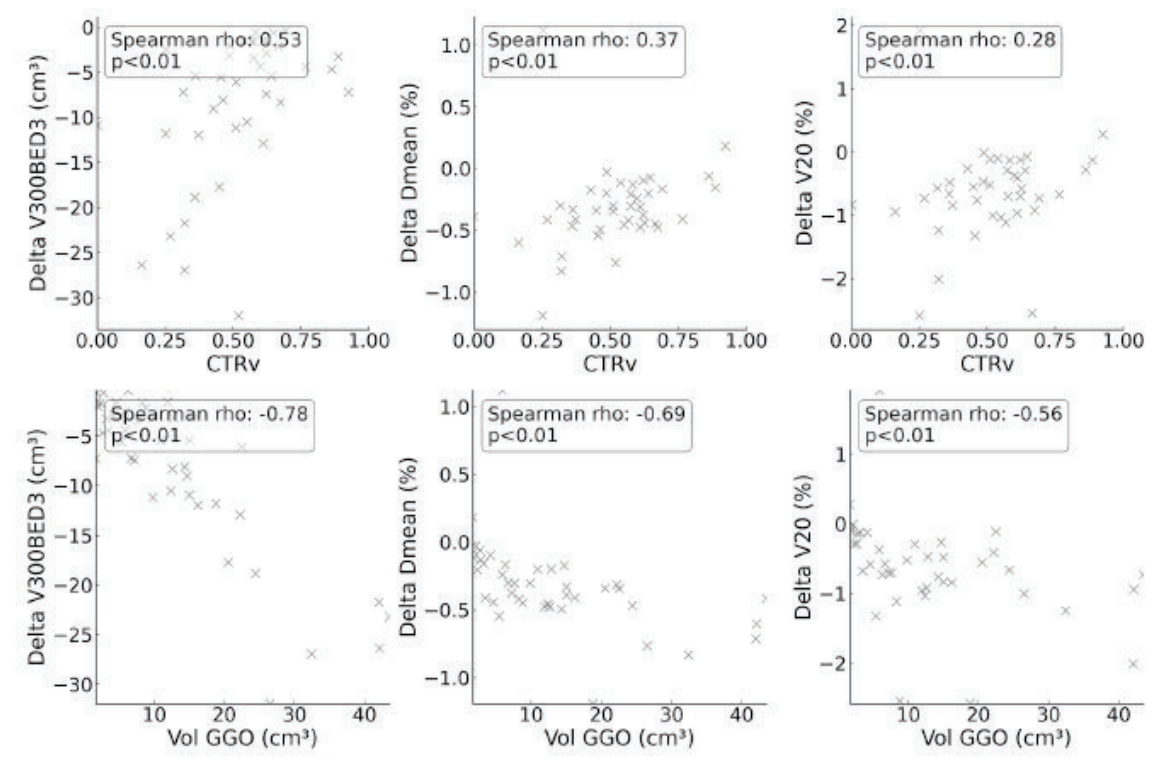


Fig. 4. Dose reduction in the lung between the standard dose prescription and the dose de-escalation approach in lung in terms of CTRv (top) or absolute Volume of the GGO PTV component (bottom). Dose reduction is analysed in terms of V300GyBED3 (Left), Dmean (centre) and V20Gy (%) (Right).

4. Discussion

In this study, we have analyzed the technical feasibility and potential benefit of a dose de-escalation strategy for the SABR treatment of lung lesions with GGO component. Regarding dose calculation accuracy, we have observed larger discrepancies when using type B calculation engines, such as AAA, for lower CTR values. These differences are lesvident for blurrier borders between the solid and the GGO components, and even less significant when breathing motion is present. Although the observed differences between AAA and AXB $_{\rm m,m}$ are similar in magnitude

to the ones previously reported [23], extra care should be taken in SABR treatments involving GGO, especially for low CTR or when using gating strategies.

Dose de-escalation strategies have been successfully used previously in the context of SABR in the lung to prevent chest wall toxicities [17]. In our study, we have demonstrated that by de-escalating the dose in the GGO region, there is a systematic reduction of lung Dmean, V20, and V300GyBED3. Although these differences are small in some cases, they become relevant for lesions that contain a higher volume of GGO. It is for this group of patients that LC rates are expected to be higher [33]. From

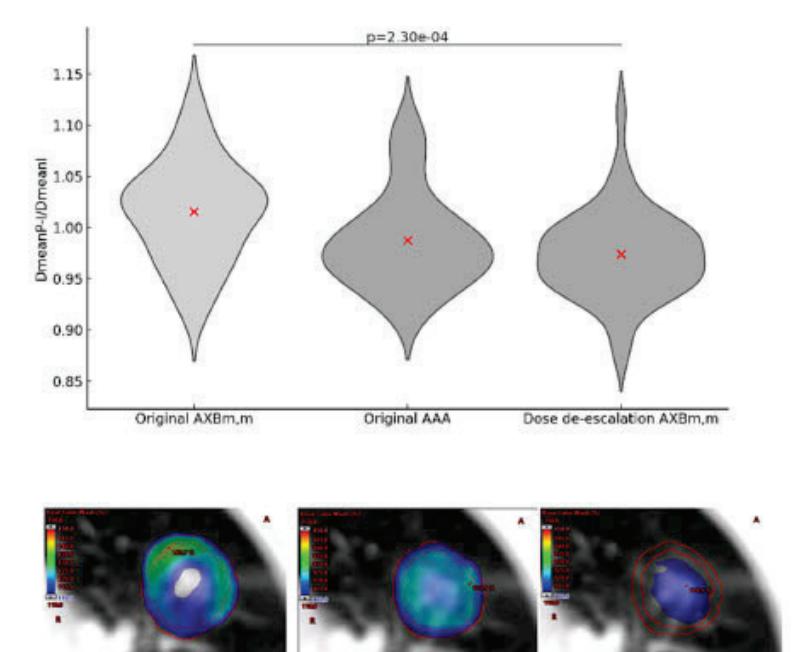


Fig. 5. Top: Robustness analysis in terms of Mean dose to the PTV -ITV area (MeanP-I) divided by mean dose to the ITV. Bottom: Dose distribution of one of the patients for the three cases of the top figure, in the same order. Colour wash levels are fixed for the three cases with the lower threshold at 110% of the prescribed dose and the upper threshold to the 150% of the prescribed dose.

the author's point of view, patients with CTR below 0.5 or absolute GGO volumes above 20 cm3 would benefit from a dose de-escalation regime.

Finally, the lower dose in the GGO area, which is generally surrounding the solid lesion, provides a naturally more robust fluence, reducing the necessity to apply any strategy to mitigate fluence peaks. In contrast to the plans obtained when the dose distribution is forced to deliver high doses to less dense tissues, a dose de-escalation to the lesser dense tissue surrounding the solid nodule allows for more robust fluences.

This study, while providing insights into dose de-escalation strategies, has some limitations. The sample size was sufficient to derive some statistical conclusions. However, a more extensive study population. including more cases of very low CTR and high GGO volume, would provide a better understanding of the impact of the dose reduction. Furthermore, this study only evaluates the technical feasibility of the technique using Ecplise as optimization and calculation engines. The results observed in this study should not be directly assumed for other planning systems.

In conclusion, this work shows that a dose de-escalation strategy to lung cancer lesions with ground glass opacities is feasible in the context of SABR and dosimetrically advantageous. The use of a de-escalation scheme, maintaining the dose to the solid component of the lesion while reducing the dose to the GGO component, could lead to lower associated lung toxicities while maintaining local control. We believe that this work sets the basis for the design of a dose de-escalation clinical trial for GGO lesions, which should evaluate whether the reduction in lung dose observed here in silico translates to a reduction of lung toxicity in patient.

Declaration of competing interest

The authors declare that they have no known competing financial

interests or personal relationships that could have appeared to influence the work reported in this paper.

REFERENCES

- [1] Barriger RB, Forquer JA, Brabham JG, Andolino DL, Shapiro RH, Henderson MA, et al. A dose-volume analysis of radiation pneumonitis in non-small cell lung cancer patients treated with stereotactic body radiation therapy. Int J Radiat Oncol
- Biol Phys 2012;82(1):457–62. https://doi.org/10.1016/j.ijrobp.2010.08.056.

 [2] Bongers EM, Botticella A, Palma DA, Haasbeek CJ, Warner A, Verbakel WP, et al. Predictive parameters of symptomatic radiation pneumonitis following stereotactic or hypofractionated radiotherapy delivered using volumetric modulated arcs. ther Oncol 2013 Oct:109(1):95-9, https://
- radone. 2013.10.011. Epub 2013 Oct 31 PMD: 24183862.

 [3] Matsuo Y, Shibuya K, Nakamura M, Narabayashi M, Sakanaka K, Ueki N, et al. Dose-volume metrics associated with radiation pneumonitis after stereotactic body radiation therapy for lung cancer. Int J Radiat Oncol Biol Phys 2012 Jul 15;83(4): e545-9. https://doi.org/10.1016/j.ijrobp.2012.01.018. Epub 2012 Mar 19 PMID: 22436782
- aha A, Beasley M, Hatton N, Dickinson P, Franks K, Clarke K, et al. Clinical and dosimetric predictors of radiation pneumonitis in early-stage lung cancer treated with Stereotactic Ablative radiotherapy (SABR) - An analysis of UR's largest cohort of lung SABR patients. Radiother Oncol 2021 Mar;156:153-9. https://doi.org/
- nc. 2020. 12.015. Epub 2020 Dec 14 PMID: 33333139. Chen H. Management of Ground-Glass Opacities in the Lung Cancer [5] Zhang Y, Pu F, Chen H. Managen Spectrum. Ann Thorac Surg 2020;110(6):1796-804. https:/
- [6] Fu F, Zhang Y, Wen Z, Zheng D, Gao Z, Han H, et al. Distinct Prognostic Pactors Patients with Stage I Non-Small Cell Lung Cancer with Radiologic Part-Solid or Solid Lesions, J Thorac Oncol 2019 Dec;14(12):2133-42, https://doi.org/10.1016/
- J.jtho. 2019.08.002. Epub 2019 Aug 19 PMID: 31437531.

 [7] Ye T, Deng I, Wang S, Xiang J, Zhang Y, Hu H, et al. Lung Adenocarcinomas Manifesting as Radiological Part-Solid Nodules Define a Special Clinical Subtype. J Thorac Oncol 2019 Apr;14(4):617–27. https://doi.org/10.1016/j. jtho.2018.12.030. Epub 2019 Jan 17 PMID: 30659988. [8] Chang B, Hwang JH, Choi YH, Chung MP, Kim H, Kwon OJ, et al. Natural history of
- [8] Chang B, Hwang JH, Choi YH, Chung MP, Xim H, Xwo OJ, et al. Natural nistory or pure ground-glass opacity lung nodules detected by low-dose CT scan. Chest 2013 Jan;143(1):172–8. https://doi.org/10.1378/chest.11-2501. PMID: 22797081.
 [9] Li H, Wang Y, Chen Y, Zhong C, Fang W. Ground glass opacity resection extent assessment trial (GREAT): A study protocol of multi-institutional, prospective, open-label, randomized phase III trial of minimally invasive segmentectomy versus

- lobectomy for ground glass opacity (GGO)-containing early-stage invasive lung ndenocarcinoma. Pront Oncol 2023 Jan;19(13):1052796.
- [10] National Lung Screening Trial Research Team; Aberle DR, Adams AM, Berg CD, Black WC, Clapp JD, Pagerstrom RM, et al. Reduced lung-cancer mortality with low-dose computed tomographic screening. N Engl J Med. 2011 Aug 4;365(5):395-409. 10.1056/NEJMoa1102873. Epub 2011 Jun 29. PMID: 21714641; PMCID:
- [11] Travis WD, Brambilla E, Noguchi M, Nicholson AG, Geisinger KR, Yatabe Y, et al. nternational association for the study of lung cancer/american thoracic society/ european respiratory society international multidisciplinary classification of lung adenocarcinoma. J Thorac Oncol 2011 Feb;6(2):244-85. https://doi.org/10.1097/
- [12] Klement RJ, Sonke JJ, Allgäuer M, Andratschke N, Appold S, Belderbos J, et al. Correlating Dose Variables with Local Tumor Control in Stereotactic Body Radiation Therapy for Early-Stage Non-Small Cell Lung Cancer: A Modeling Study on 1500 Individual Treatments. Int J Radiat Oncol Biol Phys 2020 Jul 1;107(3): 579-86. https://doi.org/10.1016/j.ijrobp.2020.03.005. Epub 2020 Mar 15 PMID: 32188579.
- [13] Huang BT, Lu JY, Lin PX, Chen JZ, Li DR, Chen CZ. Radiobiological modeling analysis of the optimal fraction scheme in patients with peripheral non-small cell lung cancer undergoing stereotactic body radiotherapy. Sci Rep 2015 Dec;11(5):
- [14] Woody NM, Videtic GM, Stephans KI, Djemil T, Kim Y, Xia P. Predicting chest wall pain from lung stereotactic body radiotherapy for different fractionation schemes. Int J Radiat Oncol Biol Phys 2012 May 1;83(1):427–34. https://doi.org/10.1016/j.
- into Facinat cincol Biol Phys 2012 May 1,33(1):427-34. https://doi.org/10.1016/j.ijrobp.2011.06.1971. Bpub 2011 Dec 23 PMID: 22197087.

 [15] Zhang J, Yang F, Li B, Li H, Liu J, Huang W, et al. Which is the optimal biologically effective dose of stereotactic body radiotherapy for Stage I non-small-cell lung cancer? A meta-analysis. Int J Radiat Oncol Biol Phys 2011 Nov 15;81(4):e305-16. https://doi.org/10.1016/j.ijrobp.2011.04.034. Bpub 2011 Jun 12 PMID: 2165805-2
- [16] Bradley JD, Hope A, El Naqa I, Apte A, Lindsay PE, Bosch W, et al. A nomogram t predict radiation pneumonitis, derived from a combined analysis of RTOG 9311 and institutional data. Int J Radiat Oncol Biol Phys. 2007 Nov 15;69(4):985-92. 10.1016/j.ijrobp.2007.04.077. Epub 2007 Aug 6. PMID: 17689035; PMCID:
- [17] Ladbury CJ, Sampath S. Lung stereotactic body radiation therapy using simultaneous integrated BED-escalation for peripherally located non-small cell lung cancer. J Radiosurg SBRT. 2022;8(3):181-187. PMID: 36861004; PMCID:
- PMC9970741.

 [18] Kenamond MC, Pokhrel D, Visak J, McGarry RC. Escalating Tumor Dose via Simultaneous Integrated Boost (SIB) Stereotactic Body Radiation Therapy (SBRT) for Large (> 5 cm) Lung Masses. Int J Radiat Oncol Biol Phys 2021;111(3, Suppl). https://doi.org/10.1016/j.jipobp.2021.07.317.

 [19] Cases C, Benegas M, Sánchez M, Vollmer I, Casas F, Gomh C, et al. Biological equivalent dose is associated with radiological toxicity after lung stereotactic ablative radiation therapy. Radiother Oncol 2023;183:109552. https://doi.org/10.1016/i.radone.2023.109552
- [20] Palma DA, Olson R, Harrow S, Gaede S, Louie AV, Haasbeek C, et al. Steres Ablative Radiotherapy for the Comprehensive Treatment of Oligometastatic Cancers: Long-Term Results of the SABR-COMET Phase II Randomized Trial. J Clin Oncol. 2020 Sep 1;36(25):2830-2838. 10.1200/JCO.20.00818. Epub 2020 Jun 2. PMID: 32484754; PMCID: PMC7460150.

- [21] Asamura H. Hishida T. Suzuki K. Koike T. Nakamura K. Kusumoto M. et al. Japan Clinical Oncology Group Lung Cancer Surgical Study Group. Radiographi determined noninvasive adenocarcinoma of the lung: survival outcomes determined noninvasive adenocarcinoma of the lung: survival outcomes of Japan Clinical Oncology Group 0201. J Thorac Cardiovasc Surg 2013 Jul;146(1):24-30.
- https://doi.org/10.1016/j.jtcvs.2012.12.047. Epub 2013 Peb 8. PMID: 233986
 [22] Chetty IJ, Devpura S, Liu D, Chen D, Li H, Wen NW, et al. Correlation of dose computed using different algorithms with local control following stereotactic ablative radiotherapy (SABR)-based treatment of non-small-cell lung cancer. Radiother Oncol 2013 Dec;109(3):498-504. https://doi.org/10.1016/j.radonc.2013.10.012. Bpub 2013 Nov 11 PMID: 24231237.
- [23] Ojala JJ, Kapanen MK, Hyödynmaa SJ, Wigren TK, Pitkänen MA. Performance of Ojain M, Kapanen Bro, 1704/Jimms W, 1704/Jimms W, 1704 H, 1704
- [24] Fogliata A, Cozzi L. Dose calculation algorithm accuracy for small fields in non homogeneous media: The lung SBRT case. Phys Med 2017;44:157–62. https://dx 016.11.104.
- [25] Healy GEA, Marsh SH, Cousins AT. The dosimetric effect of electron densit overrides in 3DCRT Lung SBRT for a range of lung tumor dir Med Phys 2018;19(6):79–87. https://doi.org/10.1002/acm2.
- Wiant D, Vanderstraeten C, Maurer J, Pursley J, Terrell J, Sintay BJ. On the validity
- y want D, vanoerstraeren C, Maurer J, Fursley J, Terrell J, Sinfay BJ. On the validity of density overrides for VMAT lung SBRT planning. Med Phys 2014 Aug;41(8): 081707. https://doi.org/10.1118/1.4887778. PMID: 25086517.

 [27] Liang X, Zheng D, Mamalui-Hunter M, Flampouri S, Hoppe BS, Mendenhall N, et al. ITV-Sasted Robust Optimization for VMAT Planning of Stereotactic Body Radiation Therapy of Lung Cancer. Pract Radiat Oncol 2019 Jan;9(1):38–48. https://doi.org/
- 10.1016/j.prto.2018.06.005. Epub 2018 Aug 20 PMID: 30138474.

 [28] Xi J, Yin J, Liang J, Zhan C, Jiang W, Lin Z, et al. Prognostic Impact of Radiological Consolidation Tumor Ratio in Clinical Stage IA Pulmonary Ground Glass Opacities. Pront Oncol 2021 Apr;12(11):616149. https://doi.org/10.3389/
- [29] Van Esch A, Kulmala A, Rochford R, Kauppinen J, Harju A. Testing of an enhanced leaf model for improved dose calculation in a commercial treatment planning system. Med Phys 2022 Dec;49(12):7754-65. https://doi.org/10.1002/mp.16019. Bpub 2022 Oct 17 PMID: 36190516.
- [30] Saez J, Hernandez V, Goossens J, De Kerf G, Verellen D. A novel procedure for determining the optimal MLC configuration parameters in treatment planning systems based on measurements with a Farmer chamber. Phys Med Biol 2020 Jul systems based on measurements with a realizable of 27;65(15):155006. https://doi.org/10.1088/1361-6560/abi
- [31] Öllers MC, Swinnen ACC, Verhaegen F. Acuros® dose verification of ultrasmall [31] Ouers Mc, Swinnen ACC, Vernaegen F. Acuross dose verification of ultrasmall lung lesions with EBT-XD film in a homogeneous and heterogeneous anthropomorphic phantom setup. Med Phys 2020 Nov;47(11):5829-37. https://doi.org/10.1002/mp.14485. Epub 2020 Oct 7 PMID: 32970849.
 [32] Bainbridge H, Dunlop A, McQuaid D, Gulliford S, Gunapala R, Ahmed M, et al. A Comparison of Isotoxic Dose-escalated Radiotherapy in Lung Cancer with Moderate Deep Inspiration Breath Hold, Mid-ventilation and Internal Target Volume Torbinizates (Elle Opend (F. Cell Benied) 2022 Mers (2015) 5.
- Volume Techniques. Clin Oncol (R Coll Radiol) 2022 Mar;34(3):151–9. https://corg/10.1016/j.clom.2021.08.012. Epub 2021 Sep 7 PMID: 34503896.
 [33] Liang X, Zhang C, Ye X. Overdiagnosis and overtreatment of ground-glass node
- like lung cancer. Asia Pac J Clin Oncol. 2024 Jan 4. 10.1111/ajco.14042. Bpub ahead of print. PMID: 38178320.

DISCUSSION

The treatment of GGO lesions with SABR presents several challenges, particularly the standard approach of treating GGOs as solid nodules. This practice can result in an overexposure of healthy lung tissue to radiation, increasing the risk of lung injury. Given that GGO lesions are often multifocal and associated with improved LC rates, ^{86,87} they may benefit from tailored SABR approaches rather than a standardized treatment strategy.

A critical first step to investigate the possibility of a tailored treatment is to accurately identify and categorize the changes in the lung parenchyma observed after radiotherapy. Once categorized, an analysis can be made evaluating potential correlations with the delivered radiation dose. While the total delivered dose is a key factor in SABR prescriptions, the BED must be considered to effectively compare different fractionation schemes. Furthermore, when implementing a dose de-escalation strategy for GGO lesions, it is essential to ensure both precise dose calculations and robust dose delivery, particularly in the context of a moving target. These considerations, along with the methodological framework for addressing them, were explored in the previous sections and will be discussed in what follows.

1. Lung parenchyma changes evaluation strategies

CT scans play an important role in both the pre-treatment planning and post-treatment follow-up phases. The CT scan is performed before treatment to delineate the tumor and surrounding structures accurately, this CT scan is usually performed using the same parameters, as it not only serves to delineate the target structures but also to calculate the dose deposition in the patient. However, there are challenges in the consistency of follow-up CT scans, which are not always performed under identical conditions between them or with the same scanner. Although efforts are made to standardize follow-up CT scans by using similar acquisition parameters, such as breathing protocols and acquisition techniques, achieving perfect consistency is not always the main priority in clinical practice. Variations in scan settings, including slice thickness, tube current, reconstruction algorithms or breathing status of the patient can occur due to differences in equipment availability, clinical workflows, and individual patient circumstances.

The density of lung tissue (Figure 17) is a critical metric used to assess treatment response and detect potential complications, such as radiation-induced pneumonitis or fibrosis. ¹⁰⁸ Variations in scanning conditions can lead to discrepancies in measured densities and significantly impacted our ability to conduct quantitative analysis of lung parenchyma densities in our work. The variability in CT scan parameters introduced discrepancies in density measurements, which could not be reliably corrected or normalized across different scans. As a result, it was challenging to draw definitive conclusions about changes in lung tissue density over time, limiting the scope of our analysis to qualitative assessment and visual evaluation by experienced clinicians.

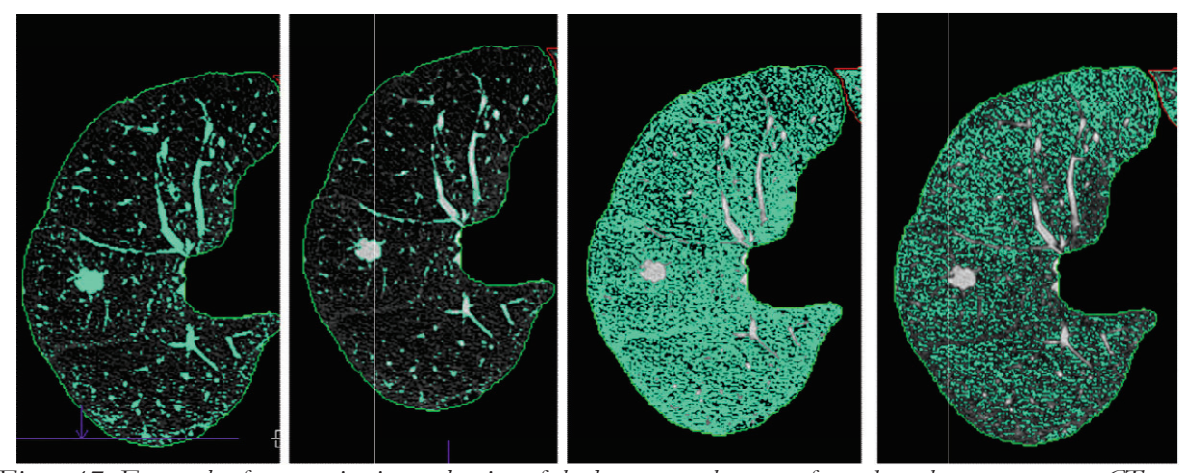


Figure 17. Example of a quantitative evaluation of the lung parenchyma performed on the pre-treatment CT scan of the right lung of a patient with a nodule. Green highlighted areas correspond to: a) solid component (200 Hounsfield Units (HU) to –200 HU), b) GGO component (-201 HU to –600 HU) c) standard lung density (-601 HU to –910 HU) and d) hypodense lung areas (-911 to –1000 HU). Original figure from the doctoral student.

Part of our follow-up period coincided also with the Coronavirus Disease 2019 (COVID-19) pandemic, which introduced additional challenges in obtaining consistent CT scans for patient follow-up. Additionally, the presence of COVID-19 infections complicated the interpretation of lung changes, as alterations in the lung parenchyma could be attributed to either treatment effects or COVID-related lung pathology.

Nevertheless, the evaluation of the grade 1 toxicities by an experienced radiologist allowed us to gain insights to categorize variations present in the lung parenchyma in terms of post radiotherapy treatment. There is extensive literature on the evaluation of radiological images post-SABR mainly to assess differences between post radiotherapy changes and local relapse, ¹¹⁷ but to the best of our knowledge, there are still no unified criteria to assess post-SABR patterns

regarding severity and typology of grade 1 toxicities. Although CTCAE score describes toxicities based on clinically observed parameters,³⁵ it does not consider a subdivision within all the radiological changes which do not have a direct clinical impact, as they all fall within grade 1 toxicities. Through the evaluation of the changes observed in our patients we developed a grading system to classify lung parenchyma changes and compare them among different patients to make it possible to evaluate different subtypes of grade 1 toxicity and its evolution with time.

2. Prescription fractionation and BED

In our cohort of patients, we employed a range of fractionation schemes, specifically prescriptions including 3 sessions of 18 Gy, 5 sessions of 11 Gy and 8 sessions of 7.5 Gy according to international guidelines.³¹ These different fractionation schemes result in significant variability in BED, a critical factor in evaluating and comparing treatment outcomes. For instance, the BED values for these fractionation schemes vary significantly from the 3 sessions of 18 Gy scheme, which nominally corresponds to a BED of 227 GyBED₃ or 126 GyBED₁₀, while the 8-session scheme corresponds to 126 GyBED₃ and 100 GyBED₁₀.

The differences in BED between these fractionation schemes requires an analysis based on BED rather than physical dose alone. This approach enabled us to assess and interpret treatment efficacy and toxicity for the different fractionation schemes. Additionally, the variation in BED provided us with a wider span of doses to analyze, potentially offering insights into doseresponse relationships and the optimization of SABR protocols.

However, the use of BED also has some limitations. Calculating BED using the linear quadratic model, especially for high-dose-per-fraction regimens like those used in SABR, is not straightforward. The model assumes a certain biological response to radiation that may not be accurate for very high doses delivered in a few fractions. This complexity requires cautious interpretation of the obtained BED values. Despite these challenges, using BED as a metric is crucial to understand the impact of fractionation strategies in lung cancer treatment and calculating BED following the linear quadratic model remains the most widespread approach and allows us to compare with different cohorts.

Over the years, several SABR regimes have been used to treat lung lesions. Some studies have analyzed the impact of different SABR regimes in terms of BED and its relation to local control and/or clinical toxicity.²³ Over the last years, lower BED regimes have been prioritized to reduce toxicity.¹⁰⁸ However, it has been reported that lowering the prescribed BED below the threshold of 100 Gy_{BED10} comes at the cost of lower LC rates.¹⁰⁸ Together with our findings

pointing to a similar dose level (300 GyBED₃) for healthy tissue complications, this justifies an approach to optimize the areas within the lesion receiving doses above 100GyBED₁₀ while maintaining the more indolent areas (GGO) as close to that lower threshold as possible (Figure 17).

This last point lead us to plan a possible de-escalation strategy which ensured a minimum dose to maintain LC rates acceptable in the GGO region of the lesion, with a minimum BED of 100 GyBED₁₀, while increasing the doses to the solid part of the lesion to the originally prescribed dose, which depending on the fractionation scheme reached up to a prescription dose of 126 GyBED₁₀ (and maximum doses up to 140% of the prescribed dose, thus 220 GyBED₁₀).

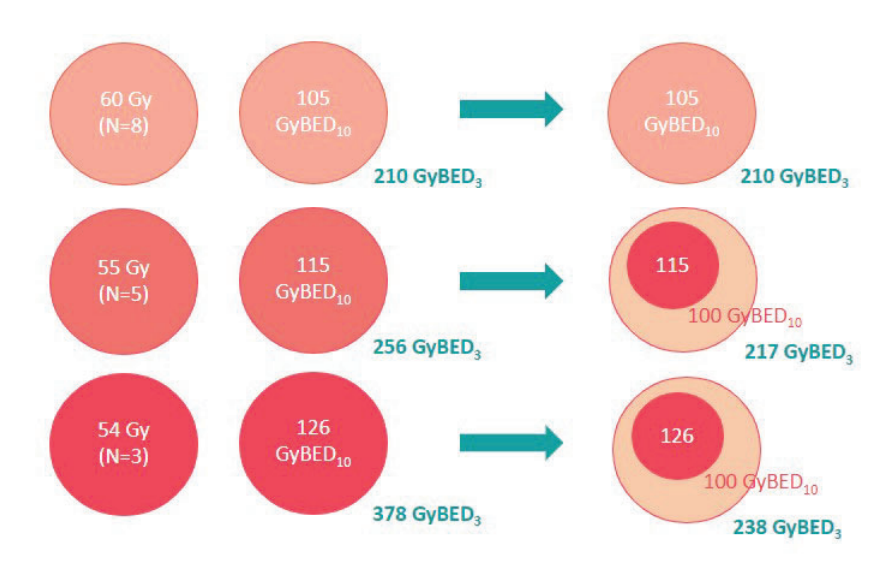


Figure 18. Schematic representation of the dose de-escalation approach proposed in this work for the three fractionation schemes analyzed. From left to right: Nominal dose and number of sessions for each fractionation scheme. Equivalent BED prescribed dose to the whole PTV in GyBED₁₀ and its equivalent dose, in GyBED₃ for the healthy tissue. On the right we can see the original prescription dose level, which is maintained in the solid region of the PTV, while the rest of the PTV is covered by a dose prescription ensuring at least 100 GyBED₁₀ and the equivalent dose to the surrounding healthy tissue for the corresponding number of sessions. Original figure from the doctoral student.

3. Comparing TPS doses AAA vs AXB

Accurately comparing TPS and dose calculation algorithms is a challenging task. One primary challenge is that the optimization process within a TPS can introduce variability even when using the same dose calculation algorithm.^{43,54} Factors such as iterative optimization steps, convergence criteria, and user-specific settings can lead to differences in the resulting dose

distribution. To address this issue and ensure consistency across our analyses, we replanned all patients' treatments following a standardized optimization process, specifically analyzed for lung SABR, that was presented in the European Society for Radiotherapy and Oncology (ESTRO) 2023 congress. This optimization protocol ensured a steep dose gradient while focusing on robust fluences.

Moreover, before proceeding with the optimization of the GGO SABR cases, we performed a study on the influence of various parameters that might affect TPS configuration as well as on the use of density overrides for optimization purposes. Some relevant parameters such as the effective spot size or the MLC characterization were evaluated to understand their impact on dose calculation algorithms. By isolating these variables, we aimed to differentiate between those differences arising from the physical description of the LINAC and those inherent to the dose calculation algorithm. Density overrides were not used as the obtained solution without the overrides was deemed robust enough and the optimization process was straightforward.

Additionally, it is important to note the differences in dose reporting between the AAA algorithm and AXB algorithm. AAA reports dose in terms of dose to water, whereas AXB reports dose in terms of dose to medium (AXB_m) or water (AXB_w) but always considering the medium in the radiation transport calculation process.¹³¹ It is important to remark that AAA and AXB_m are not comparable magnitudes. On the other hand, AXB_w is not the recommended dose reporting method by international protocols,^{39,56} as it considers dose deposition in water, which is not the tissue where dose is deposited. There is plenty of literature trying to take into consideration for these issues, to make it possible to accurately compare dose distributions obtained with both calculation engines, but it is not the aim of this work to perform a direct comparison between AAA and AXB.⁵⁵ Nevertheless, some considerations have been made when using these algorithms. First, we ensured that all detailed dose comparisons were made using the same algorithm—comparing dose to the lung for the de-escalation case to the standard case both calculated using AXB_m, for example. This approach allowed us to focus on subtle differences within the same algorithm without introducing variability from differing dose reporting methods.

4. Discussion of methodological approaches

The robustness and generalizability of the conclusions drawn by any study is highly dependent on the number of patients included in the study. To analyze the correlation between BED and grade 1 toxicities, we analyzed a cohort of over 100 patients, with a follow-up of two years after radiotherapy. This large sample size increases the likelihood that findings are

representative of the broader population undergoing SABR for lung cancer, increasing the study's validity and providing evidence to inform clinical practice.

In the second study, which examined dose de-escalation in SABR for GGO, the inclusion of over 40 cases offered a wide range of GGO sizes and CTR ratios (Figure 19). The inclusion of a phantom study allowed us to establish a baseline using a simple model that could simulate a continuous spectrum of CTRs. This approach facilitated precise control over variables and enabled a detailed analysis of the dose distribution and accuracy. Additionally, patient cases were analyzed to ensure a wide distribution of CTRs across different lesion sizes. This distribution makes it more probable that the study's findings are representative of the diverse cases found in clinical practice.

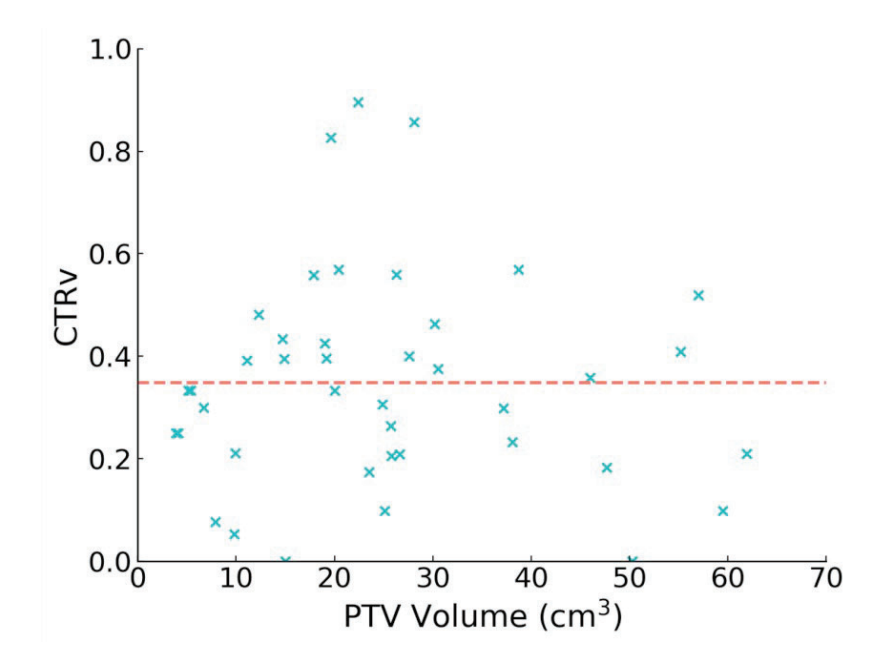


Figure 19. Relation between PTV size and the volumetric CTR for the patient lesions included in the study. The orange line represents the average CTRv value. Original figure from the doctoral student.

The unicentric nature of the study offers both potential biases and advantages. Conducting the research within a single center means that the techniques and methodologies used, such as imaging protocols and treatment planning, may be specific to that institution, potentially limiting the generalizability of the findings to other settings. Different centers might employ varying protocols and equipment, which could lead to different outcomes. Furthermore, as with most retrospective analyses, the study is subject to potential biases and confounding factors inherent in-patient data not originally collected for this specific research question.

However, a unicentric approach also provides significant advantages, particularly in ensuring a systematic follow-up and analysis of patient outcomes. This consistency allows for more controlled conditions, reducing variability in how data is collected and analyzed. A uniform follow-up protocol ensures that changes in radiological outcomes and toxicities are monitored and documented consistently, enhancing their reliability.

The treatment of the patients enrolled in this thesis was delivered using the ITV approach for motion management, which is one of the most widely adopted techniques in radiation therapy. This choice enhances the generalizability of the study's conclusions, making them more applicable to other centers that use the same approach. Nevertheless, the study also considered alternative approaches to assess the impact of GGO on dose calculation accuracy, including breath-hold and gating techniques. By exploring these options, the research acknowledged the potential benefits of active breathing management in further reducing radiation-related toxicities. High doses should be carefully managed, and techniques like gating or breath hold can potentially minimize exposure to surrounding healthy tissues, decreasing the risk of lung toxicities.

5. Implications for clinical practice

One key application is the incorporation of constraints on the absolute volume of lung tissue receiving high BED during treatment planning. By establishing such constraints, clinicians can make more informed decisions when selecting dose fractionations, thereby optimizing the balance between treatment efficacy and toxicity.

A second implementation on clinical practice may be the adoption of a dose de-escalation in SABR protocols that have a substantial impact, especially for cases intended to be treated with a lower number of sessions. This approach is beneficial for patients with significant GGO components. By tailoring the radiation dose to the specific characteristics of the tumor, such as the CTR, effective local control could be achieved while reducing the risk of damaging healthy lung tissue. These could lead to improved patient outcomes by reducing side effects and enhancing the overall quality of life. In the context of oligometastatic patients, where multiple lesions are expected to be treated sequentially, minimizing the cumulative radiation dose to healthy lung tissue is crucial.

These findings are becoming more relevant by the progressive implementation of lung cancer screening programs. As screening becomes more widespread, more lung lesions are being

detected at earlier stages.^{72,73} Many of these lesions will initially present as pure GGOs (Figure 20), which may evolve into more solid nodules over time. The natural progression of these lesions from pure GGOs to lesions with a solid component requires a reevaluation of traditional treatment strategies.

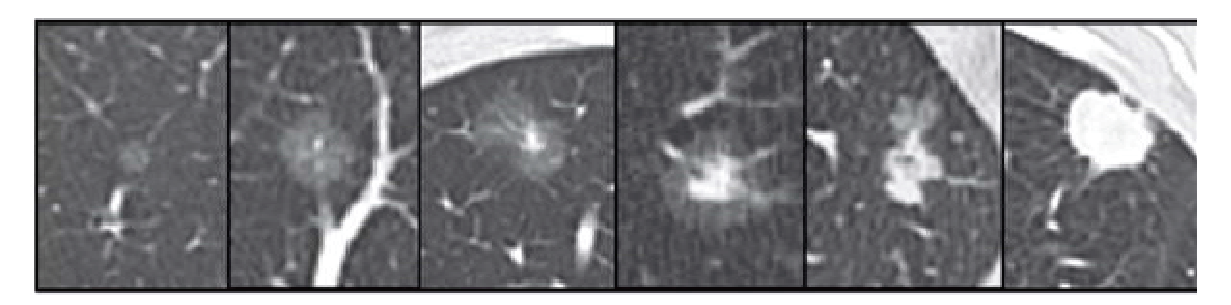


Figure 20. Different stages of the natural evolution of adenocarcinomas with various degrees of GGO component.

a) Atypical adenomatous hyperplasia b and) Adenocarcinoma in situ with different amounts of GGO component

d) Minimally invasive Adenocarcinoma e) Lepidic-predominant adenocarcinoma (non-mucinous) f) Invasive

mucinous adenocarcinoma and g) Invasive adenocarcinoma. Figure adapted from Godoy et al. 129

In conclusion, this thesis sets the bases for approaching a clinical trial for lung SABR with GGO component which could ensure similar rates of LC while reducing the risk of grade 1 toxicities.

6. Strengths and limitations

This work presents a number of aspects that give strength and consistency to the results. One of the main advantages is the inclusion of a relatively large number of patients treated in a single institution with consistent clinical protocols, which allows for homogeneity in the treatment approach, outcome analisys and imaging follow-up. This uniformity reduces variability and can lead to a more reliable analysis of the correlation between dose and radiological toxicity. The incorporation of both real patient cases and phantom-based simulations also allows for an exploration of the effects of GGO composition and respiratory motion on dose accuracy, which is not always feasible in purely clinical studies. Another important element is the proposal of a treatment adaptation strategy based on the internal structure of the lesions, which, despite being simple to implement from a planning perspective, could lead to a reduction in lung toxicity.

Even so, there are some limitations that must be acknowledged. The study is retrospective, and this type of design inevitably introduces potential biases. For instance, there is some variability in the timing and frequency of follow-up imaging, as well as in the interpretation of radiological

changes, which were not always confirmed histologically or correlated with symptoms. Furthermore, some follow up data is missing or incompleat and may lead to lack of statistical correlation with some parameters such as smoking habits. Toxicity was evaluated based on imaging findings rather quantitative analysis of the images, and although this is aligned with the study's goals, it leaves out potentially relevant outcomes. A similar approach was taken with the segmentation of GGO components, which was done visually. Moreover, while the recalculation of treatment plans with more advanced algorithms and the dose de-escalation proposal offer promising results in terms of lung sparing, these findings have not yet been confirmed in prospective clinical trials. Therefore, although the theoretical benefit appears clear, the translation to clinical practice should be done with caution. Lastly, as all data comes from a single institution, the external validity of the results may be limited, and replication in different clinical settings would be necessary to confirm the generalizability of the conclusions.

7. Future research directions

To strengthen the findings related to radiation toxicity, it is critical to validate the results in an independent cohort. This step ensures that the observed dose-toxicity relationships are not unique to the initial study population and can be generalized to a broader patient base. Validation in a different cohort helps to confirm the reliability and robustness of the results, providing a stronger foundation for clinical recommendations and potentially influencing treatment guidelines for SABR in lung cancer.

Further exploration of grade 1 toxicities is essential to fully understand the early indicators of potential long-term adverse effects. Developing a standardized protocol for evaluating and characterizing these changes would enhance the consistency of toxicity assessments across studies. By unifying the criteria and methods used to document these subtle changes, researchers can ensure more reliable data collection, which is crucial for identifying patterns and correlations that inform treatment optimization.

The application of artificial intelligence (AI) in analyzing dose-toxicity relationships presents a significant opportunity to expand the scope of toxicity studies. AI models can process large datasets efficiently, enabling researchers to examine these relationships across a more extensive cohort than would be feasible manually. By leveraging AI, the study can achieve a more nuanced understanding of the factors contributing to radiation toxicity, ultimately supporting the validation of results and the refinement of treatment protocols.

Once the toxicity results have been validated, a clinical trial could be conducted to evaluate the clinical efficacy and toxicity outcomes of a dose de-escalation strategy. This trial would be designed to confirm the potential benefits identified in the initial research, testing whether dose adjustments can maintain effective tumor control while reducing adverse effects. The findings from such a trial could lead to significant advancements in personalized radiation therapy, offering a pathway to optimize treatment for patients with lung cancer.

8. Key findings and concluding remarks

In the research conducted for this thesis we found a correlation between the lung volume receiving BED greater than 300 GyBED₃ and the occurrence and severity of observed radiological toxicities. It was also observed that changes in the lung parenchyma tend to persist or worsen in cases where the volume with D>300 GyBED₃ exceeds 20 cm³.

In the second part of the study, a positive correlation was identified between the presence of GGOs and dose calculation errors in phantom-based calculations. These discrepancies were reduced in patients, particularly in the presence of respiratory motion. When a treatment approach incorporating dose de-escalation in the GGO region was calculated, significant reductions in mean lung dose, V20, and V300GyBED₃ were achieved. Finally, it was also observed that optimizing with lower doses to the GGO area resulted in more stable fluence patterns, enhancing the robustness of the treatment.

The findings presented in this study underscore the critical role of optimizing SABR treatment protocols to enhance patient outcomes in lung cancer, particularly in cases involving GGO. By focusing on reducing grade 1 toxicities, our research offers a pathway to refine SABR strategies, potentially improving the quality of life for patients undergoing this treatment. The correlation between high BED levels and increased toxicities emphasizes the need for careful dose management and treatment planning. Although there are some challenges in clinical practice to quantify accurately lung parenchyma changes after radiotherapy, we provide a framework for categorizing and understanding post-SABR outcomes.

Looking ahead, our research lays the foundation for future clinical trials aimed at implementing dose de-escalation strategies that balance treatment efficacy with toxicity reduction. Such trials could confirm the potential benefits of tailoring SABR protocols to the specific characteristics of each patient's tumor, particularly those with larger GGO components, paving the way for a more patient-centered clinical practice.

CONCLUSIONS

- 1. Biological effective doses above 300 GyBED₃ to the lung are associated with a greater incidence of grade 1 lung toxicities after lung stereotactic radiation therapy. Furthermore, volumes greater than 20 cm³ receiving more than 300 GyBED₃ tend to present permanent parenchyma changes.
- 2. The presence of ground glass opacities within the planning target volume region induces dose calculation errors when type B algorithms, such as AAA are used. This errors are easily observed in phantom-based calculation but the discrepancies between type B and type A algorithms decrease in patient cases and especially in the presence of respiratory motion.
- 3. It is technically feasible to optimize stereotactic radiation therapy treatments for lung lesions containing ground glass opacities malignancies maintaining the expected local control to the tumor and improving calculation accuracy and robustness against breathing motion while reducing high doses to the healthy lung.

REFERENCES

- 1. Ahmad SS, Duke S, Jena R, Williams MV, Burnet NG. Advances in radiotherapy. BMJ. 2012;345:e7765. doi: 10.1136/bmj.e7765
- 2. Lievens Y, Borras JM, Grau C. Provision and use of radiotherapy in Europe. Mol Oncol. 2020;14(7):1461–1469. doi: 10.1002/1878-0261.12690
- 3. National Comprehensive Cancer Network (NCCN). NCCN Clinical Practice Guidelines in Oncology (NCCN Guidelines): Non-Small Cell Lung Cancer. Version 4.2021.
- 4. Hanna NH, Johnson DH, Temin S, Masters GA, Blumenschein GR, Govindan R. Systemic therapy for stage IV non–small-cell lung cancer: American Society of Clinical Oncology clinical practice guideline update. J Clin Oncol. 2017;35(30):3484–3515. doi: 10.1200/JCO.2017.74.6065
- 5. Turrisi AT, Kim K. Combined-modality therapy for limited-stage small-cell lung cancer. J Clin Oncol. 2001;19(4):135–149.
- 6. El Ayachy R, Giraud N, Giraud P, Durdux C, Bibault JE. The role of radiomics in lung cancer: from screening to treatment and follow-up. Front Oncol. 2021;11:603595. doi: 10.3389/fonc.2021.603595
- 7. Arroyo-Hernández M, Maldonado F, Lozano-Ruiz F, Muñoz-Montaño W, Nuñez-Baez M, Arrieta O. Radiation-induced lung injury: current evidence. BMC Pulm Med. 2021;21(1):9. doi: 10.1186/s12890-020-01376-4
- 8. Przystupski D, Górska A, Rozborska P, Bartosik W, Michel O, Rossowska J, et al. The cytoprotective role of antioxidants in mammalian cells under rapidly varying UV conditions during stratospheric balloon campaign. Front Pharmacol. 2019;10:851. doi: 10.3389/fphar.2019.00851
- 9. Little JB. Radiation carcinogenesis. Carcinogenesis. 2000;21(3):397–404. doi: 10.1093/carcin/21.3.397
- 10. Borgmann K, Dikomey E. Cellular response to ionizing radiation: DNA repair, apoptosis, and the role of p53. Adv Radiat Oncol. 2014;3(2):51–58.

- 11. Schäffer M, Barbul A. Lymphocyte function in wound healing and following injury. Br J Surg. 1998;85(4):444–460. doi: 10.1046/j.1365-2168.1998.00734.x
- 12. Gurtner GC, Werner S, Barrandon Y, Longaker MT. Wound repair and regeneration. Nature. 2008;453(7193):314–321. doi: 10.1038/nature07039
- 13. Cooke JP. Inflammation and its role in regeneration and repair. Circ Res. 2019;124(8):1166–1168. doi: 10.1161/CIRCRESAHA.118.314669
- 14. International Atomic Energy Agency. Radiation oncology physics: a handbook for teachers and students. Vienna: IAEA; 2005.
- 15. Poon RYC. Cell cycle control. In: Reference Module in Biomedical Sciences. Elsevier; 2015.
- 16. Carlos-Reyes A, Muñiz-Lino MA, Romero-Garcia S, López-Camarillo C, Hernández-de la Cruz ON. Biological adaptations of tumor cells to radiation therapy. Front Oncol. 2021;11:718636. doi: 10.3389/fonc.2021.718636
- 17. Li F, Jiang H, Bu M, Mu X, Zhao H. Dose-effect relationship of stereotactic body radiotherapy in non-small cell lung cancer patients. Radiat Oncol. 2022;17(1):211. doi: 10.1186/s13014-022-02183-3
- 18. El Naqa I, Bradley J, Blanco AI, Lindsay PE, Vicic M, Hope A, et al. Multivariable modeling of radiotherapy outcomes, including dose-volume and clinical factors. Int J Radiat Oncol Biol Phys. 2006;64(4):1275–1286. doi: 10.1016/j.ijrobp.2005.11.022
- 19. Bentzen SM, Saunders MI. The linear-quadratic approach in clinical practice. In: IntechOpen; 2001.
- 20. Shibamoto Y, Otsuka S, Iwata H, Sugie C, Ogino H, Tomita N. Radiobiological evaluation of the radiation dose as used in high-precision radiotherapy: effect of prolonged delivery time and applicability of the linear-quadratic model. J Radiat Res. 2012;53(1):1–9.
- 21. Liu L, Bassano DA, Prasad SC, Hahn SS, Chung CT. The linear-quadratic model and fractionated stereotactic radiotherapy. Int J Radiat Oncol Biol Phys. 2003;57(3):827–832. doi: 10.1016/S0360-3016(03)00634-5

- 22. Fowler JF. The linear-quadratic formula and progress in fractionated radiotherapy. Br J Radiol. 1989;62(740):679–694. doi: 10.1259/0007-1285-62-740-679
- 23. Fowler JF. 21 years of biologically effective dose. Br J Radiol. 2010;83(991):554–568. doi: 10.1259/bjr/31372149
- 24. Pérez C. Principles and practice of radiation oncology. Philadelphia: Raven Publishers; 1997.
- 25. Bratman SV, Koritzinsky M. Tumor and normal tissue response to radiotherapy. In: Harrington LA, Tannock IF, Hill RP, Cescon DW, editors. The Basic Science of Oncology. 6th ed. New York: McGraw-Hill Education; 2021.
- 26. Deloch L, Derer A, Hartmann J, Frey B, Fietkau R, Gaipl US. Modern radiotherapy concepts and the impact of radiation on immune activation. Front Oncol. 2016;6:141. doi: 10.3389/fonc.2016.00141
- 27. Van Leeuwen CM, Oei AL, Crezee J. The alfa and beta of tumours: a review of parameters of the linear-quadratic model, derived from clinical radiotherapy studies. Radiat Oncol. 2018;13(1):96. doi: 10.1186/s13014-018-1040-z
- 28. Lu Y, Hui B, Yang D, et al. Efficacy and safety analysis of hypofractionated and conventional fractionated radiotherapy in postoperative breast cancer patients. BMC Cancer. 2024;24(1):181. doi: 10.1186/s12885-024-11918-2
- 29. Castelluccia A, Tramacere F, Colciago R, Borgia M, Sallustio A, Proto T, et al. 10-year results of moderately hypofractionated postoperative radiotherapy for prostate cancer focused on treatment-related toxicity. Clin Genitourin Cancer. 2024;22:102102. doi: 10.1016/j.clgc.2024.102102
- 30. Najas GF, Stuart SR, Marta GN, Teixeira LAB, de Carvalho Gico V, Serante AR, et al. Hypofractionated radiotherapy in breast cancer: a 10-year single institution experience. Rep Pract Oncol Radiother. 2021;26(6):920–927. doi: 10.5603/RPOR.a2021.0109
- 31. Timmerman R, Paulus R, Galvin J, et al. Stereotactic body radiation therapy for inoperable early stage lung cancer. JAMA. 2010;303(11):1070–1076. doi: 10.1001/jama.2010.261

- 32. Siva S, Kron T, Bressel M, Haas M, Mai T, Vinod S, et al. A randomised phase II trial of stereotactic ablative fractionated radiotherapy versus radiosurgery for oligometastatic neoplasia to the lung (TROG 13.01 SAFRON II). BMC Cancer. 2016;16:183. doi: 10.1186/s12885-016-2227-z
- 33. Li F, Jiang H, Bu M, Mu X, Zhao H. Dose-effect relationship of stereotactic body radiotherapy in non-small cell lung cancer patients. Radiat Oncol. 2022;17(1):211. doi: 10.1186/s13014-022-02183-3
- 34. Mohan G, Hamna A, Jijo J, Saradha M, Narayanasamy A, Balachandar V. Recent advances in radiotherapy and its associated side effects in cancer—a review. J Basic Appl Zool. 2019;80(1):1–11. doi: 10.1186/s41936-019-0083-5
- 35. National Cancer Institute. Common Terminology Criteria for Adverse Events (CTCAE). Version 5.0. 2017.

https://ctep.cancer.gov/protocolDevelopment/electronic_applications/ctc.htm

- 36. Cancer Research UK. Stereotactic radiotherapy. 2022. https://www.cancerresearchuk.org/ about-cancer/cancer-in- general/treatment/radiotherapy/stereotactic-radiotherapy
- 37. Aird E, Conway J. CT simulation for radiotherapy treatment planning. Br J Radiol. 2002;75(900):937–949. doi: 10.1259/bjr.75.900.750937
- 38. Bortfeld T, Schmidt-Ullrich R, editors. Target volume delineation and field setup: a practical guide for conformal and intensity-modulated radiation therapy. 2nd ed. Cham: Springer; 2022. doi: 10.1007/978-3-030-73773-3
- 39. Hodapp N. Der ICRU-Report 83: Verordnung, Dokumentation und Kommunikation der fluenzmodulierten Photonenstrahlentherapie (IMRT). Strahlenther Onkol. 2012;188(1):97–99. doi: 10.1007/s00066-011-0015-x
- 40. Zhang S, Li S, Yang H, Zhang H, Zhang G, Hu P. Application of AIP and MIP CT on individual GTV delineation for tumor moving with respiration. In: Proceedings of the 2012 International Conference on Biomedical Engineering and Biotechnology (iCBEB); 2012. p. 736–739. doi: 10.1109/iCBEB.2012.77

- 41. Smilowitz JB, Das IJ, Feygelman V, Fraass BA, Kry SF, Marshall IR, et al. AAPM medical physics practice guideline 5.a.: commissioning and QA of treatment planning dose calculations—megavoltage photon and electron beams. J Appl Clin Med Phys. 2015;16(5):14–34. doi: 10.1120/jacmp.v16i5.5768
- 42. Mayles P, Nahum A, Rosenwald JC, editors. Handbook of radiotherapy physics: theory and practice. 1st ed. Boca Raton: CRC Press; 2007. doi: 10.1201/9781420012026
- 43. Ma CM, Chetty IJ, Deng J, Faddegon BA, Jiang SB, Li JS, et al. Beam modeling and beam model commissioning for Monte Carlo dose calculation-based radiation therapy treatment planning: report of AAPM Task Group 157. Med Phys. 2020;47(8):e1–e18. doi: 10.1002/mp.13898
- 44. Sgouros G, Bolch WE, Chiti A, Eckerman KF, Hobbs RF, Konijnenberg MW, et al. ICRU Report 96: dosimetry-guided radiopharmaceutical therapy. J ICRU. 2021;21(1):1–212. doi: 10.1177/14736691211060117
- 45. Papanikolaou N, Battista J, Boyer A, Kappas C, Klein E, Mackie T, et al. Tissue inhomogeneity corrections for megavoltage photon beams. AAPM Report No. 85; Task Group No. 65. Madison: American Association of Physicists in Medicine; 2004.
- 46. Henni A, Lauzin Y, Pirault N, Dubos B, Rogé M, Clarisse P, et al. Treatment planning for non-small cell lung tumours: VMAT versus 3DCRT—a quantitative dosimetric study. J Radiother Pract. 2020;19(1):1–6. doi: 10.1017/S1460396919000864
- 47. Bär W, Schwarz M, Alber M, Bos LJ, Mijnheer BJ, Rasch C, et al. A comparison of forward and inverse treatment planning for intensity-modulated radiotherapy of head and neck cancer. Radiother Oncol. 2003;69(3):251–258. doi: 10.1016/j.radonc.2003.08.002
- 48. Wu Q, Mohan R. Multiple local minima in IMRT optimization based on dose-volume criteria. Med Phys. 2002;29(7):1514–1527. doi: 10.1118/1.1485059
- 49. Gleeson I. Comparing the robustness of different skin flash approaches using wide tangents, manual flash VMAT, and simulated organ motion robust optimization VMAT in breast and nodal radiotherapy. Med Dosim. 2022;47(3):264–272. doi: 10.1016/j.meddos.2022.04.004

- 50. Shang H, Pu Y, Wang Y. Robust optimization of SBRT planning for patients with early stage non-small cell lung cancer. Technol Cancer Res Treat. 2020;19:1533033820916505. doi: 10.1177/1533033820916505
- 51. Liang X, Zheng D, Mamalui-Hunter M, Flampouri S, Hoppe BS, Mendenhall N, et al. ITV-based robust optimization for VMAT planning of stereotactic body radiation therapy of lung cancer. Pract Radiat Oncol. 2019;9(1):38–48. doi: 10.1016/j.prro.2018.08.005.
- 52. Van Dyk J, Rosenwald JC, Fraass B, Cramb J, Ionescu-Farca F, Sharpe M. IAEA Technical Reports Series No. 430: commissioning and quality assurance of computerized planning systems for radiation treatment of cancer. Med Phys. 2006;33(10):3871–3882. doi: 10.1118/1.2167371
- 53. American Association of Physicists in Medicine. AAPM Report No. 85: tissue inhomogeneity corrections for megavoltage photon beams. Task Group 65. Madison: AAPM; 2004. doi: 10.37206/86.
- 54. Zhou C, Bennion N, Ma R, Liang X, Wang S, Zvolanek K, et al. A comprehensive dosimetric study on switching from a Type-B to a Type-C dose algorithm for modern lung SBRT. Radiat Oncol. 2017;12(1):80. doi: 10.1186/s13014-017-0816-x
- 55. Tsuruta Y, Nakata M, Nakamura M, Matsuo Y, Higashimura K, Monzen H, et al. Dosimetric comparison of Acuros XB, AAA, and XVMC in stereotactic body radiotherapy for lung cancer. Med Phys. 2014;41(8):081715. doi: 10.1118/1.4890592
- 56. Wilke L, Andratschke N, Blanck O, Brunner TB, Combs SE, Grosu AL, et al. ICRU report 91 on prescribing, recording, and reporting of stereotactic treatments with small photon beams: Statement from the DEGRO/DGMP working group stereotactic radiotherapy and radiosurgery. Strahlenther Onkol. 2019;195(3):193–198. doi: 10.1007/s00066-018-1416-x
- 57. Bentzen SM, Constine LS, Deasy JO, Eisbruch A, Jackson A, Marks LB, et al. Quantitative analyses of normal tissue effects in the clinic (QUANTEC): an introduction to the scientific issues. Int J Radiat Oncol Biol Phys. 2010;76(3 Suppl):S3–S9. doi: 10.1016/j.ijrobp.2009.09.040
- 58. Mayo CS, Moran JM, Bosch W, Xiao Y, McNutt T, Popple R, et al. American Association of Physicists in Medicine Task Group 263: Standardizing nomenclatures in radiation oncology. Int J Radiat Oncol Biol Phys. 2018;100(4):1057–1066. doi: 10.1016/j.ijrobp.2017.12.013

- 59. Korevaar EW, Habraken SJM, Scandurra D, Kierkels RGJ, Unipan M, Eenink MGC, et al. Practical robustness evaluation in radiotherapy—a photon and proton-proof alternative to PTV-based plan evaluation. Radiother Oncol. 2019;141:267–274. doi: 10.1016/j.radonc.2019.08.005
- 60. Yock AD, Mohan R, Flampouri S, Bosch W, Taylor PA, Gladstone D, et al. Robustness analysis for external beam radiation therapy treatment plans: describing uncertainty scenarios and reporting their dosimetric consequences. Pract Radiat Oncol. 2019;9(4):200–207. doi: 10.1016/j.prro.2018.12.002
- 61. World Health Organization. Lung cancer. 2023. Available from: https://www.who.int/news-room/fact-sheets/detail/lung-cancer
- 62. International Agency for Research on Cancer. Cancer Today: Data for Spain. 2020. Available from: https://gco.iarc.fr/today/data/factsheets/populations/724-spain-fact-sheets.pdf
- 63. National Cancer Institute. Radiation Therapy for Lung Cancer. 2020. Available from: https://www.cancer.gov/types/lung/hp/lung-radiation-therapy-pdq
- 64. Iyengar P, All S, Berry MF, Boike TP, Bradfield L, Dingemans A, et al. Treatment of oligometastatic non-small cell lung cancer: An ASTRO/ESTRO clinical practice guideline. Pract Radiat Oncol. 2023;13(5):393–412. doi: 10.1016/j.prro.2023.04.004
- 65. Chen H, Stoltzfus KC, Lehrer EJ, Horn SR, Siva S, Trifiletti DM, et al. The epidemiology of lung metastases. Front Med. 2021;8:723396. doi: 10.3389/fmed.2021.723396
- 66. Palma DA, Olson R, Harrow S, Gaede S, Louie AV, Haasbeek C, et al. Stereotactic ablative radiotherapy for the comprehensive treatment of oligometastatic cancers: long-term results of the SABR-COMET phase II randomized trial. J Clin Oncol. 2020;38(25):2830–2838. doi: 10.1200/JCO.20.00818
- 67. Harrow S, Palma DA, Olson R, Gaede S, Louie AV, Haasbeek C, et al. Stereotactic radiation for the comprehensive treatment of oligometastases (SABR-COMET): extended long-term outcomes. Int J Radiat Oncol Biol Phys. 2022;114(4):611–616. doi: 10.1016/j.ijrobp.2022.05.004
- 68. Doyle E, Killean AJ, Harrow S, Phillips ID. Systematic review of the efficacy of stereotactic ablative radiotherapy for oligoprogressive disease in metastatic cancer. Radiother Oncol. 2024;196:110288. doi: 10.1016/j.radonc.2024.110288

- 69. Schellenberg D, Gabos Z, Duimering A, Debenham BJ, Fairchild A, Huang F, et al. Stereotactic ablative radiotherapy for oligo-progressive cancers: results of the randomized phase II STOP trial. Int J Radiat Oncol Biol Phys. 2023;117(2 Suppl):S58.
- 70. Paralkar VR, Li T, Langer CJ. Population characteristics and prognostic factors in metastatic non-small-cell lung cancer: a Fox Chase Cancer Center retrospective. Clin Lung Cancer. 2008;9(2):116–121. doi: 10.3816/CLC.2008.n.018
- 71. Guckenberger M, Lievens Y, Bouma AB, Collette L, Dekker A, de Souza NM, et al. Characterisation and classification of oligometastatic disease: a European Society for Radiotherapy and Oncology and European Organisation for Research and Treatment of Cancer consensus recommendation. Lancet Oncol. 2020;21(1):e18–e28. doi: 10.1016/S1470-2045(19)30718-1
- 72. Du Y, Sidorenkov G, Heuvelmans M, Groen H, Vermeulen K, Greuter M, et al. Cost-effectiveness of lung cancer screening with low-dose computed tomography in heavy smokers: a microsimulation modelling study. Eur J Cancer. 2020;135:121–129. doi: 10.1016/j.ejca.2020.05.004
- 73. Nekolla EA, Brix G, Griebel J. Lung cancer screening with low-dose CT: radiation risk and benefit–risk assessment for different screening scenarios. Diagnostics (Basel). 2022;12(2):364. doi: 10.3390/diagnostics12020364
- 74. Aberle DR, Adams AM, Berg CD, Black WC, Clapp JD, Fagerstrom RM, et al. Reduced lung-cancer mortality with low-dose computed tomographic screening. N Engl J Med. 2011;365(5):395–409. doi: 10.1056/NEJMoa1102873
- 75. Church TR, Black WC, Aberle DR, Berg CD, Clingan KL, Duan F, et al. Results of initial low-dose computed tomographic screening for lung cancer. N Engl J Med. 2013;368(21):1980–1991. doi: 10.1056/NEJMoa1209120
- 76. Sherif M, Taha M. Role of multi-detector computed tomography in differentiation between benign and malignant cavitary lung lesions. Med J Cairo Univ. 2019. doi: 10.21608/mjcu.2019.54362
- 77. Goldin JG, Brown MS, Petkovska I. Computer-aided diagnosis in lung nodule assessment. J Thorac Imaging. 2008;23(2):97–104. doi: 10.1097/RTI.0b013e318173dd1f

- 78. Schiepers C. Role of positron emission tomography in the staging of lung cancer. Lung Cancer. 1997;17 Suppl 1:S29–S35. doi: 10.1016/S0169-5002(97)00638-7
- 79. MacMahon H, Naidich DP, Goo JM, Lee KS, Leung AN, Mayo JR, et al. Guidelines for management of incidental pulmonary nodules detected on CT images: From the Fleischner Society 2017. Radiology. 2017 Jul;284(1):228–243. doi: 10.1148/radiol.2017161659
- 80. Gould MK, Tang T, Liu IL, Lee J, Zheng C, Danforth KN, et al. Recent trends in the identification of incidental pulmonary nodules. Am J Respir Crit Care Med. 2015;192(10):1208–1214. doi: 10.1164/rccm.201505-0990OC
- 81. de Margerie-Mellon C, Onken A, Heidinger BH. Characteristics and management of incidental pulmonary nodules detected on CT in the context of primary staging of non-pulmonary malignancies. Cancer Imaging. 2018;18(1):25. doi: 10.1186/s40644-018-0154-7
- 82. Henschke CI, Yankelevitz DF, Mirtcheva R, McGuinness G, McCauley D, Miettinen OS. CT screening for lung cancer: frequency and significance of part-solid and nonsolid nodules. AJR Am J Roentgenol. 2002;178(5):1053–1057. doi: 10.2214/ajr.178.5.1781053
- 83. Silvestri GA, Gonzalez AV, Jantz MA, Margolis ML, Gould MK, Tanoue LT, et al. Methods for staging non-small cell lung cancer: Diagnosis and management of lung cancer, 3rd ed: American College of Chest Physicians evidence-based clinical practice guidelines. Chest. 2013;143(5 Suppl):e211S–e250S. doi: 10.1378/chest.12-2355
- 84. Duan L, Shan W, Bo G, Lu G, Guo L. Qualitative and quantitative values of the Lung-RADS and computed tomography in diagnosing solitary pulmonary nodules. Diagnostics. 2022;12(11):2699. doi: 10.3390/diagnostics12112699
- 85. Travis WD, Brambilla E, Noguchi M, Nicholson AG, Geisinger KR, Yatabe Y, et al. International Association for the Study of Lung Cancer/American Thoracic Society/European Respiratory Society international multidisciplinary classification of lung adenocarcinoma. J Thorac Oncol. 2011;6(2):244–285. doi: 10.1097/JTO.0b013e318206a221
- 86. Lee HJ, Goo JM, Lee CH, Park CM, Leung AN. Clinical and radiologic characteristics of pulmonary subsolid nodules: part-solid and pure ground-glass opacities. AJR Am J Roentgenol. 2013;201(2):251–258. doi: 10.2214/AJR.12.8881

- 87. Travis WD, Asamura H, Bankier AA, Beasley MB, Detterbeck F, Flieder DB, et al. The IASLC Lung Cancer Staging Project: Proposals for Coding T Categories for Subsolid Nodules and Assessment of Tumor Size in Part-Solid Tumors in the Forthcoming Eighth Edition of the TNM Classification of Lung Cancer. J Thorac Oncol. 2016;11(8):1204–1223. doi:10.1016/j.jtho.2016.03.025.
- 88. Scholten ET, Jacobs C, van Ginneken B, Tempany CM, Schaefer-Prokop CM. Computeraided detection and diagnosis of pulmonary nodules. Eur Radiol. 2015;25(6):1633–1645. doi:10.1007/s00330-014-3500-3.
- 89. Siva S, Kron T, Bressel M, Haas M, Mai T, Vinod S, et al. A randomised phase II trial of stereotactic ablative fractionated radiotherapy versus radiosurgery for oligometastatic neoplasia to the lung (TROG 13.01 SAFRON II). BMC Cancer. 2016;16:183. doi:10.1186/s12885-016-2227-z.
- 90. Lagerwaard FJ, Verstegen NE, Haasbeek CJ, Slotman BJ, Paul MA, Smit EF, et al. Outcomes of stereotactic ablative radiotherapy in patients with potentially operable stage I non-small cell lung cancer. Int J Radiat Oncol Biol Phys. 2012;83(1):348–353. doi:10.1016/j.ijrobp.2011.06.2008.
- 91. Haasbeek CJ, Lagerwaard FJ, Slotman BJ, Senan S. Outcomes of stereotactic ablative radiotherapy for centrally located early-stage lung cancer. J Thorac Oncol. 2011;6(12):2036–2043. doi:10.1097/JTO.0b013e31822e5b6c.
- 92. Ball D, Mai GT, Vinod S, Babington S, Ruben J, Kron T, et al. Stereotactic ablative radiotherapy versus standard radiotherapy in stage 1 non-small-cell lung cancer (TROG 09.02 CHISEL): a phase 3, open-label, randomised controlled trial. Lancet Oncol. 2019;20(4):494–503. doi:10.1016/S1470-2045(18)30896-9.
- 93. Tekatli H, Senan S, Dahele M, Slotman BJ, Verbakel WF. Stereotactic ablative radiotherapy (SABR) for central lung tumors: Plan quality and long-term clinical outcomes. Radiother Oncol. 2015;117(1):64–70. doi:10.1016/j.radonc.2015.08.013.
- 94. Timmerman R, McGarry R, Yiannoutsos C, Papiez L, Tudor K, DeLuca J, et al. Excessive toxicity when treating central tumors in a phase II study of stereotactic body radiation therapy

- for medically inoperable early-stage lung cancer. J Clin Oncol. 2006;24(30):4833–4839. doi:10.1200/JCO.2006.07.5937.
- 95. Regnery S, Eichkorn T, Weykamp F, Held T, Weusthof K, Dinges LA, et al. Safety and efficacy of stereotactic body radiotherapy in ultracentral lung tumors using a risk-optimized fractionation scheme. Clin Lung Cancer. 2021;22(4):332–340.e3. doi:10.1016/j.cllc.2020.11.003.
- 96. Palma DA, Olson R, Harrow S, Gaede S, Louie AV, Haasbeek CJ, et al. Stereotactic ablative radiotherapy for the comprehensive treatment of oligometastatic cancers: Long-term results of the SABR-COMET phase II randomized trial. J Clin Oncol. 2020;38(25):2830–2838. doi:10.1200/JCO.20.00818.
- 97. Asamura H, Hishida T, Suzuki K, Koike T, Nakamura K, Kusumoto M, et al. Radiographically determined noninvasive adenocarcinoma of the lung: survival outcomes of Japan Clinical Oncology Group 0201. J Thorac Cardiovasc Surg. 2013;146(1):24–30. doi:10.1016/j.jtcvs.2012.12.047.
- 98. Chetty IJ, Devpura S, Liu D, Chen D, Li H, Wen NW, et al. Correlation of dose computed using different algorithms with local control following stereotactic ablative radiotherapy (SABR)-based treatment of non-small-cell lung cancer. Radiother Oncol. 2013;109(3):498–504. doi: 10.1016/j.radonc.2013.10.012.
- 99. Ojala JJ, Kapanen MK, Hyödynmaa SJ, Wigren TK, Pitkänen MA. Performance of dose calculation algorithms from three generations in lung SBRT: comparison with full Monte Carlobased dose distributions. J Appl Clin Med Phys. 2014;15(2):4–18. doi: 10.1120/jacmp.v15i2.4662.
- 100. Fogliata A, Cozzi L. Dose calculation algorithm accuracy for small fields in non-homogeneous media: The lung SBRT case. Phys Med. 2017;44:157–162. doi: 10.1016/j.ejmp.2016.11.104.
- 101. Healy GEA, Marsh SH, Cousins AT. The dosimetric effect of electron density overrides in 3DCRT Lung SBRT for a range of lung tumor dimensions. J Appl Clin Med Phys. 2018;19(6):79–87. doi: 10.1002/acm2.12446.

- 102. Wiant D, Vanderstraeten C, Maurer J, Pursley J, Terrell J, Sintay B. On the validity of density overrides for VMAT lung SBRT planning. Med Phys. 2014;41(8):081707. doi: 10.1118/1.4887778.
- 103. Liang X, Zheng D, Mamalui-Hunter M, Flampouri S, Hoppe BS, Mendenhall N, et al. ITV-Based Robust Optimization for VMAT Planning of Stereotactic Body Radiation Therapy of Lung Cancer. Pract Radiat Oncol. 2019;9(1):38–48. doi: 10.1016/j.prro.2018.08.005.
- 104. Chang JY, Senan S, Paul MA, Mehran RJ, Louie AV, Balter P, et al. Stereotactic ablative radiotherapy versus lobectomy for operable stage I non-small-cell lung cancer: A pooled analysis of two randomised trials. Lancet Oncol. 2015;16(6):630–637. doi: 10.1016/S1470-2045(15)70168-3
- 105. Guckenberger M, Allgauer M, Appold S, Dieckmann K, Ernst I, Ganswindt U, et al. Safety and efficacy of stereotactic body radiotherapy for stage I non-small-cell lung cancer in routine clinical practice: A patterns-of-care and outcome analysis. J Thorac Oncol. 2013;8(8):1050–1058. doi: 10.1097/JTO.0b013e3182993b2b.
- 106. Videtic GMM, Hu C, Singh AK, Chang JY, Parker W, Olivier KR, et al. A randomized phase 2 study comparing 2 stereotactic body radiation therapy schedules for medically inoperable patients with stage I peripheral non-small cell lung cancer: NRG Oncology RTOG 0915 (NCCTG N0927). Int J Radiat Oncol Biol Phys. 2015;93(4):757–764. doi: 10.1016/j.ijrobp.2015.07.2265.
- 107. Palma DA, Senan S, Oberije C, Belderbos J, de Dios NR, Bradley JD, et al. Predicting radiation pneumonitis after chemoradiation therapy for lung cancer: An international individual patient data meta-analysis. Int J Radiat Oncol Biol Phys. 2013;85(2):444–450. doi: 10.1016/j.ijrobp.2012.04.043.
- 108. Marks LB, Bentzen SM, Deasy JO, Kong FM, Bradley JD, Vogelius IS, et al. Radiation dose–volume effects in the lung. Int J Radiat Oncol Biol Phys. 2010;76(3 Suppl):S70–S76. doi: 10.1016/j.ijrobp.2009.06.091.
- 98. Chetty IJ, Devpura S, Liu D, Chen D, Li H, Wen NW, et al. Correlation of dose computed using different algorithms with local control following stereotactic ablative radiotherapy (SABR)-

- based treatment of non-small-cell lung cancer. Radiother Oncol. 2013;109(3):498-504. doi:10.1016/j.radonc.2013.10.012
- 99. Ojala JJ, Kapanen MK, Hyödynmaa SJ, Wigren TK, Pitkänen MA. Performance of dose calculation algorithms from three generations in lung SBRT: comparison with full Monte Carlobased dose distributions. J Appl Clin Med Phys. 2014;15(2):4-18. doi:10.1120/jacmp.v15i2.4662
- 100. Fogliata A, Cozzi L. Dose calculation algorithm accuracy for small fields in non-homogeneous media: The lung SBRT case. Phys Med. 2017;44:157-162. doi:10.1016/j.ejmp.2016.11.104
- 101. Healy GEA, Marsh SH, Cousins AT. The dosimetric effect of electron density overrides in 3DCRT Lung SBRT for a range of lung tumor dimensions. J Appl Clin Med Phys. 2018;19(6):79-87. doi:10.1002/acm2.12446
- 102. Wiant D, Vanderstraeten C, Maurer J, Pursley J, Terrell J, Sintay B. On the validity of density overrides for VMAT lung SBRT planning. Med Phys. 2014;41(8):081707. doi:10.1118/1.4887778
- 103. Liang X, Zheng D, Mamalui-Hunter M, Flampouri S, Hoppe BS, Mendenhall NP, et al. ITV-Based Robust Optimization for VMAT Planning of Stereotactic Body Radiation Therapy of Lung Cancer. Pract Radiat Oncol. 2019;9(1):38-48. doi:10.1016/j.prro.2018.08.005
- 104. Chang JY, Senan S, Paul MA, Mehran RJ, Louie AV, Balter P, et al. Stereotactic ablative radiotherapy versus lobectomy for operable stage I non-small-cell lung cancer: A pooled analysis of two randomised trials. Lancet Oncol. 2015;16(6):630-637. doi:10.1016/S1470-2045(15)70168-3
- 105. Guckenberger M, Allgauer M, Appold S, Dieckmann K, Ernst I, Ganswindt U, et al. Safety and efficacy of stereotactic body radiotherapy for stage I non-small-cell lung cancer in routine clinical practice: A patterns-of-care and outcome analysis. J Thorac Oncol. 2013;8(8):1050-1058. doi:10.1097/JTO.0b013e318293dc45
- 106. Videtic GMM, Hu C, Singh AK, Chang JY, Parker W, Olivier KR, et al. A randomized phase 2 study comparing 2 stereotactic body radiation therapy schedules for medically inoperable patients with stage I peripheral non-small cell lung cancer: NRG Oncology RTOG 0915

- (NCCTG N0927). Int J Radiat Oncol Biol Phys. 2015;93(4):757-764. doi:10.1016/j.ijrobp.2015.07.2268
- 107. Palma DA, Senan S, Oberije C, Belderbos J, de Dios NR, Bradley JD, et al. Predicting radiation pneumonitis after chemoradiation therapy for lung cancer: An international individual patient data meta-analysis. Int J Radiat Oncol Biol Phys. 2013;85(2):444-450. doi:10.1016/j.ijrobp.2012.04.043
- 108. Marks LB, Bentzen SM, Deasy JO, Kong FM, Bradley JD, Vogelius IS, et al. Radiation dose–volume effects in the lung. Int J Radiat Oncol Biol Phys. 2010;76(3 Suppl):S70-S76. doi:10.1016/j.ijrobp.2009.06.091
- 109. Bradley JD, Paulus R, Komaki R, Masters G, Blumenschein G, Schild S, et al. Standard-dose versus high-dose conformal radiotherapy with concurrent and consolidation carboplatin plus paclitaxel with or without cetuximab for patients with stage IIIA or IIIB non-small-cell lung cancer (RTOG 0617): A randomised, two-by-two factorial phase 3 study. Lancet Oncol. 2015;16(2):187-199. doi:10.1016/S1470-2045(14)71158-8
- 110. Chen H, Senan S, Nossent EJ, Boldt RG, Warner A, Palma DA. Evidence-based approaches to minimize radiation-induced lung toxicity in precision radiation therapy. Lancet Oncol. 2017;18(12):e698-e708. doi:10.1016/S1470-2045(17)30667-0
- 111. Kocak Z, Evans ES, Zhou SM, Miller KL, Folz RJ, Shafman TD, et al. Challenges in defining radiation pneumonitis in patients with lung cancer. Int J Radiat Oncol Biol Phys. 2005;62(3):635-638. doi:10.1016/j.ijrobp.2004.12.005
- 112. Matsuo Y, Shibuya K, Nakamura M, Narabayashi M, Sakanaka K, Ueki N, et al. Dosevolume metrics associated with radiation pneumonitis after stereotactic body radiation therapy for lung cancer. Int J Radiat Oncol Biol Phys. 2012;83(4):e545-e549. doi:10.1016/j.ijrobp.2011.12.057
- 113. Cases C, Benegas M, Sánchez M, Vollmer I, Casas F, Gomà C, et al. Biological equivalent dose is associated with radiological toxicity after lung stereotactic ablative radiation therapy. Radiother Oncol. 2023;183:109552. doi:10.1016/j.radonc.2023.109552

- 114. Qiao X, Tullgren O, Lax I, Sirzén F, Lewensohn R. The role of radiotherapy in treatment of stage I non-small cell lung cancer. *Lung Cancer*. 2003 Jul;41(1):1–11. doi: 10.1016/s0169-5002(03)00152-1
- 115. Borghaei H, Paz-Ares L, Horn L, Spigel DR, Steins M, Ready NE, et al. Nivolumab versus Docetaxel in advanced nonsquamous non-small-cell lung cancer. *N Engl J Med.* 2015 Oct 22;373(17):1627–1639. doi: 10.1056/NEJMoa1507643
- 116. Chalkidou A, Macmillan T, Grzeda MT, Peacock J, Summers J, Eddy S, et al. Stereotactic ablative body radiotherapy in patients with oligometastatic cancers: a prospective, registry-based, single-arm, observational, evaluation study. *Lancet Oncol.* 2021 Jan;22(1):98–106. doi: 10.1016/S1470-2045(20)30537-4
- 117. Dahele M, Palma D, Lagerwaard F, Slotman B, Senan S. Radiological changes after stereotactic radiotherapy for stage I lung cancer. *J Thorac Oncol.* 2011 Jul;6(7):1221–1228. doi: 10.1097/JTO.0b013e318219aac5
- 118. Ronden MI, Palma D, Slotman BJ, Senan S. Brief report on radiological changes following stereotactic ablative radiotherapy (SABR) for early-stage lung tumors: a pictorial essay. *J Thorac Oncol.* 2018 Jun;13(6):855–862. doi: 10.1016/j.jtho.2018.02.023
- 119. Horne ZD, Dohopolski MJ, Clump DA, Burton SA, Heron DE. Thoracic reirradiation with SBRT for residual/recurrent and new primary NSCLC within or immediately adjacent to a prior high-dose radiation field. *Pract Radiat Oncol.* 2018 May–Jun;8(3):e117–e123. doi: 10.1016/j.prro.2017.11.011
- 120. John C, Dal Bello R, Andratschke N, et al. In-field stereotactic body radiotherapy (SBRT) reirradiation for pulmonary malignancies: a multicentre analysis of the German Society of Radiation Oncology (DEGRO). *Sci Rep.* 2021;11:4590. doi: 10.1038/s41598-021-83210-3
- 121. Maranzano E, Draghini L, Anselmo P, Casale M, Arcidiacono F, Chirico L, et al. Lung reirradiation with stereotactic body radiotherapy. *J Radiosurg SBRT*. 2016;4(1):61–68.
- 122. Klement RJ, Sonke JJ, Allgäuer M, Andratschke N, Appold S, Belderbos J, et al. Correlating dose variables with local tumor control in stereotactic body radiation therapy for early-stage non-small cell lung cancer: a modeling study on 1500 individual treatments. *Int J Radiat Oncol Biol Phys.* 2020 Jul 1;107(3):579–586. doi: 10.1016/j.ijrobp.2020.03.005

- 123. Huang BT, Lu JY, Lin PX, Chen JZ, Li DR, Chen CZ. Radiobiological modeling analysis of the optimal fraction scheme in patients with peripheral non-small cell lung cancer undergoing stereotactic body radiotherapy. *Sci Rep.* 2015 Dec 11;5:18010. doi: 10.1038/srep18010
- 124. Woody NM, Videtic GM, Stephans KL, Djemil T, Kim Y, Xia P. Predicting chest wall pain from lung stereotactic body radiotherapy for different fractionation schemes. *Int J Radiat Oncol Biol Phys.* 2012 May 1;83(1):427–434. doi: 10.1016/j.ijrobp.2011.06.1971
- 125. Saha A, Beasley M, Hatton N, Dickinson P, Franks K, Clarke K, et al. Clinical and dosimetric predictors of radiation pneumonitis in early-stage lung cancer treated with stereotactic ablative radiotherapy (SABR) An analysis of the UK's largest cohort of lung SABR patients. Radiother Oncol. 2021 Mar;156:153–159. doi: 10.1016/j.radonc.2020.12.015
- 126. Bradley JD, Hope A, El Naqa I, Apte A, Lindsay PE, Bosch W, et al. A nomogram to predict radiation pneumonitis, derived from a combined analysis of RTOG 9311 and institutional data. *Int J Radiat Oncol Biol Phys.* 2007 Nov 15;69(4):985–992. doi: 10.1016/j.ijrobp.2007.04.077
- 127. Gay HA, Niemierko A. A free program for calculating EUD-based NTCP and TCP in external beam radiotherapy. *Phys Med.* 2007 Dec;23(3–4):115–125. doi: 10.1016/j.ejmp.2007.07.001
- 128. Sarudis S, Karlsson Hauer A, Nyman J, Bäck A. Systematic evaluation of lung tumor motion using four-dimensional computed tomography. *Acta Oncol.* 2017 Apr;56(4):525–530. doi: 10.1080/0284186X.2016.1274049
- 129. Palma DA, Senan S, Haasbeek CJA, Verbakel WFAR, Vincent A, Lagerwaard FJ. Radiological and clinical pneumonitis after stereotactic lung radiotherapy: a matched analysis of three-dimensional conformal and volumetric-modulated arc therapy techniques. *Int J Radiat Oncol Biol Phys.* 2011;80(2):506–513. doi: 10.1016/j.ijrobp.2010.02.032
- 130. Godoy MC, Naidich DP. Subsolid pulmonary nodules and the spectrum of peripheral adenocarcinomas of the lung: recommended interim guidelines for assessment and management. *Radiology.* 2009 Dec;253(3):606–622. doi: 10.1148/radiol.2533090179
- 131. Muñoz-Montplet C, Fuentes-Raspall R, Jurado-Bruggeman D, Agramunt-Chaler S, Onsès-Segarra A, Buxó M. Dosimetric impact of Acuros XB dose-to-water and dose-to-medium

reporting modes on lung stereotactic body radiation therapy and its dependency on structure composition. *Adv Radiat Oncol.* 2021;6(4):100722. doi: 10.1016/j.adro.2021.100722